UNIVERSITY OF OKLAHOMA

GRADUATE COLLEGE

ADVANCES TOWARD THE UTILIZATION OF CUCURBIT[7]URIL AND SELECTED VIOLOGENS IN MOLECULAR MACHINES AND DEVICES

A DISSERTATION

SUBMITTED TO THE GRADUATE FACULTY

in partial fulfillment of the requirements for the

Degree of

DOCTOR OF PHILOSOPHY

By

SHAWNA BETH ELLIS
Norman, Oklahoma
2013

ADVANCES TOWARD THE UTILIZATION OF CUCURBIT[7]URIL AND SELECTED VIOLOGENS IN MOLECULAR MACHINES AND DEVICES

A DISSERTATION APPROVED FOR THE
DEPARTMENT OF CHEMISTRY AND BIOCHEMISTRY

BY

_____
Dr. Ronald Halterman, Chair

_____
Dr. Daniel Glatzhofer

_____
Dr. Kenneth Nicholas

_____
Dr. Ann West

_____
Dr. Lloyd Bumm

Dedication

I dedicate this work to my husband, Trevor Ellis, and my children, Aidan and Ryker Ellis. I am in addition grateful to my mother, my father, and my grandparents, who have been instrumental in my educational success. I also thank my co-workers and collaborators as mentioned throughout this document. This work would not be possible without the guidance and support of my advisor, Dr. Ronald Halterman. In addition, throughout this process and in all things I do, God has been my driving and guiding strength.

Acknowledgements

I acknowledge and appreciate the work of Ronald Halterman, Michael Ashby, Daniel Glatzhofer, Josef Kalmar, Susan Nimmo, Jason Moore, and Jillian Moore as detailed throughout the pages of this document.

Table of Contents

List of Tables

List of Figures

Abstract

The study of technology at the molecular level is the perhaps the final frontier in materials science, and is fertile ground for the application of supramolecular chemistry. Cucurbit[7]uril is a particularly unique macrocycle that encapsulates smaller molecules and has potential application in enhancing the properties of guest molecules. This study has highlighted the reasons that the application of cucurbit[7]uril should be in the forefront of these emerging fields. The studies herein have gathered sound data supporting the use of cucurbit[7]uril in a variety of molecular scale devices. For example, cyclic voltammetry is used to demonstrate the protective effects provided by cucubit[7]uril to prevent photobleaching of small molecules that are potentially useful in dye-sensitive solar cells. Also, modes of binding, kinetic binding constants, and equilibrium binding constants have been determined for a variety of host-guest complexes which could lead to the strategic incorporation of these molecules into molecular machines and devices. Not only has previously held knowledge about the interactions of this macrocycle been confirmed, but the results here have increased the sphere of knowledge and may also guide future studies in this promising field.

Chapter 1: Introduction

Recently, macrocycles of all types have found useful application in chemistry in recent years, including supramolecular structures and polymers, reaction catalysis, drug delivery, removal of heavy metals, molecular machines, nanosensors, and physical property enhancement.[1] Though most of the applications have employed the use of cyclodextrin and crown ethers, more recently, cucurbit[n]urils (CB[n]) (Figure 1) have shown unique properties that have expanded the field.[1]

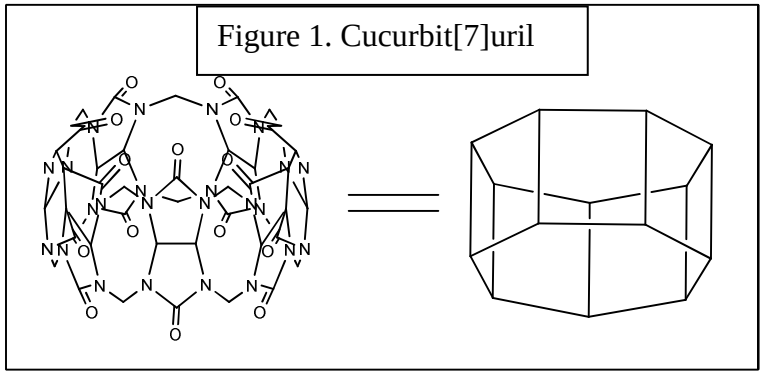

Figure 1. Cucurbit[7]uril

By use of hydrophobic interactions, and to a smaller extent electrostatic interactions, these macrocycles can bind various small molecules with abnormally high binding constants in the range of 10^5 to 10^{12} M^{-1}.[1] The size of the hydrophobic interior cavity in these pumpkin shaped tubes depends on the number of methylene bridged glycoluril units, which can range from five to ten units, with CB[6], CB[7], CB[8] finding most practical use.[1] The hydrophobic guest, of complimentary size and shape, seeks the interior of the cavity in whole or part, and the final alignment of host and guest is determined in milliseconds by secondary electrostatic interactions. In particular, electron dense amide groups create a negative electrostatic potential around both portals. Due to this feature, cucurbit[n]uril can bind cationic, electrostatically positive, and hydrophobic molecules, leading to very high binding constant to a wide variety of guests.

Although the field of molecular machines and devices remains in its infancy stages, there have been a few industrial applications of true chemically synthesized molecular technology. Many of the targeted applications of this field will remain a pipe dream until the body of scientific knowledge has been established to understand the underlying nuances. Cucurbit[7]uril[1] has the possibility of solving many of the problems associated with weakly binding systems, but brings its own complications. CB[7], by itself, is poorly soluble in any solvent but water[1] and when encapsulating other molecules, its strong binding properties are severely weakened when any other solvent is introduced to the system, limiting its usefulness in some ways, while elevating it in others. After all, cucurbituril's strong binding properties are primarily tied to the propensity of hydrophobic compounds to exit their environment in favor of CB[7]'s cavity. In addition, this same feature of CB[7] renders it extremely difficult to functionalize, as most organic reactions must be conducted in organic solvent. This makes CB[7] nearly impossible to attach directly to any other molecule or surface. This problem can be solved by associating CB[7] with other molecules through a rotaxane or catenane,[2] but remains a limiting factor in many situations, such as flow through systems, in vivo applications, and overall it decreases the creativity of structures that can be produced. Although CB[7] can bind a wide variety of guest molecules,[3] there also needs to be greater depth of guest molecules available through the literature.

The limitations of these systems are superseded by the vast potential of the field of molecular machines. At this early data gathering stage, there is much to be learned from this unique compound, and the potential applications in the medical and materials fields are staggering. It is therefore advantageous to be involved in these studies from

the ground up, improving the science and participating in any problem solving along the way. It is probable that improvement in key areas of the field will continue to promote the science of molecular machines and lead to innovation both planned and unplanned in coming years. In particular, our work focuses on problems such as surface attachment, rotaxane formation, various methods of functionalization, and the gathering of inclusion data from a wider depth of compounds. The context of these studies may not be attainable until the next decade, but as growth continues, it is realistic to expect future technologies that are literally built up atom by atom.

Chapter 2 will take advantage of the ability of CB[7] to encapsulate organic fluorescent dyes and enhance fluorescent properties for application in dye-sensitized solar cells[4] (DSSC). The appeal of DSSC lies in the opportunities for the cheap construction of these solar harvesting devices and their subsequent mass production.[4] However, current versions have low efficiency compared to the traditional silicon solar cells, therefore the practical application of these cells has not become widespread.[5] The encapsulation of Rhodamine B and Pyronin Y dyes with CB[7] results in the formation of strong, non-covalent intramolecular interactions between host and cationic guest, which is envisioned to modify the photo-chemical properties of the dye.[6] These properties will be tested in bulk solution by cyclic voltammetry experiments.

Chapter 3 addresses the difficulty of producing a CB[7]-containing rotaxane due to the lack of solubility of the macrocycle.[1] In particular, a fascinating viologen guest molecule is targeted in this study due to the potential stabilizing effects CB[7] could provide. A subset of rotaxanes, called "psuedo rotaxanes," are less stable[2] and can be temporarily separated in equilibrium, especially by the presence of a competitive

binding group; however, a full rotaxane must be physically blocked with a large stopper at both ends of the linear axle. Full rotaxanes may be neccessary in certain situations such as flow through techniques and in vivo applications. However, there is currently a dearth in the production of accessible CB[7]-containing rotaxanes. The wider difficulty of creating suitable rotaxane stoppers is studied in order to meet this need.

Chapter 4 focuses on increasing the depth of knowledge concerning CB[7] guests. In particular, if CB[7]'s strong equilibrium binding constants are to be taken advantage of in order to be used in molecular devices, there must be a library of kinetic and equilibrium binding data upon which to draw on. This was addressed through the lens of potential cancer sensor applications, and by doing so, highlights the many questions that are bound to surface when constructing a complicated molecular device. A molecular sensor is described that proposes the use of cucurbit[7]uril as a shuttle that allows for communication between the receptor and signaling group of the molecular sensor.

Chapter 2: Dye-sensitized Solar Cells (DSSC)

2.1 Introduction

Inspired by nature, dye-sensitized solar cells (DSSCs) have the potential to be a powerful source of renewable energy in the coming years.[4] DSSCs mimic the process of photosynthesis, but instead of using chlorophyll pigments to harvest light in order to produce biochemical energy, light is harvested by manmade fluorescent dyes and converted into electricity.[4] The mechanism of this manmade approach to photosynthesis is initiated when an electron, belonging to a synthetic fluorescent dye, is excited by absorbed light and injected into the conduction band of a titanium (IV) oxide semiconductor. This leaves behind an electron hole in the dye, which is now a temporary radical dication. For this to happen, it is optimal for the dye to be chemically attached or absorbed onto the semi-conducting surface at a physical length that maximizes electron injection, and that the energy level of the excited dye is sufficiently higher than the Fermi level of the semi-conductor[5] (Figure 2). The electron then travels through a conducting glass anode to the cathode by wire, providing a current to perform work, before it is returned to the dye by an iodide/triiodide electrolyte through diffusion.

Figure 2. DSSC[4]

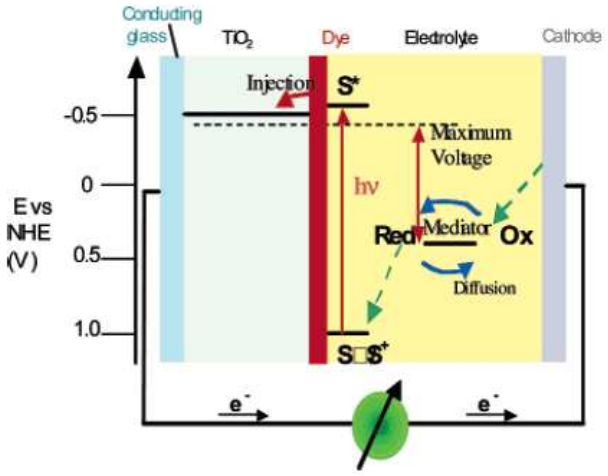

The appeal of DSSC lies in the opportunities for the cheap construction of these systems and their subsequent mass production. However, current versions have low efficiency (~11-13 %) compared to silicon solar cells (~25%), as well as low durability (silicon lasts 25 years); therefore the practical application of these cells has not become widespread.[5] In addition, current versions of these systems require the use of toxic and expensive Ru-based dyes.[4] Therefore an important target area for improvement of solar cells and photovoltaic devices is the development of cheaper, environmentally friendly, more redox stable dyes which will therefore increase electron injection. Most importantly, the target dye system should have a limited ability to aggregate, which will prevent the system from breaking down over time due to photo-oxidation.

To a limited extent, these problems could be resolved by the use of cheap organic dyes with a higher molar extinction coefficient, which would not only increase efficiency of the photo-chemical process, but would also increase the overall system's efficiency by increasing sheer numbers of excited electrons.[6] Another approach would be to improve the efficiency of the photo-chemical process by increasing excitation lifetime. However, this may prove difficult to accomplish by solely modifying the dyes themselves. A better approach could be to stabilize the radical dication of the excited dye by strategic supramolecular interaction, such as the use of a molecular cage to encapsulate the dye, thereby creating a stabilizing environment around the excited dye leading to increased fluorescence, reducing the recombination of the excited electron with the dye. This method would have the added benefit of preventing the dyes from aggregating with other dyes in their cationic states, which leads to an undesirable

electron transfer which destroys the dye through the irreversible process of photo-oxidation.

2.2 Specific Aims

The goal of this project was to study host guest systems as possible candidates for use in dye-sensitized solar cells. Specifically, cucurbit[7]uril (CB[7]) has been studied in combination with commercially available organic dyes, Rhodamine B and Pyronin Y (Figure 3). These dyes were chosen primarily for their strong binding (K_a) with CB[7] ($1.6 \pm 0.4 \times 10^5\ M^{-1}$ and $9.7 \pm 5.4 \times 10^6\ M^{-1}$, respectively), their absorbance in the visible spectrum (lambda max 510 nm and 547 nm, respectively), and their high molar extinction coefficients (>50,000 $M^{-1}\ cm^{-1}$).[5] The encapsulation of these dyes with CB[7] results in the formation of strong intramolecular interactions[6] between host and cationic guest, which is envisioned to modify the photo-chemical properties of the dye. In addition, CB[7] is expected to increase the durability and overall lifetime of the cell by protecting the dye from aggregating[7] with neighboring substances leading to undesirable electron transfer and photo-degradation. These properties will be tested in bulk solution by cyclic voltammetry experiments, using Indium Tin Oxide (ITO) as the conducting electrode as is used commonly in DSSCs. We will evaluate the redox

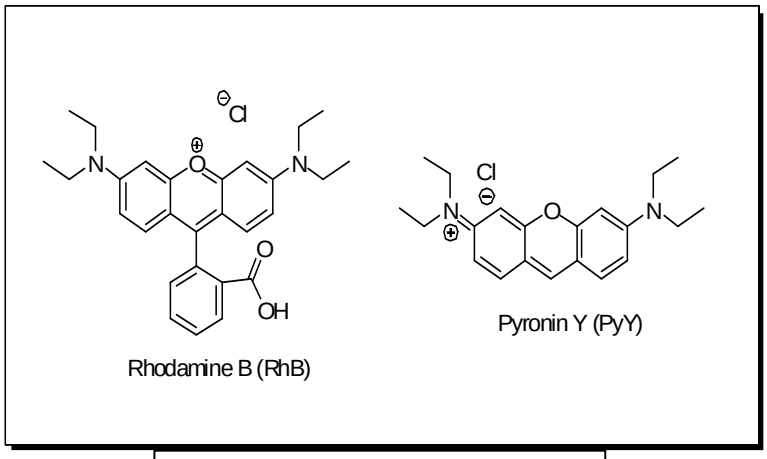

Figure 3. Dye structures

properties of organic dyes (Rhodamine B, Rhodamine B with a tether, and Pyronin Y in the presence and absence of CB[7] for application in DSSC in order to assess the encapsulating molecule's ability to provide stability to the excited state to and to protect against photo-oxidation. These general effects have been demonstrated in the literature for other CB[n]/dye systems[6] that are less suitable for use in DSSC, necessitating the following study in this area.

In order to keep the dye in optimum proximity to the semiconducting layer thereby increasing the injection rate of electrons, it was desirable to develop a way to attach the dye to the titanium dioxide (TiO_2) semiconductor via a tether. Phosphonic acid is a common tether utilized for TiO_2; however, the fragile surface is not ideal for use in cyclic voltammetry studies which would be necessary to confirm the success of a surface attachment. Therefore; an indium tin oxide (ITO) coated glass slide was substituted for TiO_2 due to literature precedence for a phosphonic acid group to attach to both TiO_2 and ITO[7], allowing for the use of the attachment point as the conducting electrode for a direct measurement of redox properties using cyclic voltammetry. Due to synthetic accessibility, Rhodamine B was chosen to be further functionalized with this phosponic acid tether.

2.3 Synthesis and Experimental Procedure

The first goal of this project was to obtain cucurbit[7]uril in good yield and purity for the purpose of dye encapsulation. The cyclic structure of CB[7] consists of methylene bridged glycoluril units [n] and contains a hydrophobic interior cavity which is lined by electron dense amide groups, creating a negative electrostatic potential around both portals. Due to this feature, cucurbit[n]uril can bind cationic,

electrostatically positive, and hydrophobic molecules, leading to very high binding to a variety of guests.[1] Since Rhodomine B and Pyronin Y are cationic organic molecules, this dye-CB[n] system is suitable for this study. CB[7] in particular has become the focus of this study for several reasons. Due to its larger cavity size, CB[7] can bind a wider range of guests than CB[6] and CB[5][1,3], including the organic dyes herein; Rhodamine B and Pyronin Y. Also, CB[7] is more soluble in water than other

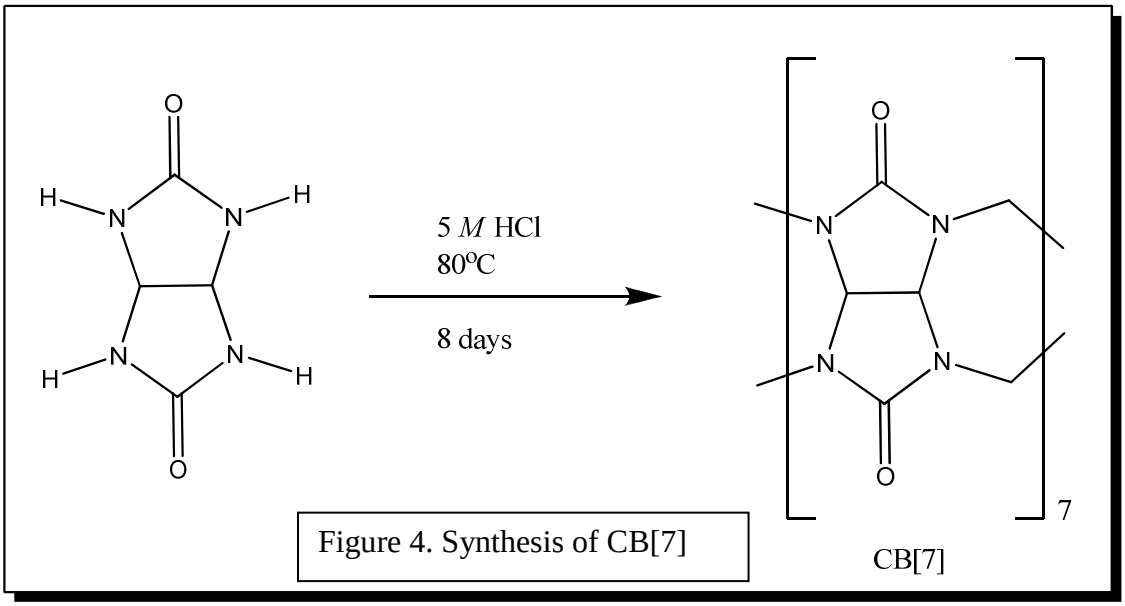

Figure 4. Synthesis of CB[7]

oligomers of CB[n].

Cucurbit[7]uril was synthesized via the literature procedure from glycouril and para-formaldehyde[1] (Figure 4). Because longer reaction times favor higher order oligomerization, the reaction conditions have been optimized to favor the formation of the desired product with seven repeating subunits. The common side products, CB[5], CB[6], CB[8], and CB[10] are removed by a rigorous purification process that uses the differing solubility properties of the macromolecules.[1] The isolated CB[7] can then be further purified by recrystallization to give white crystals.

2.4 Cyclic Voltammetry of Rhodamine B and Pyronin Y

The fluorescent dyes Rhodamine B and Pyronin Y were purchased from Fischer Scientific. They are similar in structure, color, and properties, and may be oxidized and reduced by the application of an electrical current (Figure 5). The following redox studies of these dyes were conducted using cyclic voltammetry (CV), in collaboration with Professor Glatzhofer,[8] in order to assess the oxidation potential that would be necessary to promote an electron to the excited state. Then, CB[7] was added to each solution and an electrical current was cycled multiple times by CV to determine the protective effect this encapsulating molecule would have on the oxidation potentials and durability of the dyes.

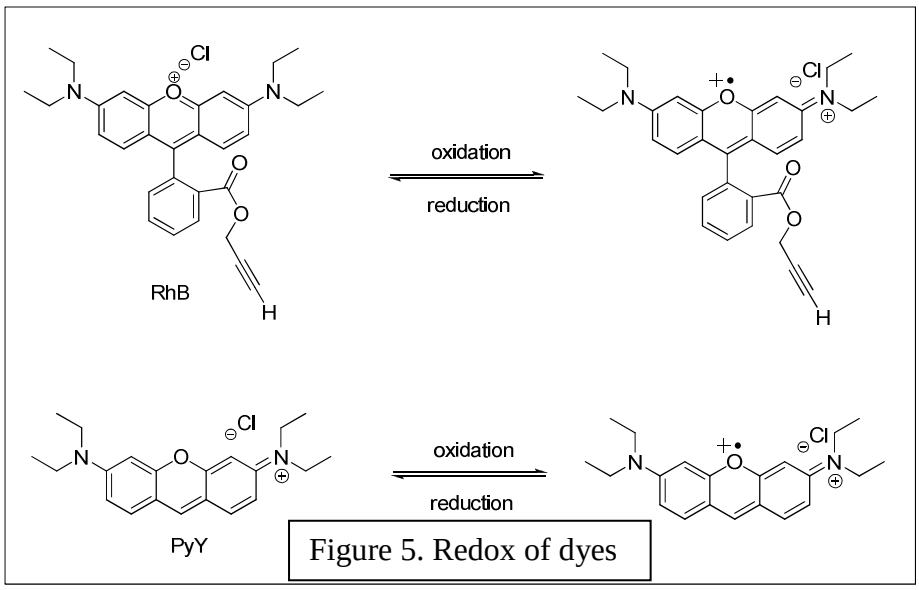

Figure 5. Redox of dyes

The cyclic voltammagrams of both dyes were taken for three scans each. The dyes showed a peak for both an oxidation potential and a diffusion delayed return reduction potential which restores the original composition of the structure. Rhodamine B (RhB) was found to give an oxidation peak at 960 mV which is reduced to 920 mV

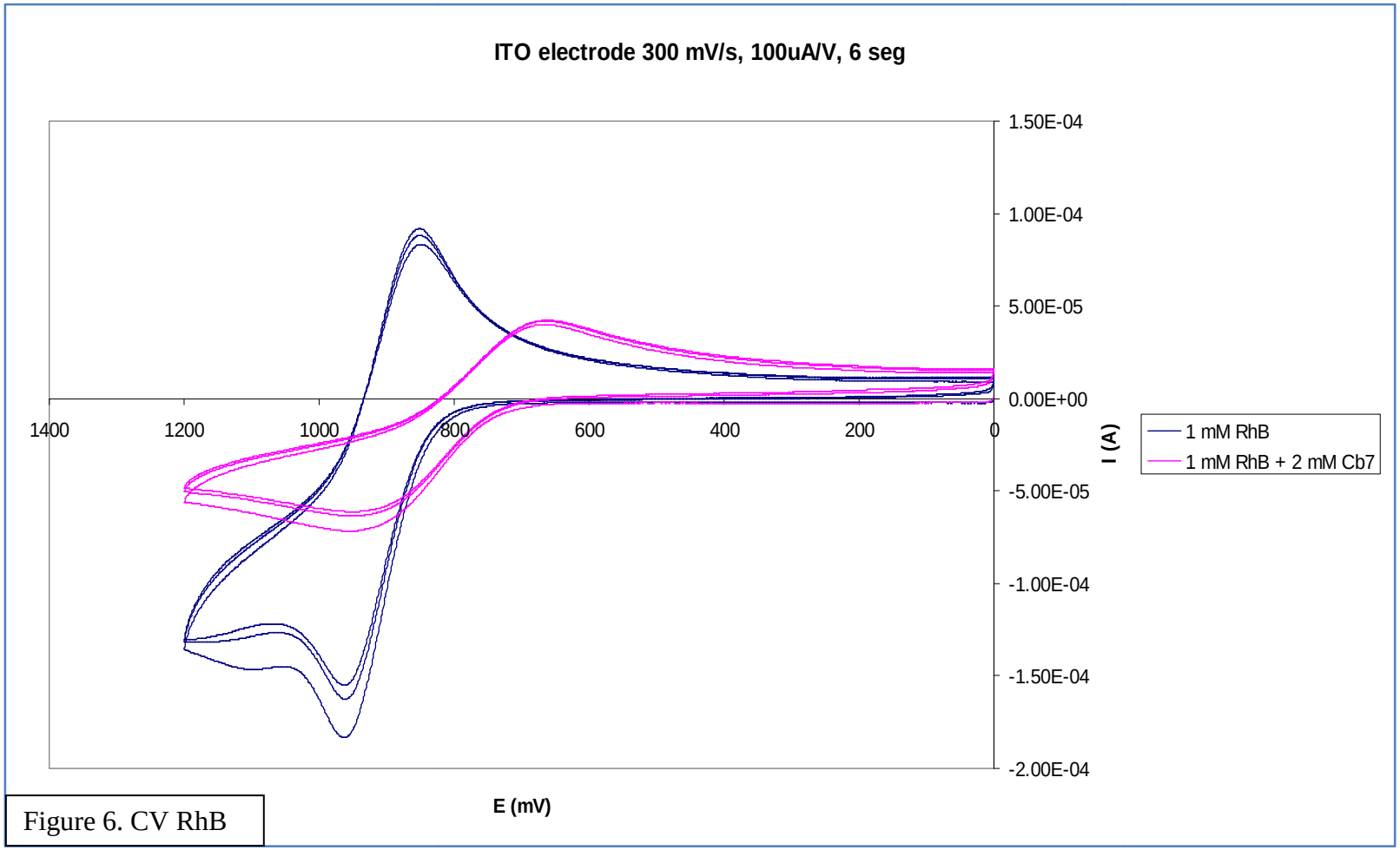

Figure 6. CV RhB

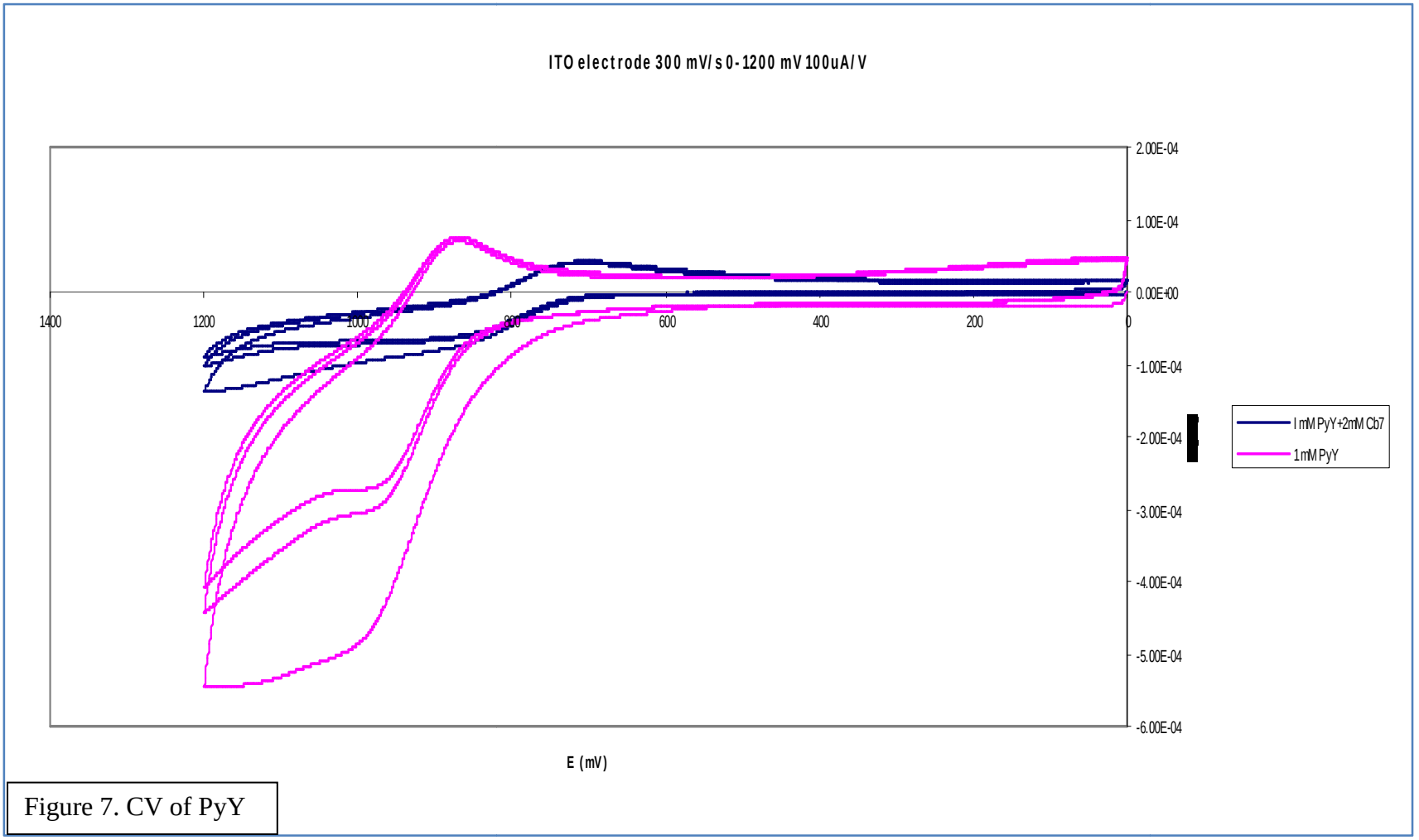

Figure 7. CV of PyY

with the addition of CB[7] (Figure 6). This could indicate that CB[7] is stabilizing the radical di-cation of the dye upon oxidation. An similar effect can be seen for Pyronin Y (PyY) (Figure 7). Its oxidation potential is reduced from 970 mV to 830 mV with the addition of CB[7]. This could be caused by better encapsulation of Pyronin Y in the cavity of CB[7] due to less steric interference, increasing the ability of CB[7] to stabilize the radical di-cation. If this high energy species can be stabilized, then logic dictates that the excited electron of a dye-sensitized solar cell has a better chance of being injected into the semiconducting material. These observations are consistent with results obtained by Halterman et. al.[7], showing that the encapsulation of a rhodamine dye by CB[7] increases the fluorescence lifetime of the dye, providing visual evidence of increased stability of the radical di-cation. In addition, the authors demonstrated that for a Rhodamine 6G dye/CB[7] system, the lifetime of the organic dye, during which the electron is in its excited state, was increased. This is due to the protective properties of the hydrophobic moieties within the cavity, the electron rich areas provide a surface that allows for the stabilization of the charged form of the dye, through non-covalent interactions. Now, with cyclic voltammetry evidence of the oxidation and reduction of the dyes in hand, the stability of these dyes over time can be studied.

The cyclic voltammetry cycles for Rhodamine B were then increased to investigate photobleaching of the dye. Over time, it is clear that the signal degrades as the dye undergoes photobleaching (Figure 8). However, with the addition of CB[7], the coordinated dye signal does not degrade nearly as much as the dye by itself, indicating

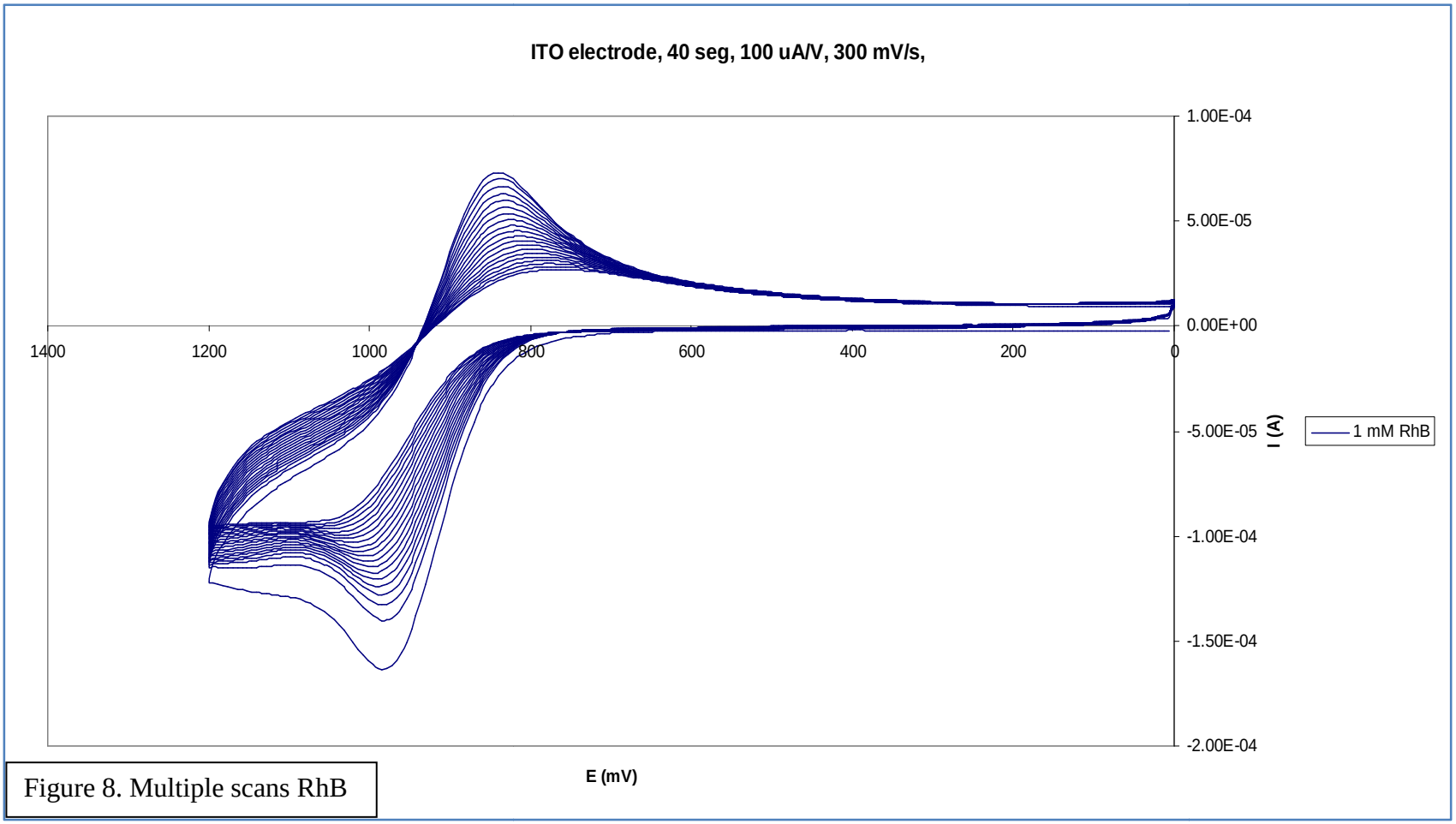

Figure 8. Multiple scans RhB

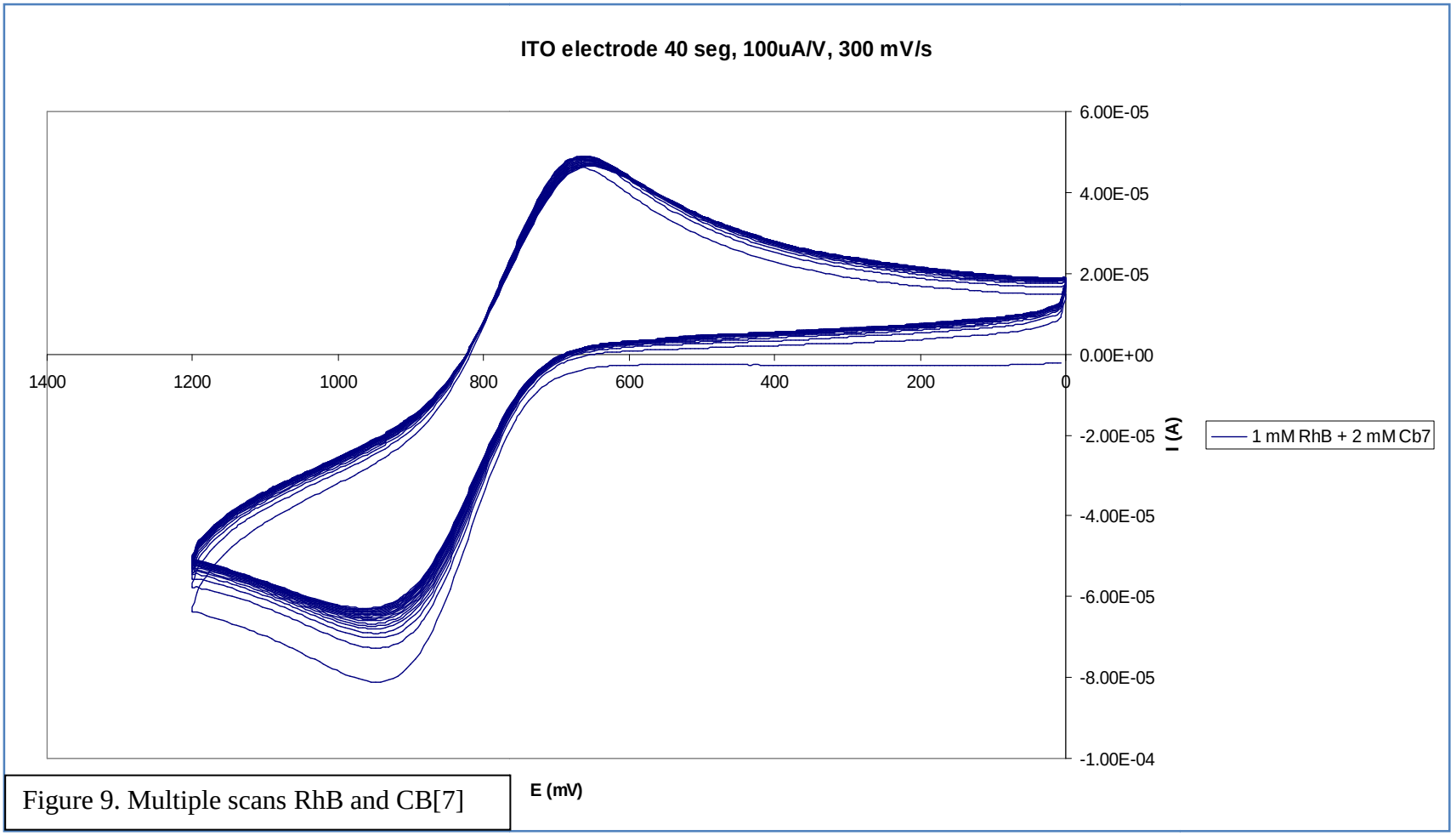

Figure 9. Multiple scans RhB and CB[7]

that the CB[7] could be providing a protective effect by isolating the radical-dication from other reactive species in the solution (Figure 19). This type of effect has been observed in the literature for Rhodamine 6G dye by Nau, et al.[9] using CB[7] as a means of protection against photo-bleaching and aggregation with other species. Nau et. al. measured the diminishing florescence of R6G solutions over time, and quantified the

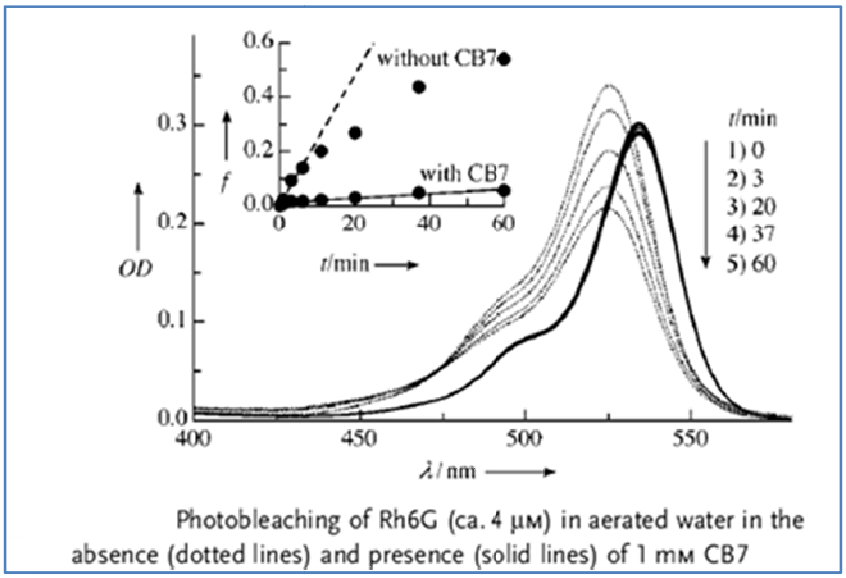

Figure 10. Rh6G photobleaching

protective benefits of CB[7]. This is important because photo-oxidation represents an interruption in the oxidation/reduction cycle via a chemical reaction between the cationic form of the dye and another chemical entity. This competitive reaction results in the formation of a modified dye skeleton that is no longer photo-active (Figure 10). These results are supporting evidence that the inert and robust chemical composition of organic dye/CB[7] systems are capable of withstanding the chemical environment necessary for a DSSC with less degradation over time.

2.5 Surface attachment of Rhodamine B

In order to make these dyes more applicable to DSSCs, it was necessary to consider the ultimate goal of attaching them to the surface of titanium oxide. If the surface attachment is successful, the redox properties of an organic dye in the presence and absence of CB[7] could be evaluated for application in DSSC. This would determine the encapsulation molecule's ability to provide stability to the excited state and to protect against photo-oxidation. In order to conduct cyclic voltammetry studies more easily, it was necessary to substitute titanium dioxide for an indium tin oxide coated slide as the conducting electrode and attachment point for the dye. In addition, we chose Rhodamine B as the model system for surface attachment due to synthetic accessibility, even though it was not as promising a candidate for DSSC as compared to PyY, indicated by solution studies herein. Rhodamine B has a carboxylic acid functionality which was envisioned as a potential attachment point for the tether. This attachment point could then be linked to surfaces that could test the feasibility of the dye-CB[7] system in repeating cycles of current and light, as would be applicable in DSSC. This study narrowly focuses on studying the potentially protective effects of CB[7] on Rhodamine B when it undergoes multiple cycles of oxidation and reduction using cyclic voltammetry. To achieve this purpose, Rhodamine B is envisioned to be attached to an Indium Tin Oxide electrode by a phosponic acid tether that is added to RhB via a triazole linker.

2.6 Synthesis of Rhodamine Propargyl Ester (3)

The precursors of **8** were initially envisioned to be an ester of Rhodamine B containing a terminal alkyne, and an azide tether that is pre-attached to the ITO surface.

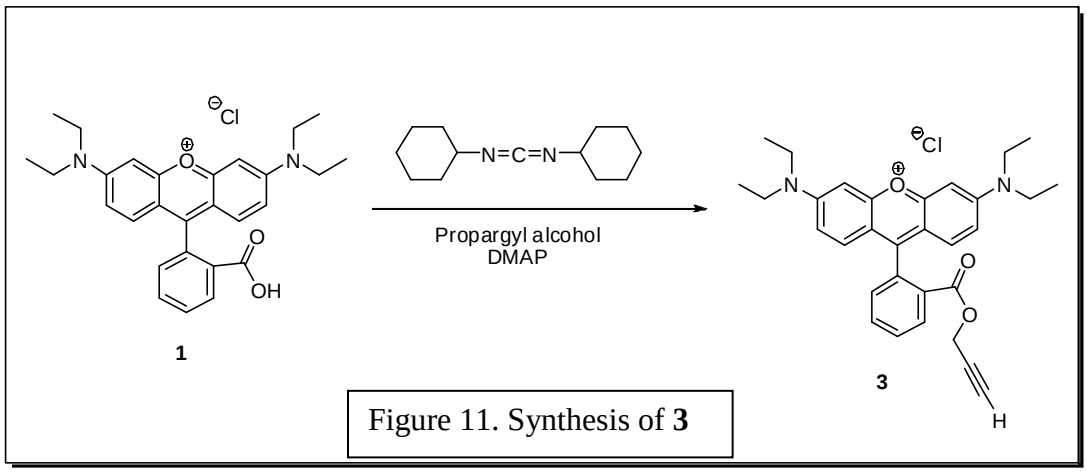

Figure 11. Synthesis of **3**

These compounds could then be joined together by an azide alkyne Huisgen cycloaddition.[10] Rhodamine propargyl ester **3** was formed from Rhodamine B under mild conditions using Steglich Esterification (Figure 11).

N,*N'*-Dicyclohexylcarbodiimide (DCC) was added to activate the carboxylic acid to be reacted with the propargyl alcohol, and 4-dimethylaminopyridine (DMAP) was used as a catalyst. The final pure product was a deep purple and highly reflective solid **3**.

2.7 Synthesis of Phosphoric Acid Tether and surface attachment

The production of precursor **7** was attempted by a three step synthesis (Figure 12). First, triethyl phosphite was added in small excess to 1,8-dibromooctane **4** to give a

Figure 12. Synthesis of **7**

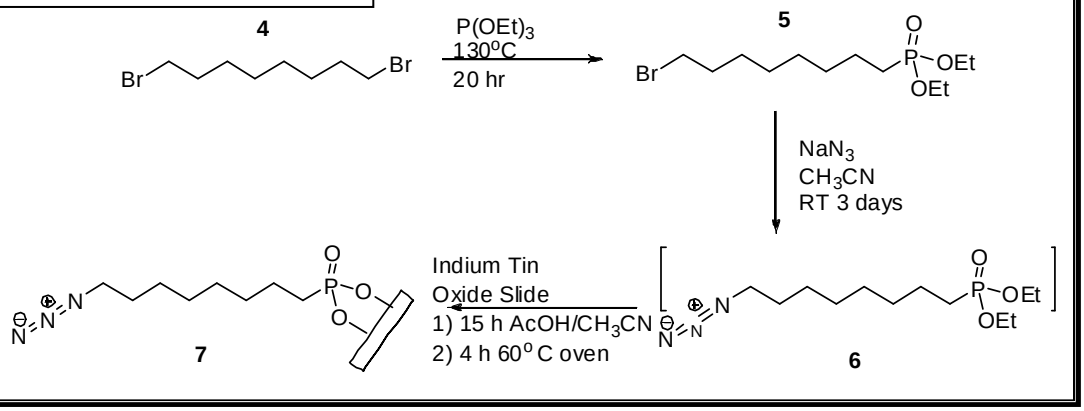

statistical mixture of substitution products.[11] The mono substituted product **5** was purified to give a yellow oil, verified by ^{1}H NMR. Next, the phosphonic azide **6** was obtained from ester **5** by an S_N2 addition of sodium azide. The crude product **6** was utilized immediately without isolation, in order to prevent destruction of the heat sensitive azide group. The procedure for the attachment of the azide tether **6** was carried out by an intitial hydrolysis of the phosphonic ester to the phosphonic acid, which allows the phosphonic acid to physically absorb to the surface of a cleaned and activated ITO slide. This is followed by a final heat curing at 60C which induced a chemical reaction between the OH functionality of the ITO slides and the phosphonic acid. Unfortunately, the success of these steps could not be determined experimentally as they occurred, and would have to be determined by the analysis of subsequent steps. After the curing step was completed, the slides were then rinsed to remove any unattached tether. A mixture of RhB ethyl ester **3**, Nolan's[10] sIMesCuBr catalyst, an ITO slide presumably with attached tether **7**, and a solution of *tert*-butyl alcohol and water was allowed to diffuse for three days at room temperature in order to 'click' the precursors together by the cyclo-addition of the azide to the alkyne. (Figure 13) The

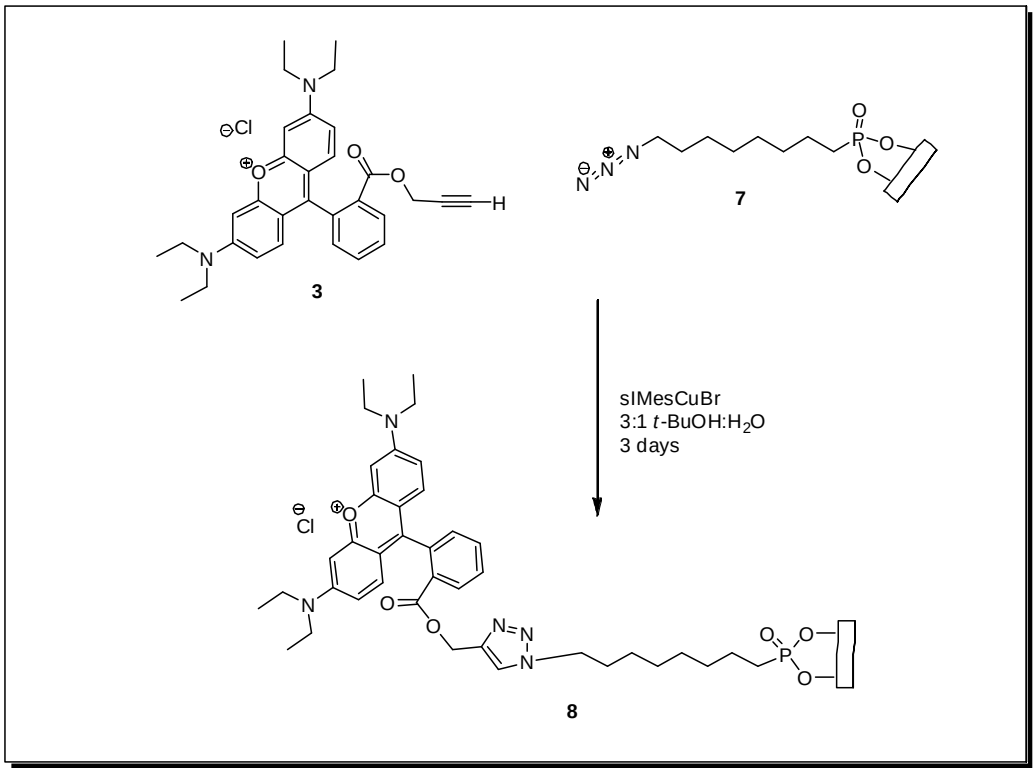

Figure 13. Synthesis of **8**

slides were then removed and rinsed, and the success of the surface attachment was then tested by cyclic voltammetry. It was expected that successful attachment of this complex system would yield an oxidation and reduction potential, but no peaks were observed experimentally. This outcome suggests failure at one or more of the previous steps including surface attachment, curing, the click reaction, hydrolysis, or azide substitution. It is very likely that the final curing step was the point of failure, as literature examples suggest that higher curing temperatures than we used are necessary to complete chemical bonding of the phosphonic acid to the ITO surface. However, if we had used a higher temperature, we would have run the increased risk of

decomposition of the azide. It is also possible that the attachment step was the point of failure. The problem is that successful attachment depends on a sensitive balance of solvent polarity and surface activation to achieve a successful attachment. Though many solvent combinations were attempted with the phosphonic acid tether, a successful system for surface attachment was either not found, or was not ultimately successful because proper curing was not possible. Alhough other members of the Halterman Group[12] had success attaching silane tethers to glass slides; however, the phosphonic acid/ITO system was notably different. It is additionally possible that the failure of the synthesis occurred with the click reaction. Nolan's sIMesCuBr catalyst[10] was employed for this synthesis, which is a well-documented and proven method of producing a robust click reaction as an alternative to the more common CuII/sodium ascorbate system.[10] However, it is possible that the crowded, attached tethers on the surface of the ITO were interfering with the success of the azide alkyne Huisgen cycloaddition.

2.8 Redesign of Surface attachment of Rhodamine B and cyclic voltammetry

In an attempt to bypass these difficulties, it was decided to click tether **5** with functionalized Rhodamine B propargyl ester **3** prior to surface attachment. (Figure 14) By producing the isolatable compound **9**, we were able to confirm the success of the click reaction by NMR spectra of the intermediate, due to the triazole's characteristic peak at 5.5 ppm. An attachment procedure was followed, and this time the possibility of destroying the azide by heat was eliminated. CVs were taken of these slides, with only one slide yielding possible evidence for the presence of attached product (Figure 15). In both the second and third scan, there was a small but promising oxidation peak

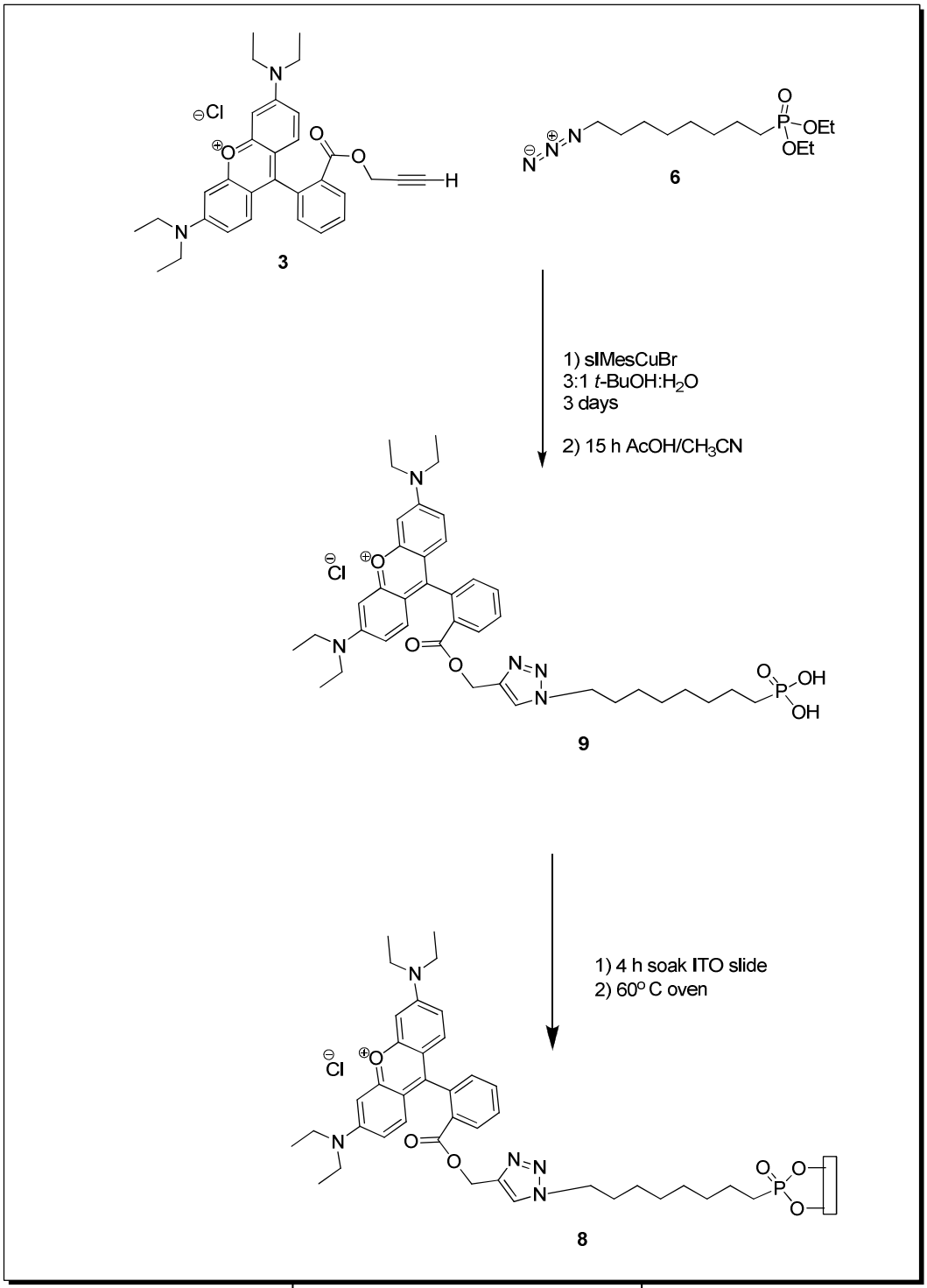

Figure 14. Synthesis of **8b**

at 970 mV, which was unfortunately not reproducible. This study was limited by the small amount of compound that was produced by the synthetic scheme, and in the

future could be aided by even higher curing temperatures (above 60C) in an effort to increase the amount of chemically attached dye.

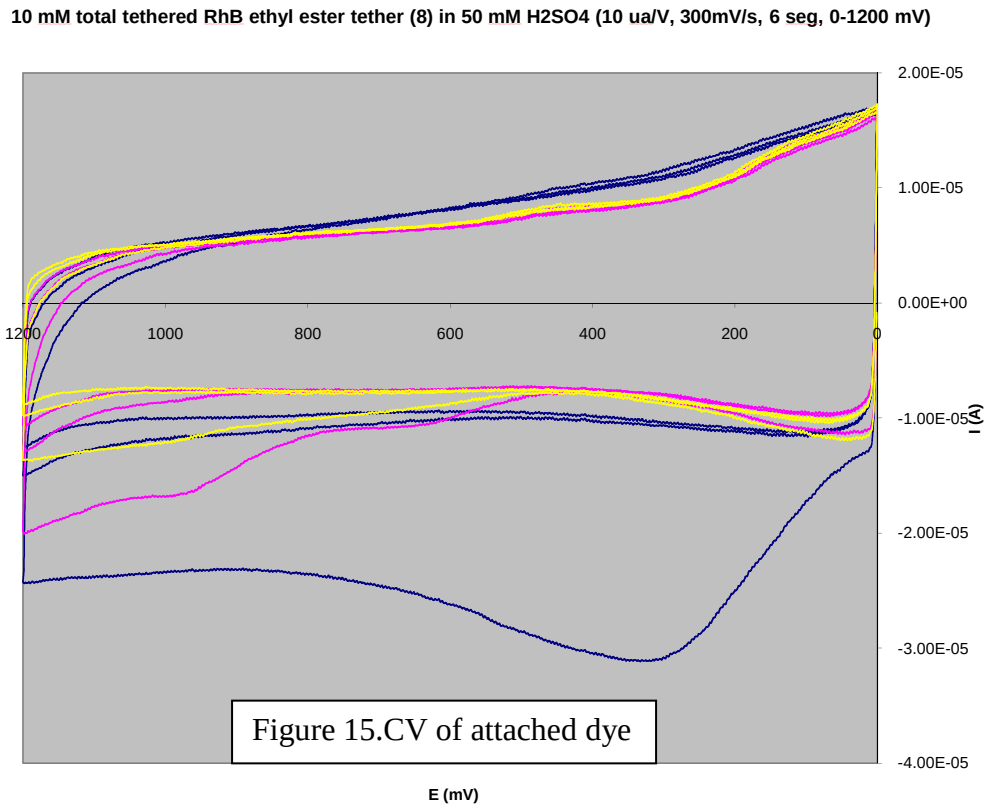

Figure 15.CV of attached dye

If this peak could be confirmed, it would indicate that the dye was successfully attached to the ITO surface. The peak of 970 mV is shifted 10 mV up from the original position of the oxidation peak of free Rhodamine B. This would be consistent with literature indicating that surface attachment to ITO causes a small increase in potential due to the electron density increase upon anchoring.[6] Notably, the return reduction peak is absent or too small to be visible, which would indicate that the oxidation at 980 mV could be irreversible, possibly due to decomposition, putting into question the viability of this system. In future studies, if this result could be repeated, it would be interesting to see if the introduction of CB[7] could cause the return oxidation peak to be visible.

Ultimately, the decision was made to put DSSC research aside in favor of promising research results in the following chapters.

In summary, these studies have found that CB[7] coordinated dyes, undergoing multiple cycles of oxidation and reduction, do not degrade nearly as much as an uncoordinated dye. This indicates that the CB[7] is likely providing a protective effect by isolating the radical-dication from other reactive species in the solution, thus preventing photobleaching. This effect would be vitally important if applied to the use of DSSC, because longer lasting solar cells are more economically feasible.

2.9 Experimental

General Cyclic Voltammetry Procedure- In general, all solutions that underwent cyclic voltammetry were bubbled with nitrogen prior to analysis, in order to prevent oxygen signals. The solutions were prepared with an electrolyte of 20 mM KCl to improve conductivity of the solution while also keeping the range of the experiment clear of noise. All experiments were conducted in the presence of ambient light. We attempted to conduct the experiments in acetonitrile, however the solubility of CB[7] became a limiting factor. This was unfortunate because the use of DI water as the solvent limited the range of the CV that was free of background noise. All experiments were conducted with a range of 0-1200 V, a scan rate of 300 mv/s, a sensitivity of 10 μA/V, and 6 or 40 segments were taken. In some experiments, CB[7] was present in a 1 mM concentration. The working electrode and reference-electrode were ITO and SCE, respectively.

Synthesis of Cucurbit[7]uril[1] – A mixture of glycouril (20g, 141 mmol) and para-formaldehyde (8.45 g, 281 mmol) were dissolved into concentrated 5 *M* HCl (150 mL). The slurry was stirred at 80C for 8 d, in a beaker covered by a watchglass. The solution was then cooled to room temperature and MeOH (400 mL) were added in order to precipitate CB[7]. The solid was filtered and washed two times with methanol. To remove any remaining impurity, the solid was dissolved in 20% aqueous glycerol in a beaker. The mixture was heated to 60C for 3 h while stirring, and then allowed to cool. Next, the CB[7] was collected on a filter. CB[7] and then washed five times with MeOH (400 mL) which was added to the filter one at a time and pulled off by vacuum, yielding approximately 15% of CB[7]. For improved purity, CB[7] was recrystallized with vapor diffusion recrystallization. First, CB[7] was sonicated in dilute sulfuric acid to give a concentrated solution in a small vial. The vial was then placed into a Erlenmeyer flask containing a small amount of 1:1 acetone:THF, being careful to keep the solutions separate. The top of the flask was sealed, and the apparatus was left at room temperature for three days until crystals appeared. This occurred as the acetone and THF vapor slowly diffuses into the CB[7] solution, lowering the solubility of CB[7]. The crystals were then collected in a filter to provide a yield of 3% spectroscopically pure CB[7]. ^{1}H NMR spectra were consistent with those found in the literature.[1]

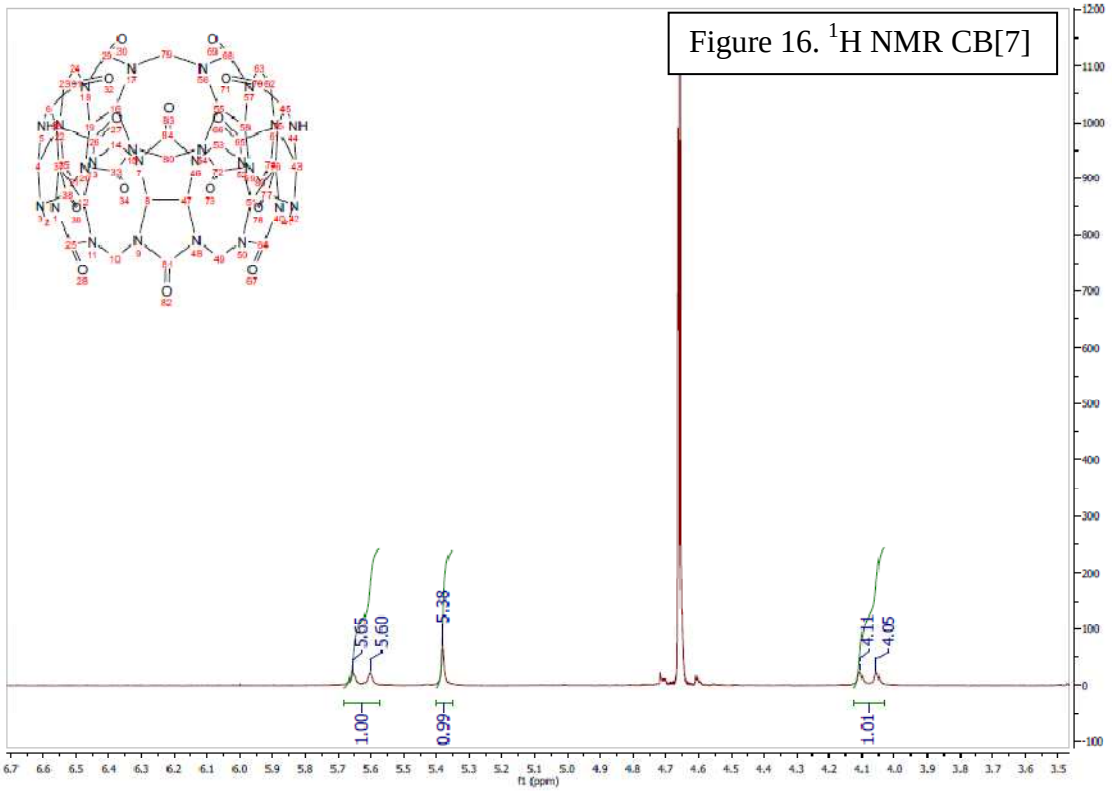

Figure 16. ^{1}H NMR CB[7]

ITO slide cleaning procedure - Indium Tin Oxide coated glass slides were ordered from commercial sources to be used in surface studies. In order for the phosphonic acid tether to chemically bond to the slide, the surface of the slide had to be properly cleaned and activated. The following procedure was applied whether the slide was new or was being reused. The slides were first submerged in acetone in a glass beaker and sonicated for ten minutes to remove any organic residue. The slides were further sonicated in methylene chloride for the same reason. Next, the organic solvent was replaced by DI water, which had been passed through a millipore filter, and sonicated for two minutes. This was repeated five times, replacing the water each time, to remove any water soluble residue. The slides were then placed in the oven overnight to completely dry, as organic solvent residue would not be desirable in the next step.

After the slides were cooled, they were placed in a solution of 1:1:5 30% NH_4OH, 30% H_2O_2, and millipore purified DI water. This step is key in producing uniform hydroxyl groups on the surface of the slide and removing any oxides that may have been left behind from its previous use. Finally, the slides were sonicated in copious amounts of millipore water in order to remove the remains of the reactive solution.

Synthesis of Rhodamine B Propargyl Ester 3: A mixture of rhodamine B (1.00 g, 2.08 mmol), methylene chloride (35 mL), 1,3-dicyclohexylcarbodiimide (DCC) (0.54 g, 2.6 mmol), propargyl alcohol (0.58 g, 10.4 mmol), and 4-dimethylaminopyridine (DMAP) (0.03 g, 0.28 mmol) was stirred under nitrogen at room temperature for 3 d. The methylene chloride was evaporated and the resulting product was purified by silica gel column chromatography with 9:1 methanol/chloroform, followed by 1:1:0.1 methanol/chloroform/glacial acetic acid, to give ester (**3**) (0.09 g, 0.18 mmol, 82%) as a purple solid: ^{1}H NMR (300 MHz, CD_3CN): δ 8.28 (m, 1 H), 7.84 (m, 2 H), 7.40 (m, 1 H),7.06 (d, *J*=9.5 Hz, 2 H), 6.93 (dd, *J*=2.5, 9.5 Hz, 2 H),6.84 (d, *J*=2.5 Hz, 2 H), 4.59 (d, *J*=2.5 Hz, 2 H), 3.61(q, *J*=7.1 Hz, 8 H), 2.64 (t, *J*=2.5 Hz, 1 H), 1.24 (t, *J*=7.1 Hz, 12 H).

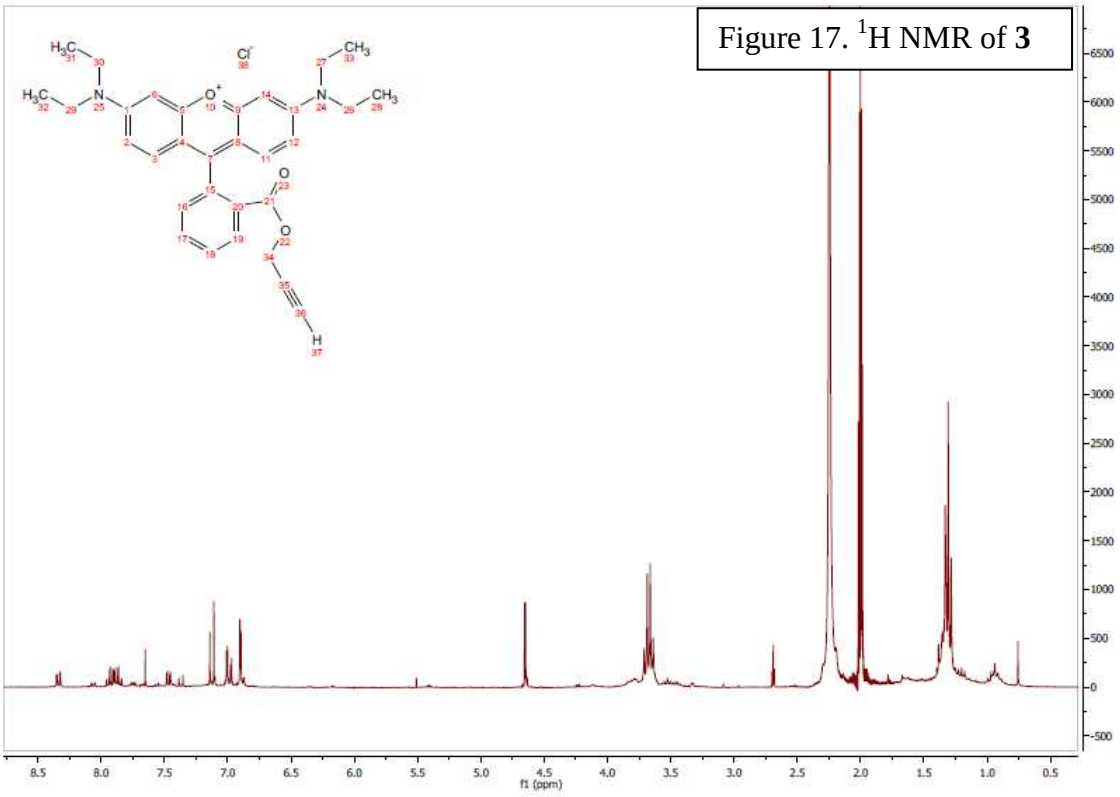

Figure 17. ^{1}H NMR of **3**

Synthesis of 8-bromooctylphosphonic acid 5- Clear liquid triethyl phosphite (3.1 mL, 18.2 mmol) was added neat to 1,8-dibromooctane **4** (3 mL, 16.6 mmol) under a dry nitrogen atmosphere dropwise by syringe. The mixture was constantly stirred for 30 m before being heated to 130C for 20 h. Upon completion, the reaction mixture was cooled and quenched with distilled water and stirred for two h. The crude product was then extracted with methylene chloride and washed with water and brine three times. The methylene chloride layer was dried with magnesium sulfate, filtered, and evaporated to give a crude liquid. The product **5** was purified by silica column with a one to one mixture of hexane and ethyl acetate to give a yellow oil (0.34 g, 7%). ^{1}H NMR (300 MHz; $CDCl_3$): δ 1.33 (t, J = 12.6 Hz, 6H), 1.45–1.85 (m, 14H), 3.45 (t, 2H), 4.15 (q, 4H).[6]

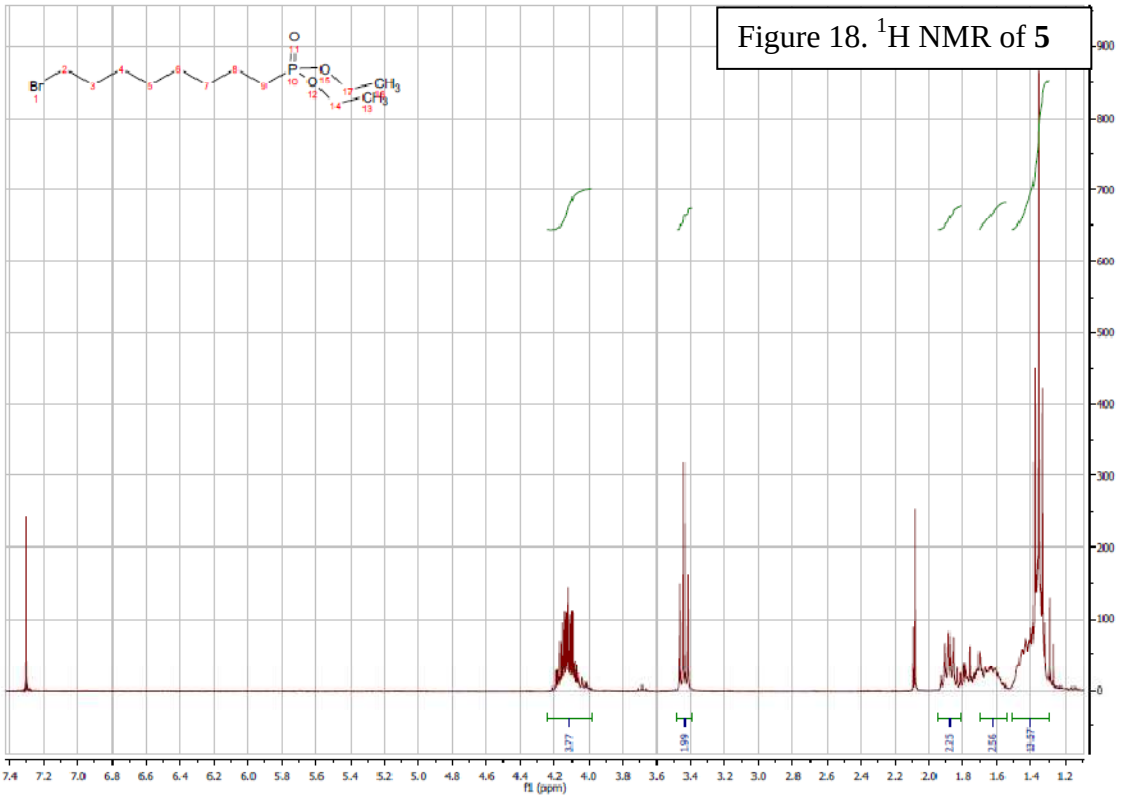

Figure 18. ^{1}H NMR of **5**

Synthesis of 8-azidooctylphosphonic acid 7: A mixture of phosphonic ester (**5**) (0.30 g, 1.1 mmol) and sodium azide (0.08 g, 1.2 mmol) were combined in acetonitrile (45 mL) at 60C for 3 d under nitrogen. Upon completion, the mixture was cooled and acetonitrile was evaporated. The crude product was triturated with methylene chloride, and the methylene chloride was evaporated without heat to give product **6** (0.22 g, 85% yield). The product was soaked in a 1:1 mixture of acetic acid and acetonitrile for 15 hours in the presence of an ITO slide, followed by curing in the oven to give product **7**. This product would not be confirmed at this stage of the synthesis.

Synthesis 1of 3,6-bis(diethylamino)-9-(2-(((1-(8-phosphonooctyl)-1H-1,2,3-triazol-4-yl)methoxy)carbonyl)phenyl)xanthylium chloride 8a- Activated ITO slides were soaked in a 1 mM solution of tether **7** for 15 h in a 1:1 mixture of acetonitrile and acetic acid. Afterwards, the slides were rinsed with acetonitrile and then cured in the oven for 4 h at 60C. After the curing step was completed, the slides were dipped in a solution of RhB propargyl ester **5** (1 mM) and Nolan's[10] sIMesCuBr catalyst (10%) in a 1:1 mixture of *tert*-butyl alcohol and water for six hours at room temperature. The slides were then dried by centrifuge and then rinsed with copious amounts of ethanol and water before CV analysis of the slide in 20 mM KCl was conducted; however, the desired compound was not found in the analysis.

Synthesis of 3,6-bis(diethylamino)-9-(2-(((1-(8-phosphonooctyl)-1H-1,2,3-triazol-4-yl)methoxy)carbonyl)phenyl)xanthylium chloride 9-The reaction was run in a 3:1 mixture of *t*-butyl alcohol and water containing RhB propargyl ester **3** and sIMesCuBr (10 mol%) and tether **6** for 15 h at room temperature. The mixture was immediately used to soak several activated ITO slides for four hours in a 3:1 mixture of *t*-butyl alcohol and acetic acid, and at that time a ^{1}H NMR sample of the soaking mixture was taken to confirm the presence of click product **9**. ^{1}H NMR (300 MHz, CD_3CN): δ 8.36 (m, 1 H), 7.86 (m, 2 H), 7.42 (m, 1 H),7.14 (d, J=9 Hz, 2 H), 6.98 (dd, J=2.5, 9 Hz, 2 H),6.89 (d, J=2 Hz, 2 H), 5.51(s,1 H), 3.67 (m, 2H), 3.60 (d, J=7 Hz, 2 H), 3.58(m, J=7 Hz, 8 H), 1.31 (m, 12 H), 1.25 (14 H).

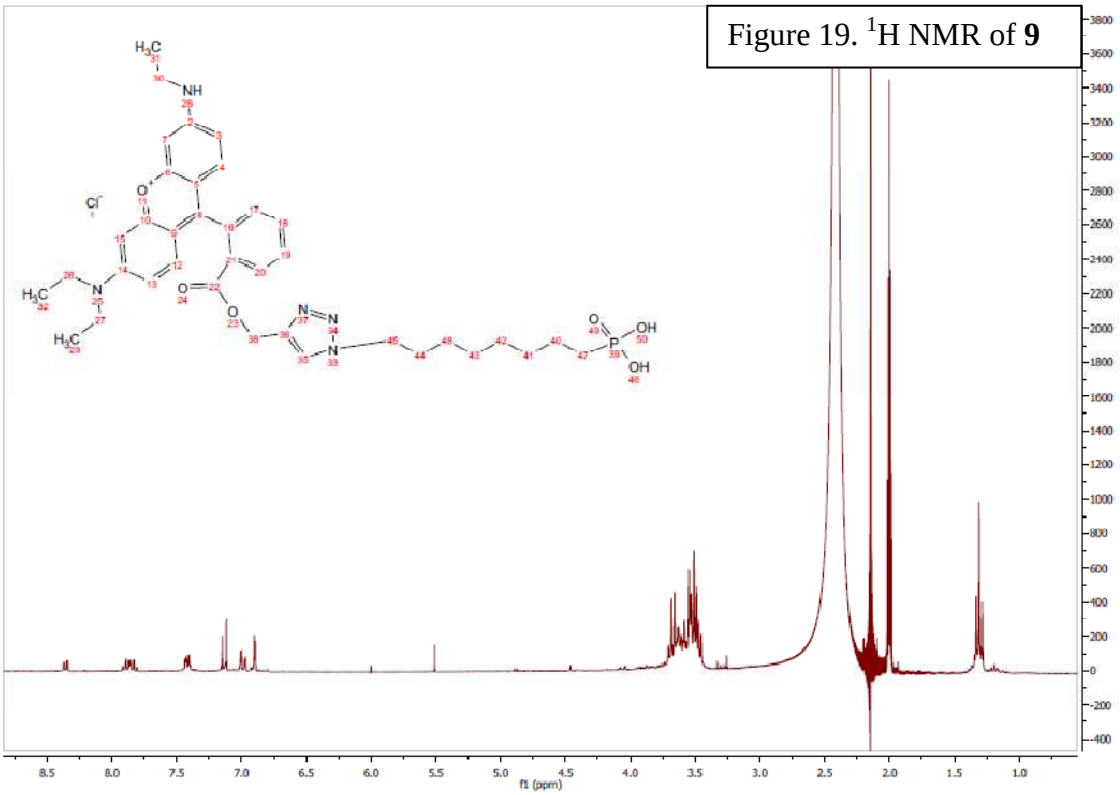

Figure 19. ^{1}H NMR of **9**

Synthesis 2 of 3,6-bis(diethylamino)-9-(2-(((1-(8-phosphonooctyl)-1H-1,2,3-triazol-4-yl)methoxy)carbonyl)phenyl)xanthylium chloride 8b- A mixture of click product **9** was soaked with ITO slides in a 1:1 mixture of *t*-butyl alcohol and acetic acid for 4 h. These slides were then rinsed with ethanol and water and cured at 60C for 4 h before CV analysis of the slide in 20 mM KCl was conducted, and it appeared that the desired compound produced an oxidation peak in the CV analysis.

Chapter 3: Introduction to molecular rotaxanes

3.1 Background

Molecular machines, such as shuttles and sensors, can involve the use of host-guest chemistry that reacts to stimuli such as light, pH, electric potential, and temperature.[3,4,5] When the host molecule is shaped like a ring, it can be locked to a structure containing the guest, sometimes becoming part of a catenane or rotaxane (Figure 20 and 21).[2] A molecular rotaxane is simply a cyclic macrocycle threaded onto a linear axle that stays in place due to supramolecular forces or steric barrier.[2] A subset of rotaxanes, called "psuedo rotaxanes," are less stable and can be temporarily separated in equilibrium, especially by the presence of a competitive binding group; however, a full rotaxane must be physically blocked with a large stopper at both ends of the linear axle.[2] A useful way of forming a rotaxane is by pre-coordinating and capping a psuedorotaxane.[2] Supramolecular chemistry has found increasing application in molecular devices such as molecular sensors and shuttles. An

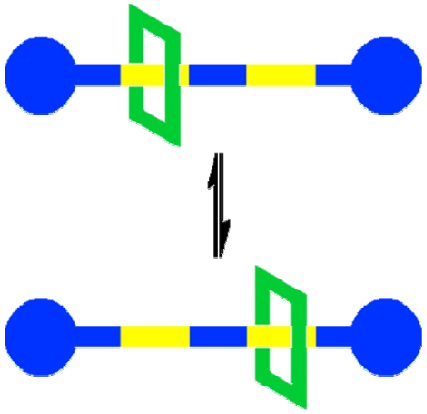

Figure 20. Stoddart Rotaxane[2]

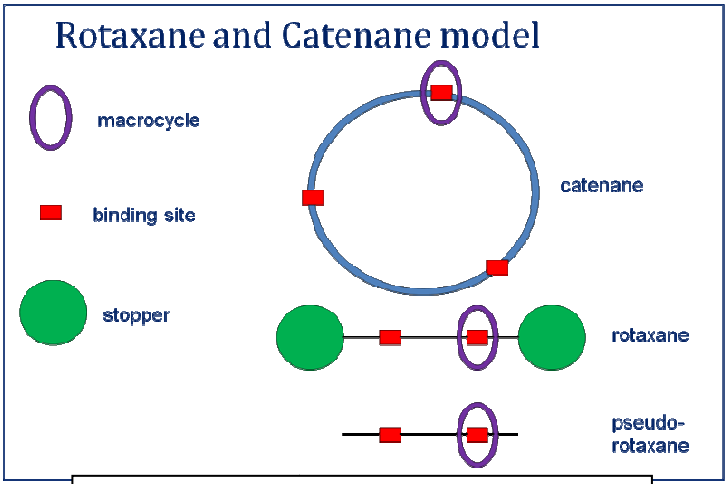

Figure 21. Rotaxane and Catenane model

excellent example of this is in the work of Stoddart et. al. [2] (Figure 21). Stoddart developed a molecular shuttle device of the simplest form in 1991, consisting of two binding sites on an axle, and one molecular ring that could dock from one station to the other through pi-pi interaction through space. The dumbbell construction of the axle prevents the ring from slipping off. The axle is composed of an ethyleneglycol chain, and the docking stations consist of arene groups. The bead is a tetracationic cyclophane that interacts with the two identical stations by weak pi-pi interactions and moves continually between them. Since Stoddart's initial work in the area of molecular shuttles, others[13,14,15] have attempted to improve the versatility of molecular shuttles by composing structures with unique binding sites and rings that are capable of reacting to outside stimuli including light, pH, temperature, and electricity. The study of the exact nature of supramolecular binding is a first step toward the construction of a stimuli-controlled molecular shuttle or sensor. Therefore, kinetic and thermodynamic binding in these types of systems is also an important target for study. Rotaxanes have enormous potential in the application of molecular switches and molecular motors.

Figure 22: Light driven shuttle[13]

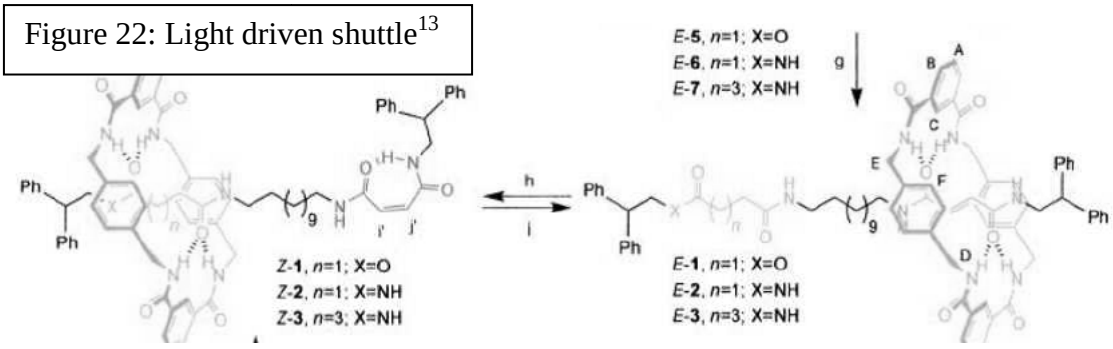

Zerbetto et. al. developed a switchable rotaxane that contained two binding sites as pictured[13] (Figure 22). The macrocycle contains amide moieties that form hydrogen bonds to ester and amide functionalities on the axle. One of the binding sites on the

rotaxane was strategically designed to contain two amides that can hydrogen bond to form a seven member ring when the axle is in the *Z* conformation, which stabilizes the system when the macrocycle occupies the other binding site. When the axle is thermally converted to the *E* conformation, the seven member ring is disrupted, and the macromolecule can shuttle to bind at that site. This process is reversible with light which converts the axle back to the *Z* conformation. Another example of a switchable shuttle consists of crown ether macrocycle that has the possibility of two binding sites along an axle within a stoppered system.[14] (Figure 23) The shuttling action is pH controlled, and one of the binding sites is a secondary amine and the other is a viologen. Initially, the macrocycle resides with the protonated amine, but upon deprotonation with a non-nucleophilic base, the macrocycle prefers to bind with viologen. This chemically controlled shuttle system is completely reversible by the addition of acid. The third example of a molecular switch uses redox control to switch from a Cu I complex to a Cu II complex[15] (Figure 24). Copper I prefers a low coordination number such as four, while Cu II prefers a higher coordination number such as five or six. The macrocycle is pre-equipped with two binding sites suitable to the coordination with copper, while the axle contains the complementary binding sites that are strategically chosen for each

Figure 23: Acid Base controlled shuttle[14]

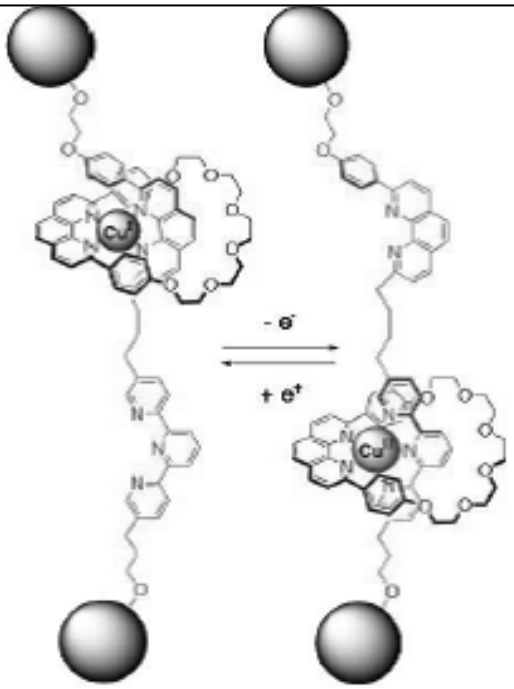

oxidation state of copper, by creating the necessary geometry and coordination number.

Figure 24: Redox controlled shuttle[15]

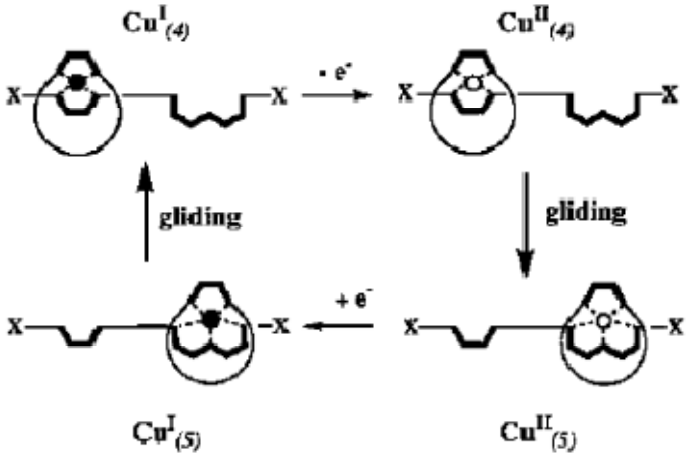

Upon reversible reduction or oxidation, the copper complex can switch from one stable complex and docking site to another (Figure 24).

To date, only two full rotaxanes containing CB[7] have been constructed and studied,[16] leaving many questions as to the nature of this macrocycle. CB[7] has become the focus of our group as a host molecule for molecular machine construction. Due to its larger cavity size, CB[7] can bind a wider range of guests than CB[6] and CB[5][1], also, it has better water solubility than CB[6] and CB[8][1], which is important to any application of CB[7] to molecular machines. CB[7] binds particularly well with ammonium and viologen species, whose size, shape, and electronic properties are ideally suited for the cavity. Viologens themselves are of particular interest to the construction of molecular machines due to their unique binding and redox properties. For example, a one-electron reduction of the viologen guest results in a two-fold decrease of the binding constant with CB[7].[17] This type of switching could easily be envisioned to be useful in the construction of a molecular shuttle, but redox applications of this molecule have had limited success due to the tendency of viologen to undergo diligamerization, a problem that would potentially be solved with CB[7].

In order to form a full rotaxane of viologen with CB[7], it will need to be precoordinated and capped. The binding position, or mode, of CB[7] with the viologen then becomes an important consideration in order to acheive successful capping. In general, viologens are unique in the way that they bind with CB[7] in that they have two possible modes of binding. If the viologen has hydrophobic groups that are at least four carbons long, CB[7] will prefer to bind in an external position, with the cavity of CB[7] enclosing the hydrophobic group, and the electronegative portals of CB[7] lining up with the nearby electropositive portion of the viologen.[18] Otherwise, CB[7] will bind with an internal mode (Figure 21).[18] Perhaps this schizophrenia between modes of binding is due in part to the imperfect alignment of the portals of CB[7] (6 angstroms) with both cationic sites of the viologen (7 angstroms), weakening the supramolecular interactions and allowing competition between internal and external binding modes.

Figure 25: Binding modes of CB[7][18]

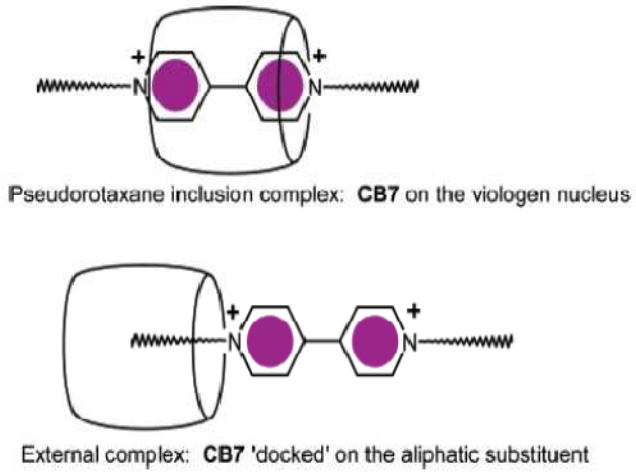

Full rotaxanes are desirable targets particularly for in vivo, surface-attached, and flow through systems. However, the synthesis of some molecular systems (sensors, shuttles, or surface-attached tethering systems) may be difficult to achieve with CB[7] due to its hydrophilic nature, which could hinder crucial steps of a total synthesis of a complex macromolecule. Therefore, the development of stoppering groups, reaction

conditions, and synthetic strategies that address these concerns is an important area of study concerning molecular machines containing CB[7].

3.2 Specific Aims

In this chapter, two stoppers will be investigated as to their ability to sterically block CB[7] and also their ability to induce internal binding modes. Then the stoppers will be investigated as to their synthetic utility in forming a rotaxane. The particular stoppers proposed are 3,5-dimethylbenzyldipridinium dibromide **10** and 3,5-dimethoxybenzyldipridinium dibromide **11** (Figure 26). The first stopper attempts to use just enough steric hindrance to block CB]7], while the second uses a combination of steric hindrance and electronics. If one of these compounds is determined to be a good stopper, that stopper will again be used in an attempt to form a permanent full rotaxane.

Figure 26. Compounds **10** and **11**

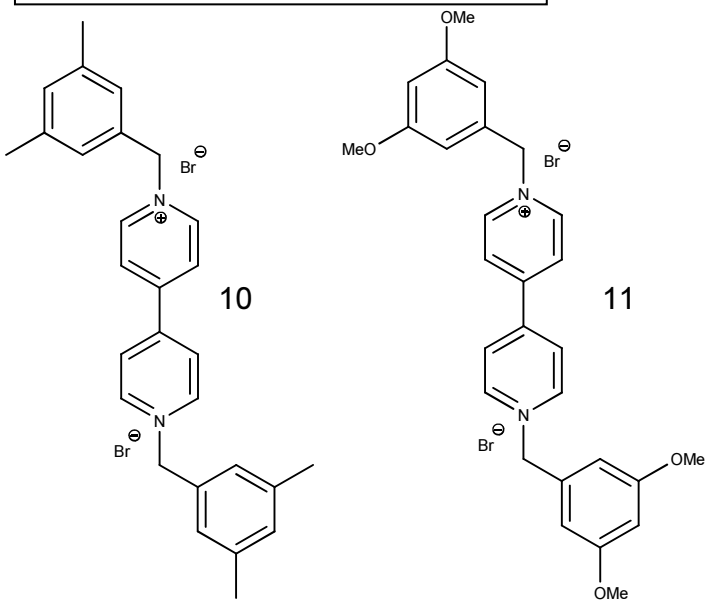

3.3 Synthesis of proposed stoppers

A series of mono-substituted dipyridines were synthesized by substitution, from the starting dipyridine and a series of 3,5-disubstituted benzyl bromides (Figure 27). In all cases, the reactions were conducted in an experimentally optimized organic solvent, allowing the resulting salt to precipitate out upon completion of the reaction, while the starting materials remain in solution. The impure product salt, containing some residual disubstituted side product, could then be triturated on a filter, and further purified by column chromatography or by recrystallization. Compounds **10** and **11** were prepared from mono-substituted starting material **13** and **14**, respectively. A threefold excess of the appropriate 3,5-disubstituted benzyl bromide was added to the starting material and refluxed for two days in acetonitrile (Figure 28).

Figure 27. Synthesis of **12-14**

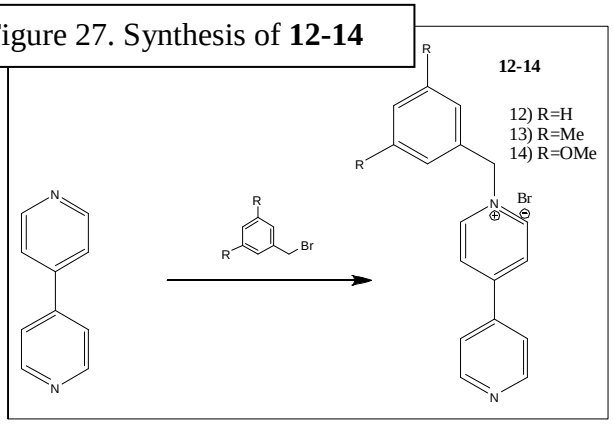

Figure 28. Synthesis of **10** and **11**

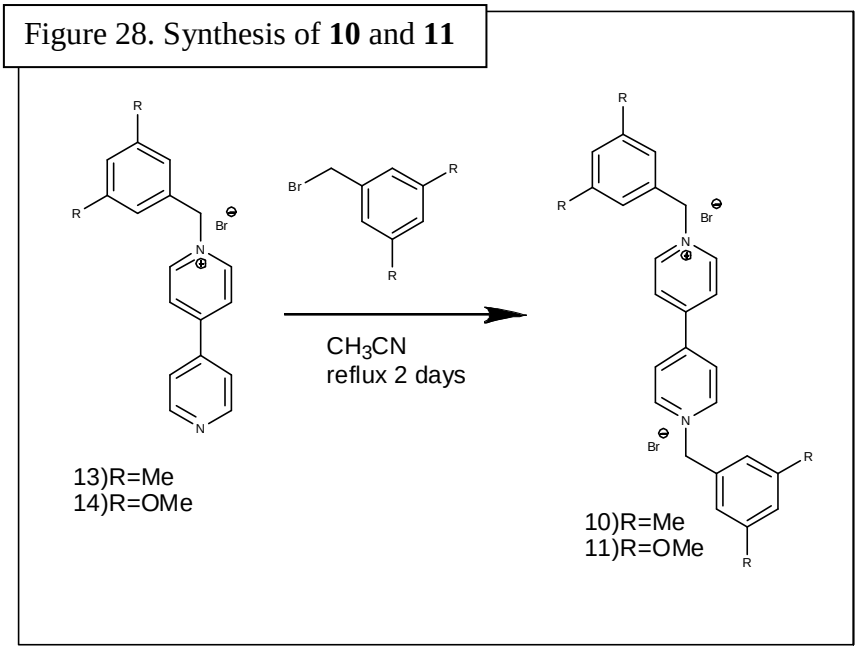

3.4 Determination of stopper effectiveness

The potential surface plots of compound **10** and **11** in combination with 1 equivalent of CB[7] were calculated by Spartan 08 (PM-3 gas-phase).

Figure 29. Spartan model of compound **10**

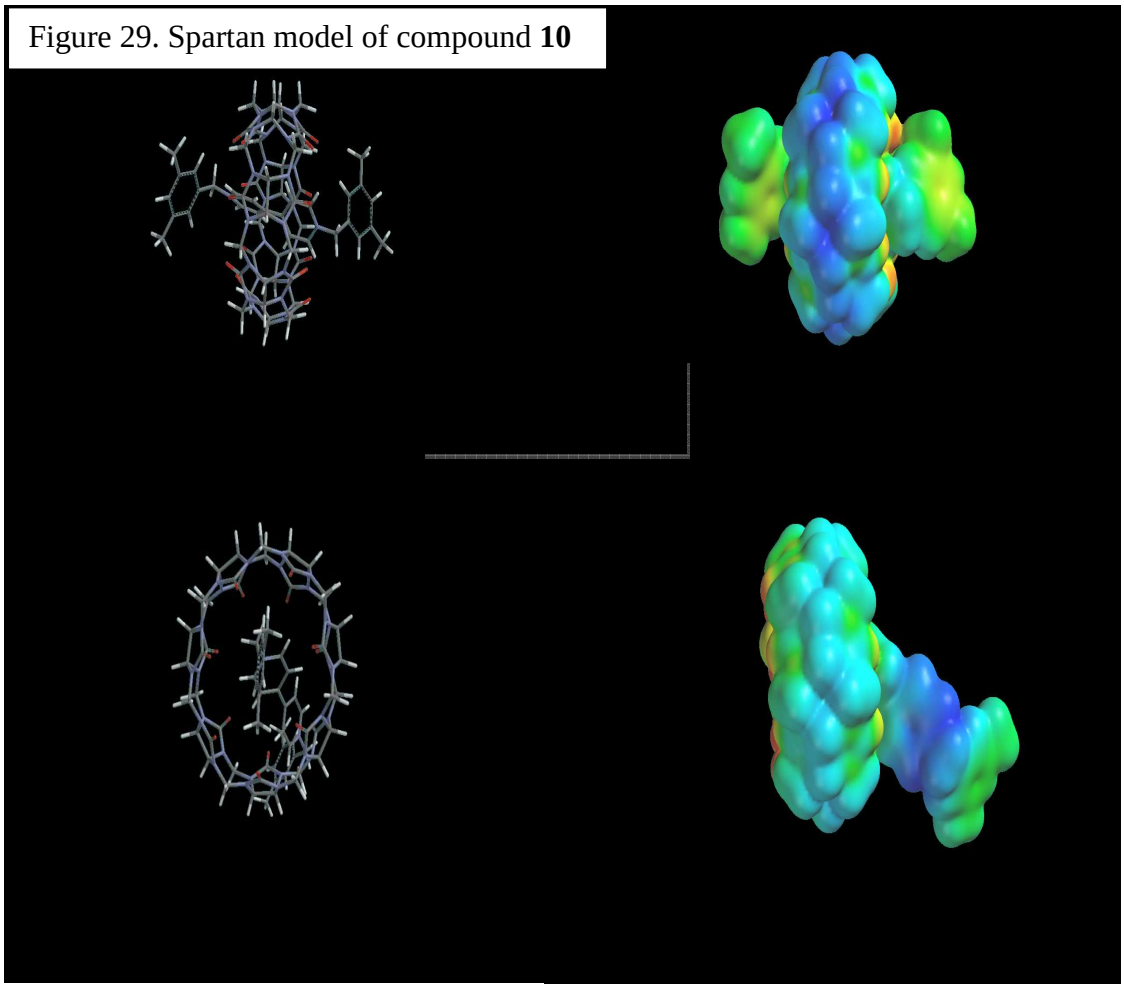

Compound **10** (Figure 29) was initially positioned in a center binding position and a local energy minimum of 2021 kJ/mol was found by PM-3 calculations. Then, cucurbit[7]uril was moved along the axis to an external binding site, and new local minimum of 1918 kJ/mol was found. Compound **11** (Figure 30) was initially positioned in a center binding position and a local energy minimum of 1518 kJ/mol was found by

PM-3 calculations. Then, cucurbit[7]uril was moved along the axis to an external binding site, and new local minimum of 1416 kJ/mol was found. Both rotaxanes showed an overall decrease in energy from the central binding site to the external one. In summary, compound **10** gave a decrease of 24 kJ/mol and Compound **11** gave a decrease of 41 kJ/mol. In both cases, there is no evidence that CB[7] is able to slide off over the stopper, so further study was necessary.

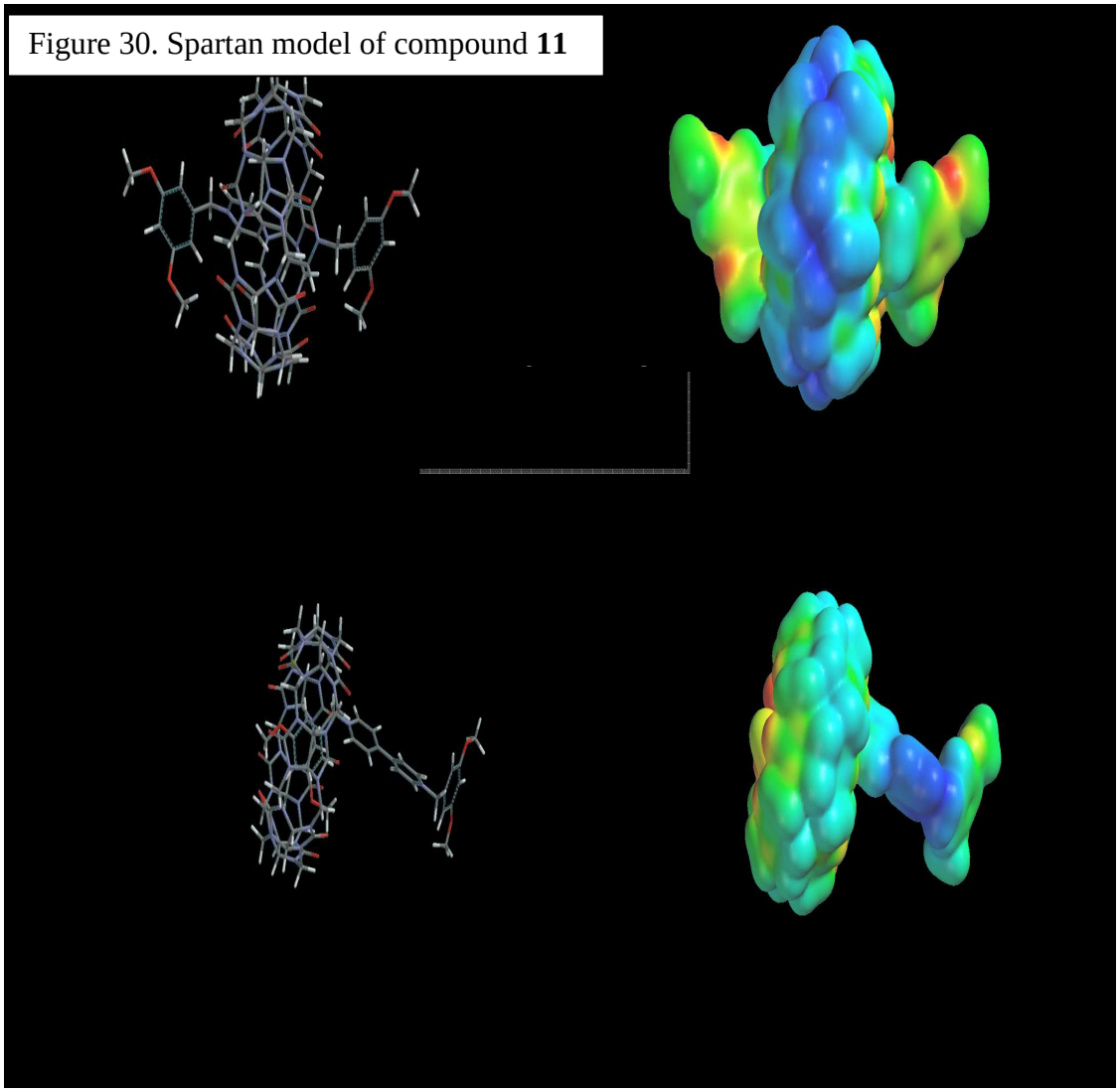

Figure 30. Spartan model of compound **11**

In order to further determine the effectiveness of the stopper, one equivalent of CB[7] was combined with both Compound **10** and Compound **11**. Both compounds showed evidence of a downfield shift of the methyl peaks and no movement of the hydrogens alpha to the nitrogen cations, indicating that, unlike the models above, the 1:1 mixtures were unable to reach their lowest energy because cucurbit[7]uril could not pass over the stopper. This provides strong evidence that the stoppers are effective.

3.5 Preparation of Psuedorotaxanes and determination of binding modes

Products **12-14** were separately combined with one and two equivalents of CB[7] and analyzed by NMR titration in neutral D_2O to determine the mode of binding. The first compound that was analyzed was compound **12**, which was initially combined with CB[7] in a 1:1 mmol solution.The peaks associated with CB[7] in the 1:1 complex can be found at 4.1 ppm, 5.5 ppm, and 5.8 ppm, which are the 14 outer methylene protons, the 14 methyne protons, and the 14 inner methylene protons, respectively. In the 1:1 complex, 1-benzyl-4-(pyridin-4-yl)pyridinium bromide **12** showed three major upfield shifts of greater than 0.5 ppm from its unbound state as these protons were shielded by encapsulation of CB[7]. The NMR shifts representing the protons of the aromatic ring showed the largest displacement, moving from a tight cluster at 7.45 ppm to a broadened group of three peaks with an average of 6.80 ppm (Figure 31). This broadening indicates fast exchange on the NMR time scale between either bonded or nonbonded CB[7] with compound **12**. The NMR shifts of the methylene protons of the benzyl group shifted upfield from 5.80 to 5.2 ppm, and the NMR shifts of the dipyridyl protons alpha to the benzyl group shifted upfield from 9.20 to 8.70. The identification of the shift values was aided by a full titration of compound **9** with CB[7], in which the

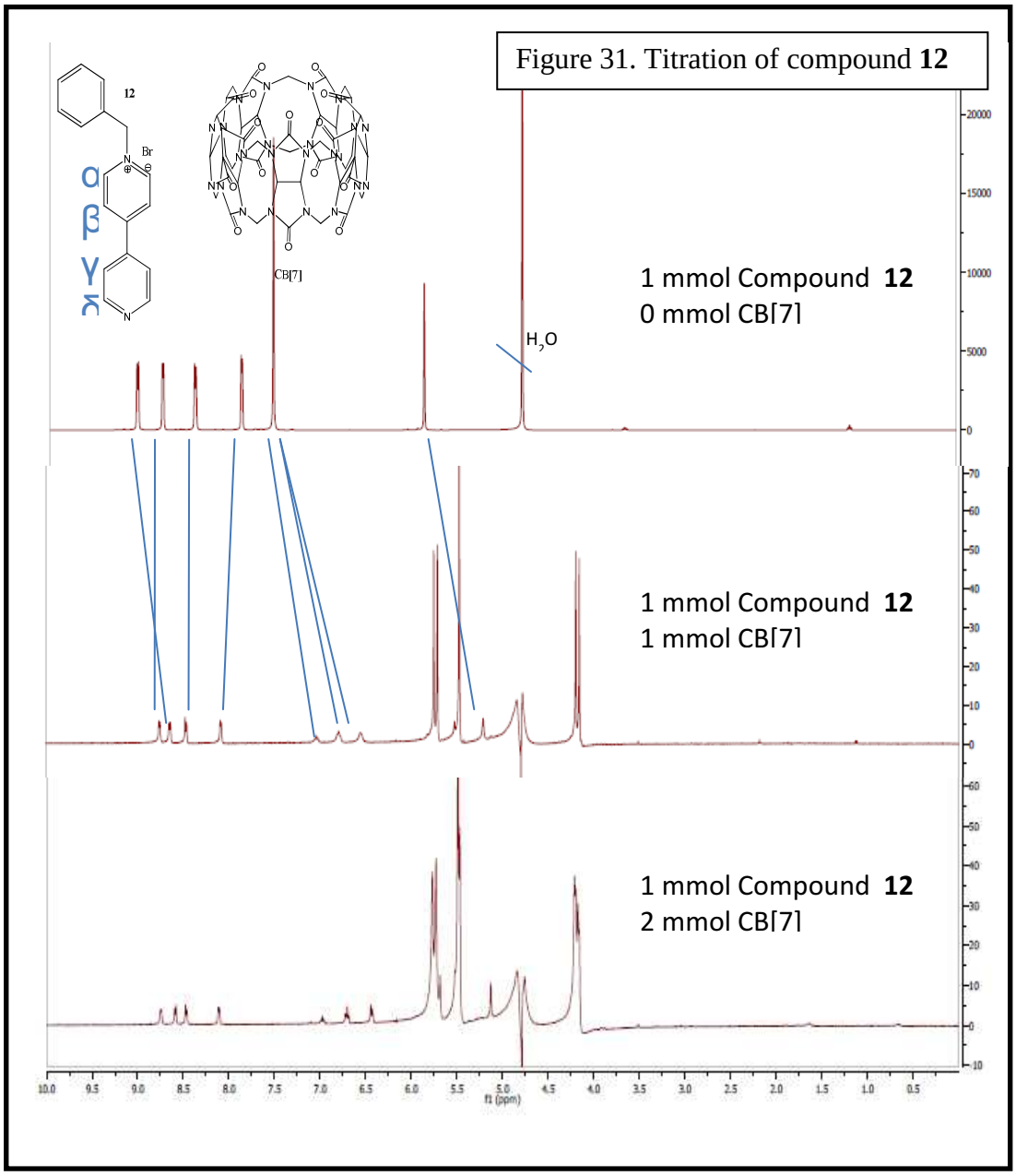

Figure 31. Titration of compound **12**

addition of CB[7] gave broad NMR shifts that were the weighted average of bound and unbound axle, indicating fast exchange of CB[7] with all molecules of the axle. When these observations and individual shift changes are considered together, they suggest an external mode of binding of CB[7] with compound **12**, in which the macromolecule encapsulates the entire benzyl group and the alpha protons of the dipyridyl group

(Figure 32). This is consistent with the literature findings[18] that external binding modes occur in dipyridyl compounds when the length of the carbon chain is greater than four.

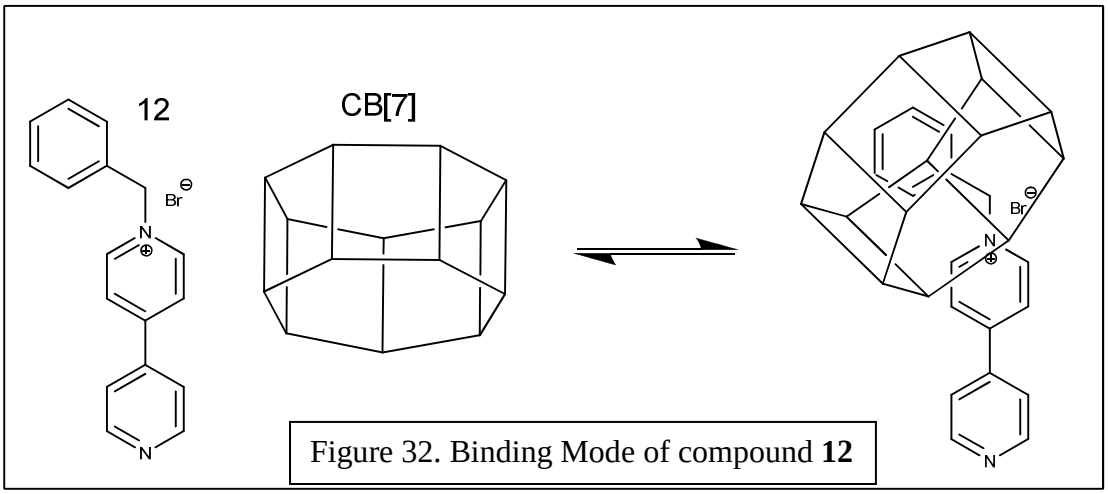

Figure 32. Binding Mode of compound **12**

In this particular case, the possibility of an internal binding is disfavored in comparison, maybe due to repulsion of the uncharged nitrogen of compound **12** with the oxygens in the carbonyls of CB[7]. Importantly, when a second equivalent of CB[7] is added, the chemical shifts of compound **12** do not shift further, indicating that 2:1 binding modes do not exist. This conclusion is also supported by the fact that 2:1 concentration NMRs show the chemical shifts expected for unbound CB[7], shifts not seen in 1:1 concentration ^{1}H NMRs. This decisively shows the presence of unbound CB[7] in 2:1 concentration, likely due to the fact that the carbonyl groups of two CB[7]s would be electronically repulsive in close proximity, and so being a relatively short axle, will not allow two equivalents to be associated with it.

Compound **14** (Figure 33) was also studied by a titration of CB[7] in increasing concentration, beginning with the 1:1 binding ^{1}H NMR of CB[7] with compound **14**.

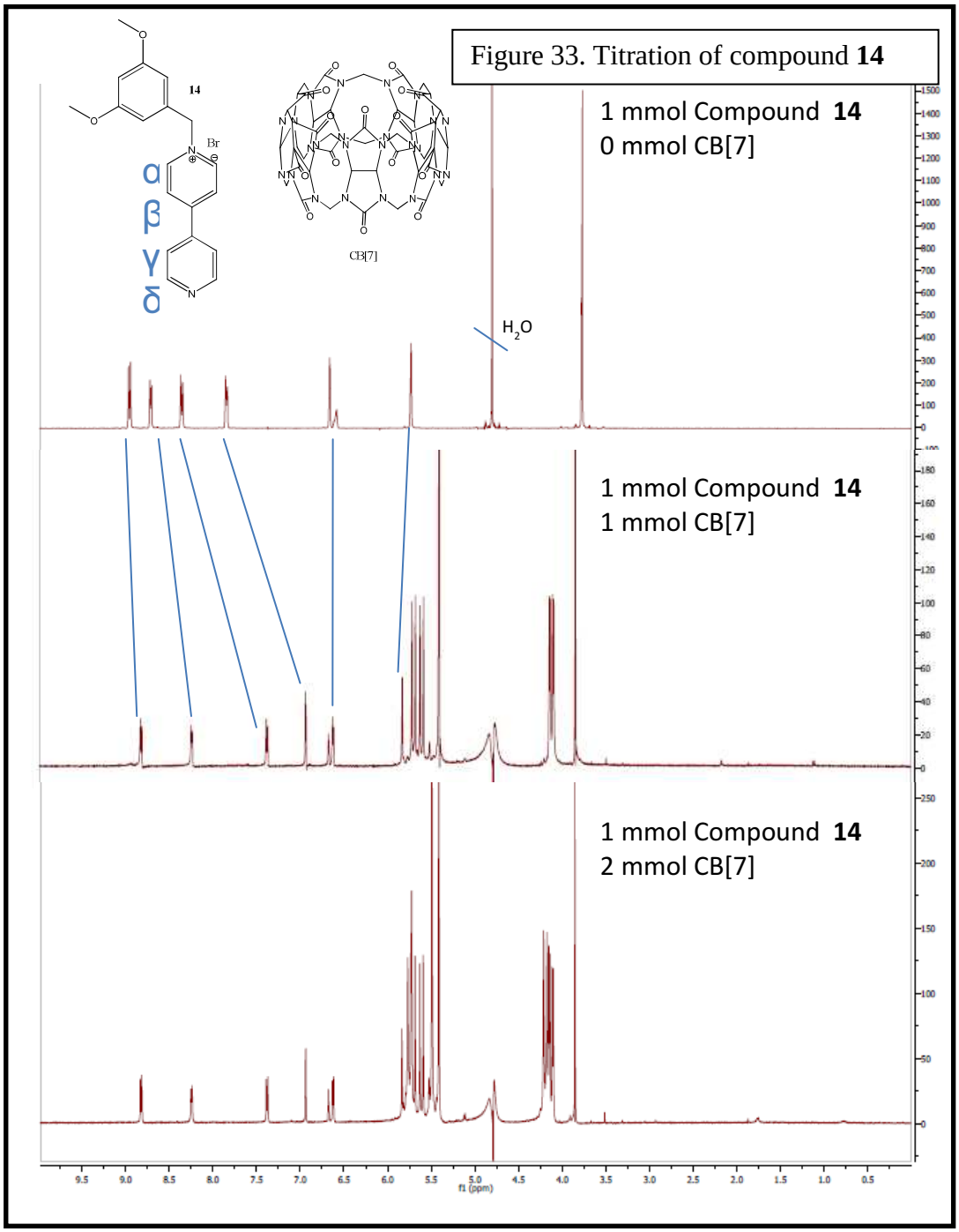

The peaks associated with compound **14** remained sharp in general and do not display averaging as CB[7] is titrated into solution, indicating an overall slow exchange on the NMR time scale. This is supported by the splitting pattern of the inner methylene protons of CB[7] as it appears at 5.6 ppm. When CB[7] is unbound, its inner methylene

protons experience essentially the same average electronic environment on the ^{1}H NMR time scale. However, in the 1:1 binding ^{1}H NMR spectra, the inner methylene protons give a signal of two doublets which have an integration of seven protons each. This supports the idea that the top inner methylene protons are experiencing a different electronic environment than the bottom inner methylene protons, and therefore are encapsulating the axle in some way that causes visibly different ^{1}H NMR shifts. Turning our attention to the ^{1}H NMR shifts of the axle, the methoxy proton ^{1}H NMR shifts in particular remain largely unchanged, moving slightly downfield to 3.8 ppm, suggesting that the methoxy groups do not play a large role in the supramolecular interactions with CB[7]. The methylene protons, the benzene protons, the beta protons of the dipyridyl group, and the alpha protons also show little movement, moving slightly downfield to 5.8, 6.6, and slightly upfield to 8.25 and 8.8 ppm, respectively. The proton NMR signal on the axle that experienced the greatest shift upon binding to the axle was by far the delta proton of the dipyridyl moity (from 8.7 to 7.4) and the gamma proton (from 7.8 to 6.9). These large upfield shifts indicate encapsulation by CB[7], suggesting an internal binding mode (Figure 34). This internal binding could be

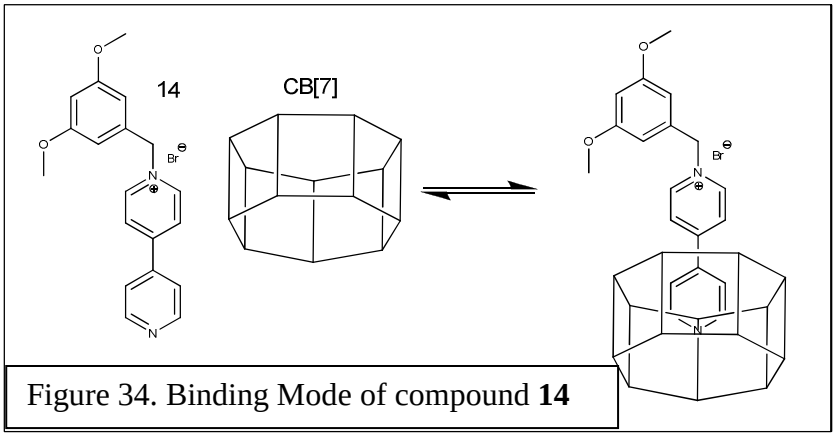

Figure 34. Binding Mode of compound **14**

strongly favored as opposed to external binding due to the steric bulkiness of the methoxy groups in combination with the electronic repulsion of the electronegative oxygens of the methoxy groups with the electronegative portals of CB[7]. Notably, the CB[7] group does not thread very far onto the dipiridyl axle despite the lack of steric opposition, possibly due to the positively charged nitrogen preferring an aqueous environment for stabilization and so avoiding the lipophilic cavity of CB[7]. When the possibility of the axle **14** binding with two equivalents of CB[7] was considered and tested, the first observation was that the NMR shifts of the axle did not change. New peaks were observed whose shifts were consistent with free CB[7], which led to the conclusion that 2:1 binding of CB[7] with the axle **14** did not occur.

The analysis of compound **13** is more speculative than the analysis of compounds **12** and **14** due to the complicated overlapping of the NMR spectra, but it is still possible to garner important information from the analysis of a 1:1 mixture of CB[7] and compound **13** (Figure 35). First, the vast majority of the peaks are broad, indicating intermediate exchange on the ^{1}H NMR time scale. Notably, one peak remains sharp at 9.0 ppm, which corresponds to the alpha proton of compound **13**. This indicates a lack of interaction with CB[7] during the binding event. As labeled in Figure 36, I have speculated an additional peak corresponding to the alpha proton at 8.7 ppm, which could indicate a small percentage of the alpha protons in solution are shielded by CB[7] at any one time. The most interesting feature of the 1:1 mixture of CB[7] and compound **10** are the peaks associated with the methyl protons of the benzyl ring. Before the addition of CB[7], the methyl groups share an ^{1}H NMR shift at 2.3, but

after the addition of one equivalent, they split into two broad peaks at 1.7 and 2.4 ppm, indicating unique electronic environments. The upfield shift to 1.7 ppm indicates

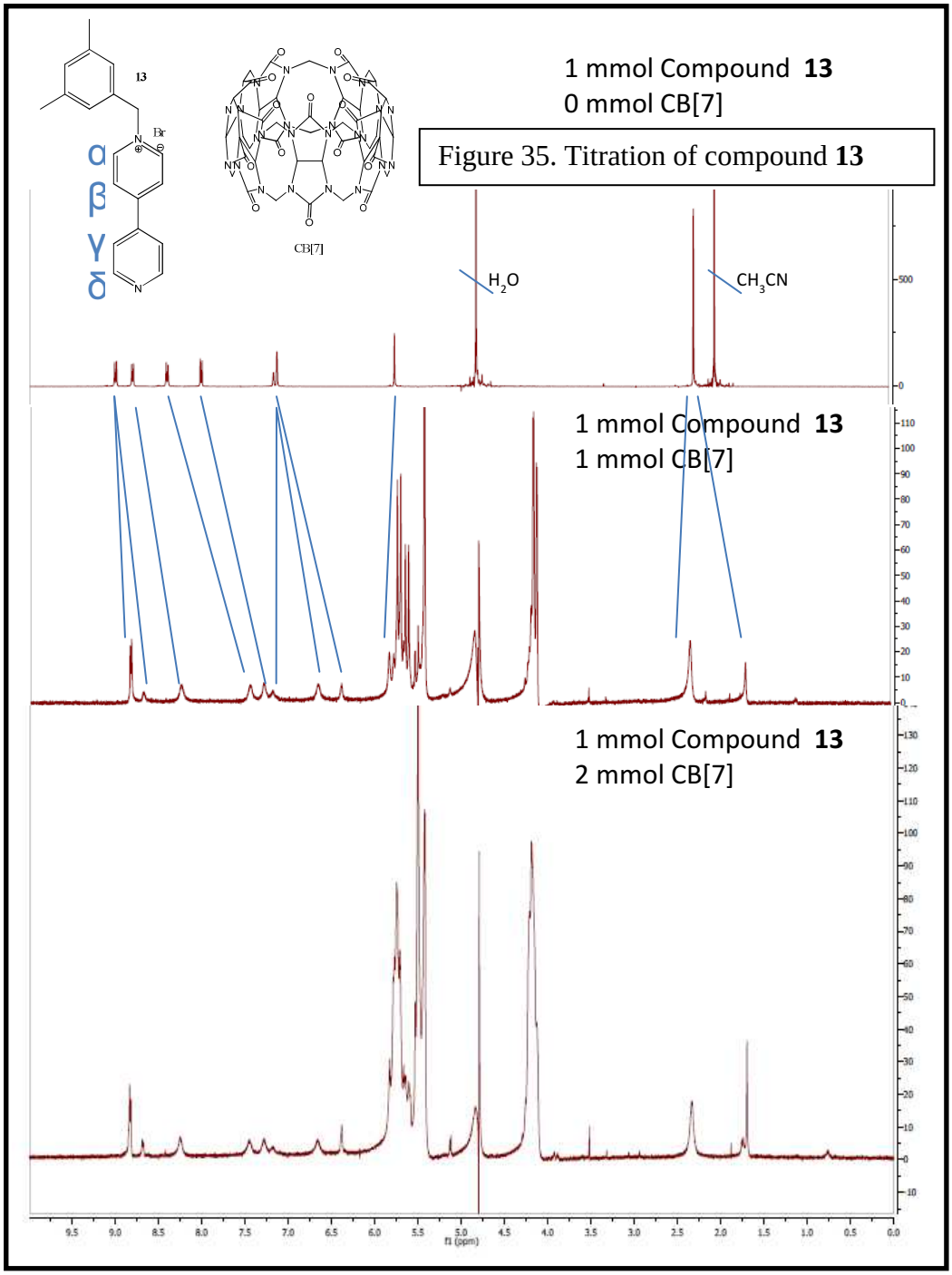

Figure 35. Titration of compound **13**

that one of the methyl groups is encapsulated inside CB[7], while the other methyl group is outside or right along the portals of CB[7]. The encapsulation of the 2,4-dimethyl benzyl group is also supported by the shifts of the benzyl protons from a cluster at 7.1 ppm to individual broader peaks at 7.2, 6.7, and 6.4. It is unclear exactly where CB[7] sits in relation to axle **13**, in particular if the 2,4-dimethyl benzyl group is acting as a stopper as postulated, the CB[7] could either be located in a capping position centered around one of the methyl groups, or the CB[7] could be threaded onto axle **13** in so called external binding, similar to its position when combined with axle **12**, but frustrated by the stoppering of the bulky dimethylbenzene. The former description seems more plausible considering the lack of shift of the alpha proton. In contrast to compounds **12** and **14**, there is more than one binding site, this time in the internal position similar to compound **14**. This is evidenced by the downfield shifts of the beta, gamma, and delta protons (from 8.7, 7.7 and 8.2 ppm to 8.3, 7.3 and 7.2, respectively). The proposed binding modes of axle **13** can be found in Figure 36. In addition, when 2:1 concentrations of CB[7] and axle **13** are combined, the shifts associated with CB[7] do not indicate the presence of unbound CB[7], but rather suggest that all molecules of CB[7] are taking turns interacting with the axle **13**. Also, the complex still appears to have a 1:1 ratio of axle **13** and CB[7] at any one time, due to a lack of new chemical shifts. This occurs despite the presence of two possible binding sites, indicating steric and electronic interactions between the oxygens along the portals of CB[7] do not allow the 2:1 complex. Finally, sharper peaks at 1.7, 6.3, and 8.7 ppm suggest faster exchange occurring on the NMR time scale, due to an increase in concentration of CB[7].

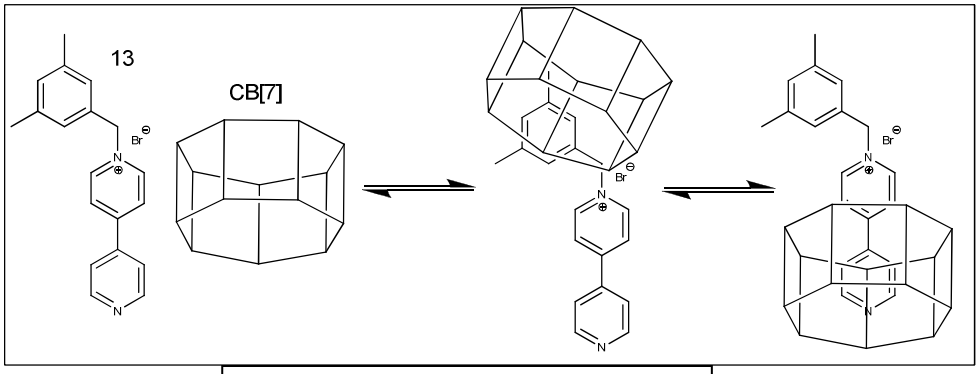

Figure 36. Binding Mode **13**

3.6 Efforts to produce a rotaxane from Compound 13

The synthesis of a tight viologen rotaxane with CB[7] was attempted by reflux in a 1:1 solution of acetonitrile and water. However, no expected product was formed. This could be due to the insolubility of 3,5-dimethylbenzyl bromide in this solvent , as well as due to the binding mode of CB[7] along the rotaxane. According to some of the predicted binding modes in Figure 36, CB[7] could be either surrounding the nucleophile, or is binding on the outside of the stopper, causing the reaction to occur without incorporation of CB[7].

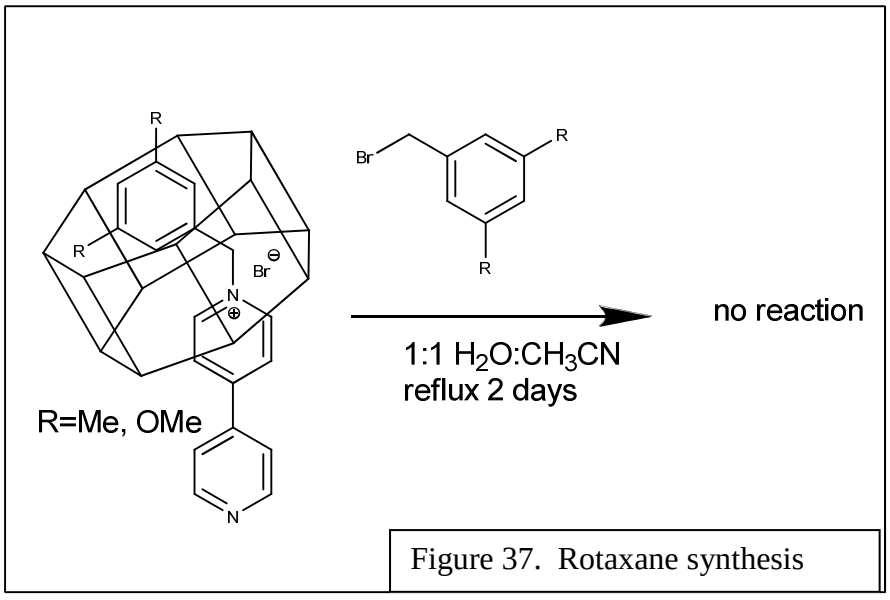

Figure 37. Rotaxane synthesis

The desirable initial binding mode depicted in Figure 37 was probably never achieved. It is possible that the second binding mode depicted in Figure 36 could be prevented by incorporation of a triethylene glycol group on the open end of the axle. The hydrophilicity of this group would certainly help the solubility of the axle in water prior to the reaction. It may also repel the encapsulation by CB[7], which would help to favor the binding mode in Figure 37. This type of structure will be further explored in Chapter 4. If a structure with a desirable binding mode can be found, a synthesis could potentially be designed to cap the pseudorotaxane at the end of a functionalized triethylene glycol group.

3.8 Experimental

1-benzyl-4-(pyridin-4-yl)pyridinium bromide 12- 4,4-bipyridine (2.00 g, 13 mmol) and benzyl bromide (10 mmol) were dissolved in dry acetone under nitrogen at 70C and the solution was stirred for 1 h. A yellow precipitate was then collected on a filter and washed with ether. The remaining solid was recrystallized in ethanol and ether overnight. The pure crystals were collected on a filter to give (0.42 g, 1.3 mmol, 13%) ^{1}H NMR (400 MHz, D_2O): 8.88 (d, *J*=6Hz, 2H), 8.25 (d, *J*=6Hz, 2H), 7.74 (d, *J*=6Hz, 2H), 7.38 (d, *J*=6Hz, 2H), 5.72 (s, 5H), 4.65 (s, 2H). ^{13}C NMR (400 MHz, D_2O): 153.66, 149.79, 144.61, 142.00, 132.42, 129.87, 129.47, 128.99, 125.85, 122.25, 64.09.

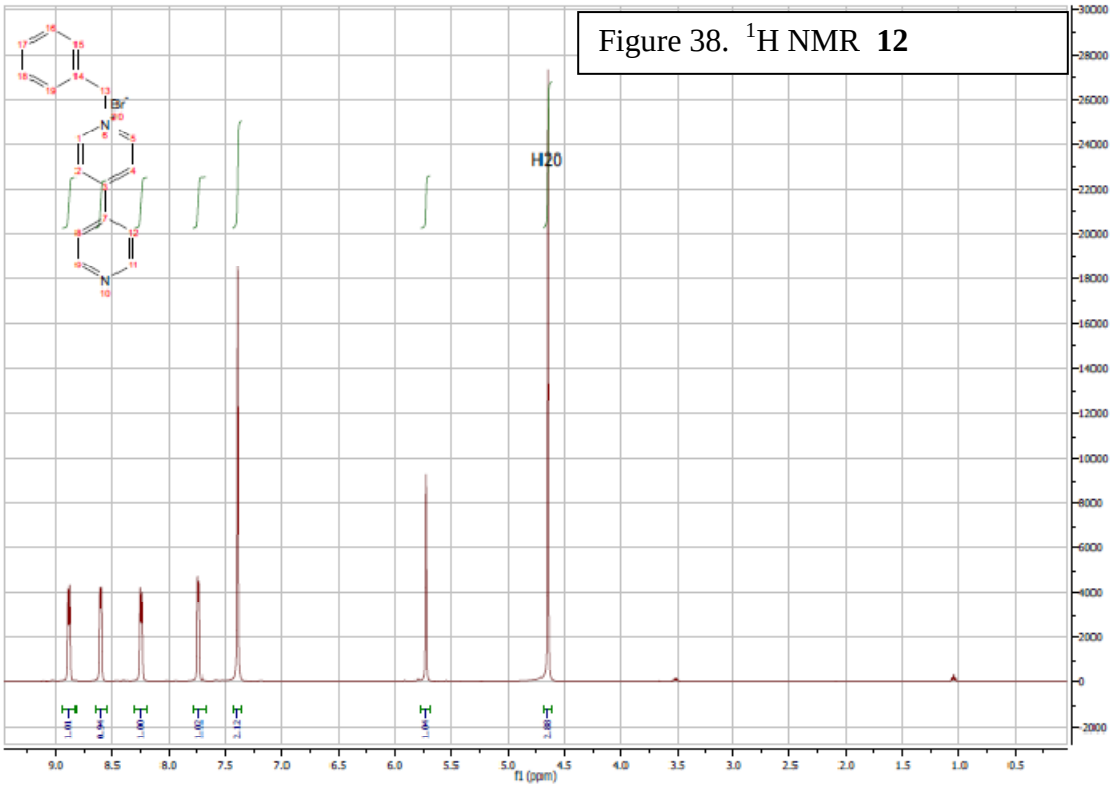

Figure 38. ^{1}H NMR **12**

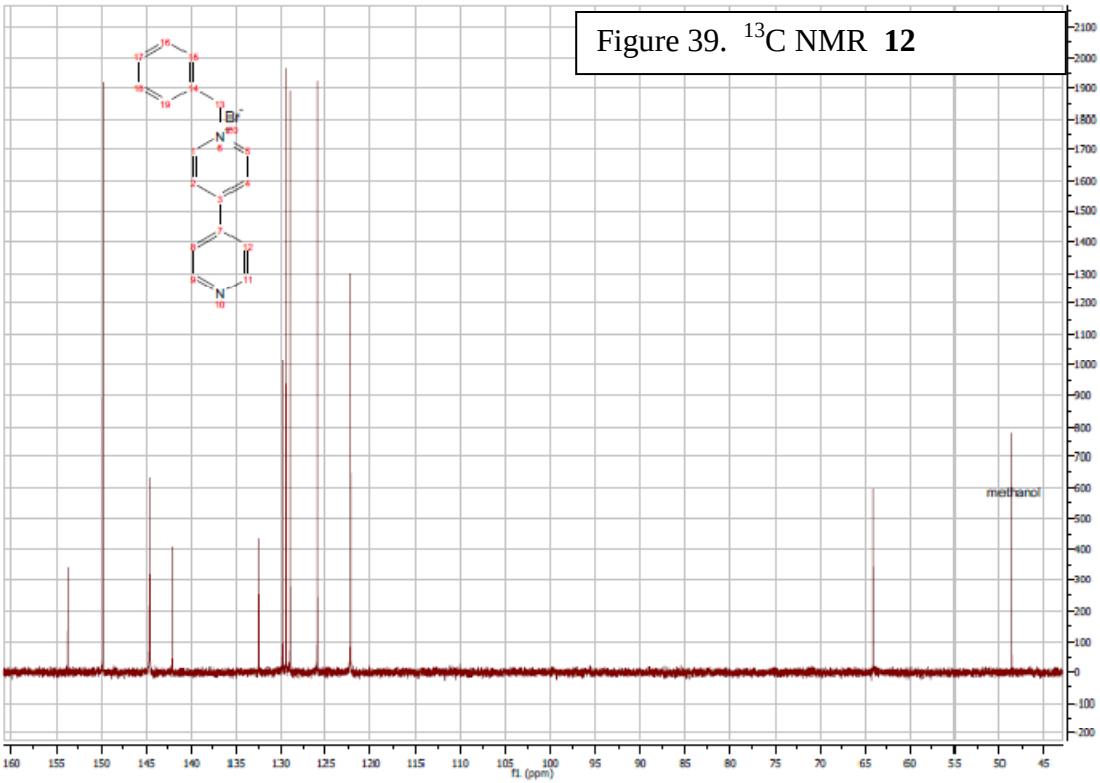

Figure 39. ^{13}C NMR **12**

1-(3,5-dimethylbenzyl)-4-(pyridin-4-yl)pyridinium 13- 4,4-bipyridine (1.02 g, 6.5 mmol) and 3,5-dimethylbenzyl bromide (5 mmol) were dissolved in 50 mL dry acetone under nitrogen. The temperature was raised to 85C and the solution was stirred for 1 h. After cooling, the solvent was evaporated down to 10 mL and a yellow precipitate was then collected on a filter and washed with ether. The crude mixture was purified by silica gel column of 8:1:1 methanol:methylene chloride: acetic acid. The column yielded pure yellow solid (0.37 g, 1.1 mmol, 21%) ^{1}H NMR (300 MHz, D_2O): 8.90 (m, 2H), 8.70 (m, 2H), 8.31 (m, 2H), 7.89 (m, 2H), 7.10 (s, 1H), 7.03 (s, 2H), 5.67 (s, 6H)

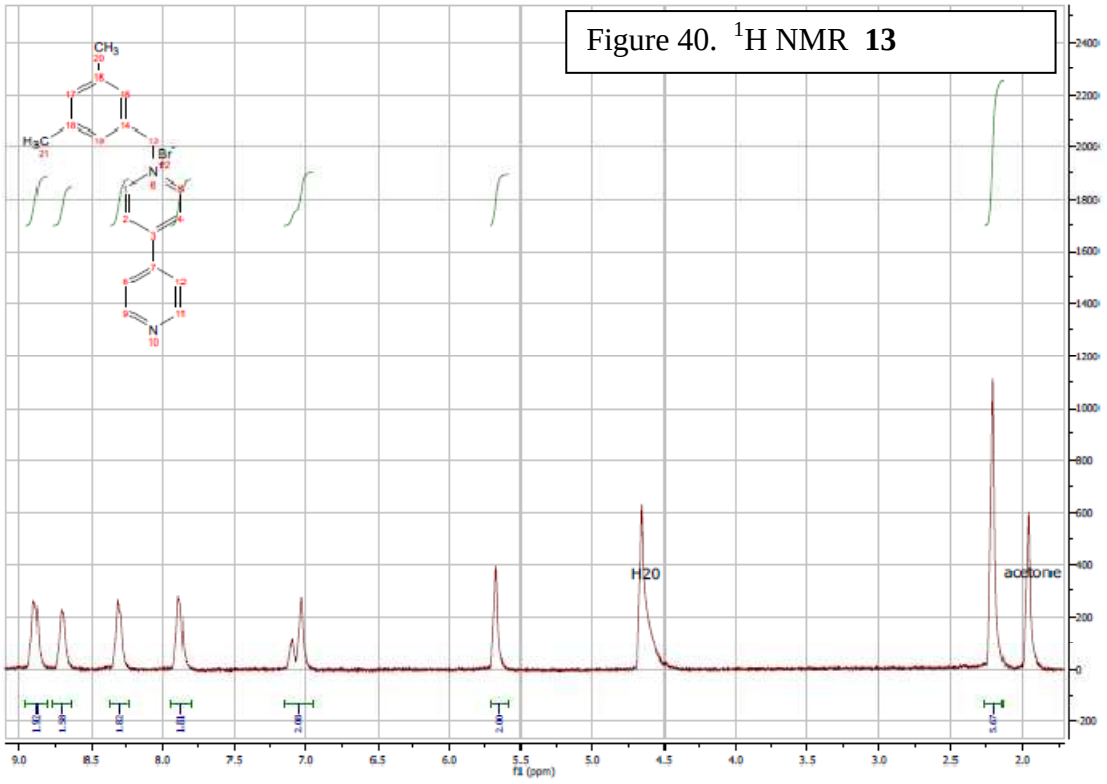

Figure 40. ^{1}H NMR **13**

1-(3,5-dimethoxybenzyl)-4-(pyridin-4-yl)pyridinium 14- 4,4-bipyridine (1.02, 2.2 mmol) combined with 3,5-dimethoxy benzyl bromide (1.3 g, 8.4 mmol) and 70 mL of acetone. The reaction mixture was flushed with nitrogen, and allowed to reflux for 1 h.

The resulting crude mixture was cooled and evaporated to 10 mL. The resulting precipitate was collected in a filter and purified by column chromatography (1:10:90 glacial acetic acid:methanol:methylene chloride) to give a yellow solid. (1.1 mmol, 21%) ^{1}H NMR (300 MHz, D_2O): 8.87 (d, *J*=7Hz, 2H), 8.63 (d, *J*=7Hz, 2H), 8.27 (d, *J*=7Hz, 2H), 7.75 (d, *J*=7Hz, 2H), 6.58 (s, 2H), 6.50 (s, 1H), 5.64 (s, 2H), 3.68 (s, 6H). ^{13}C NMR (400 MHz, D_2O): 160.84, 160.50, 149.81, 144.85, 144.57, 134.59, 125.92, 122.29, 107.38, 101.24, 63.84, 55.42. HRMS (ESI): *m/z*307.1451 $[M]^+$, ($M=C_{26}H_{33}N_2O_3^+$ requires 307.1441).

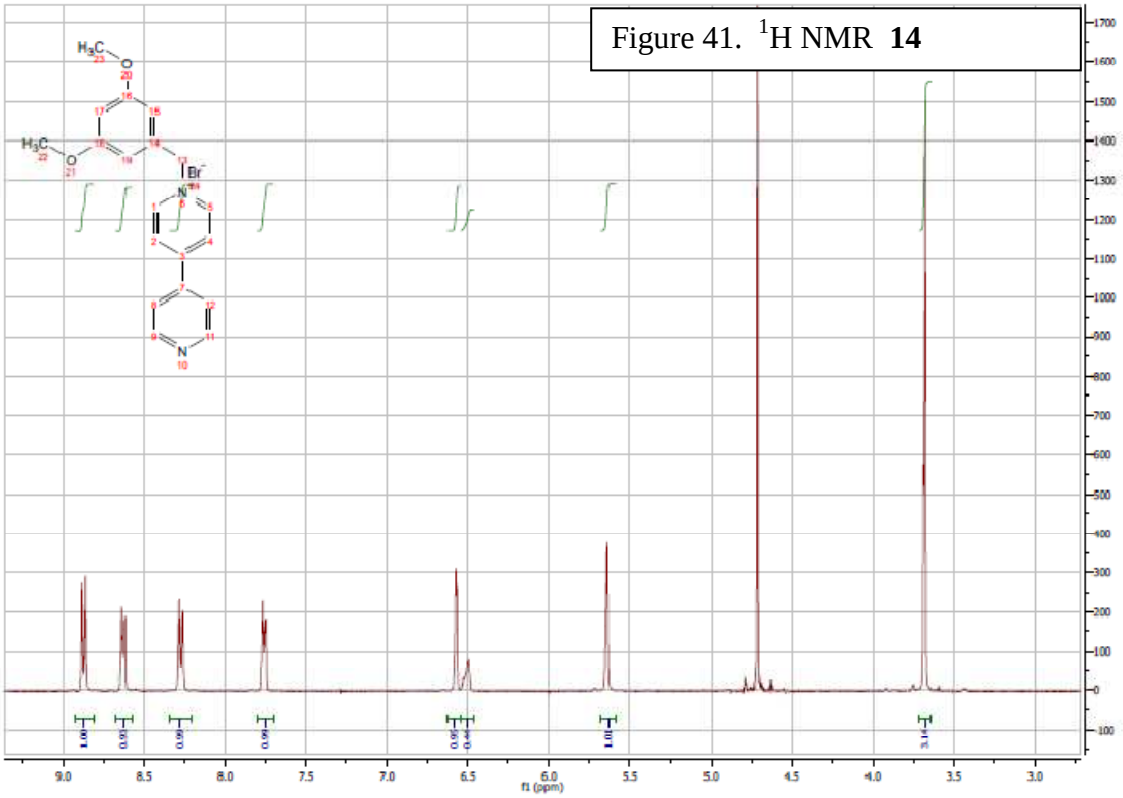

Figure 41. ^{1}H NMR **14**

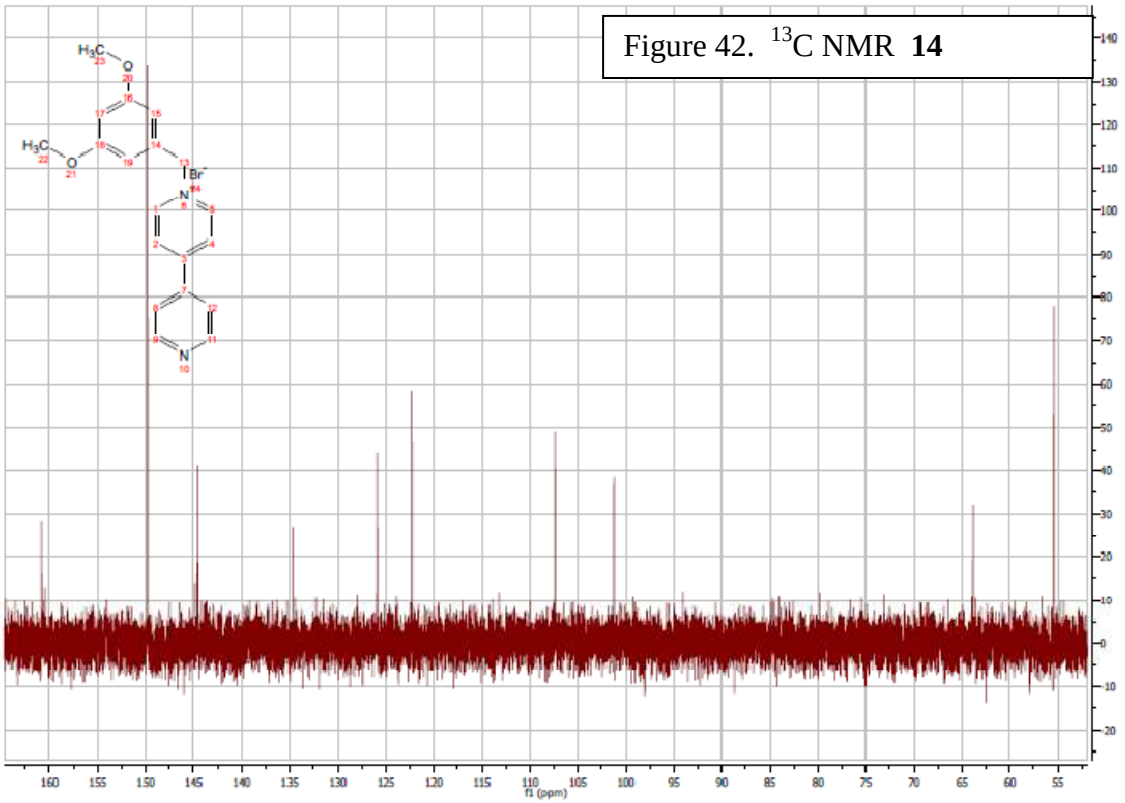

Figure 42. ^{13}C NMR **14**

1,1'-bis(3,5-dimethylbenzyl)-4,4'-bipyridine-1,1'-diium bromide 10- (3,5-dimethylbenzyl)-4-(pyridin-4-yl)pyridinium (0.18 g, 0.52 mmol) and 3,5-dimethylbenzyl bromide (1.6 mmol) were dissolved in dry acetonitrile under nitrogen and heated to 85C for 2 d. The mixture was allowed to cool, and an orange precipitate was then collected on a filter and washed with acetonitrile and ether. The remaining solid was recrystallized in ethanol. The pure crystals were collected on a filter to give (0.14 g, 0.3 mmol, 48%) ^{1}H NMR (300 MHz, D_2O): 9.01 (d, *J*=8Hz, 4H), 8.41 (d, *J*=8Hz, 4H),7.11 (m, 2H), 7.05 (m, 4H), 5.73 (s, 4H), 2.21 (s, 12H).

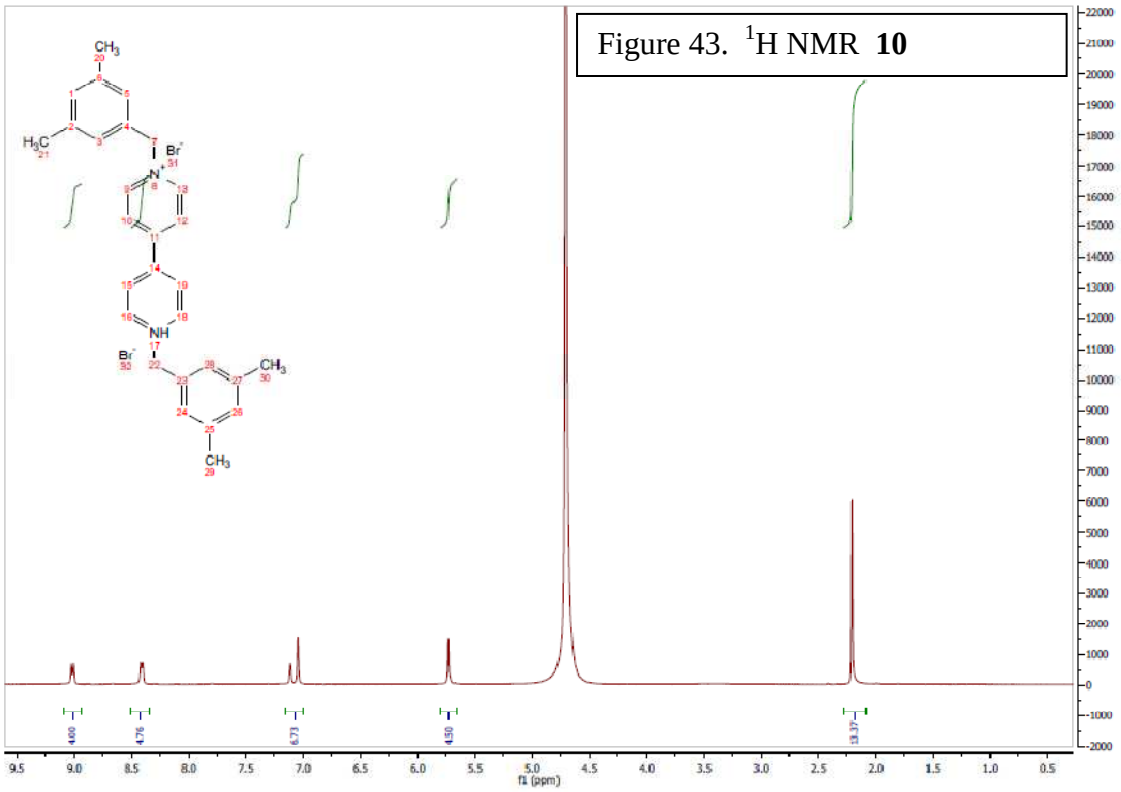

Figure 43. ^{1}H NMR **10**

1,1'-bis(3,5-dimethoxybenzyl)-4,4'-bipyridine-1,1'-diium bromide-11 (3,5-dimethoxybenzyl)-4-(pyridin-4-yl)pyridinium (0.55 g, 1.4 mmol) and 3,5-dimethoxybenzyl bromide (4.3 mmol) were dissolved in dry acetonitrile under nitrogen and heated to 85C for 2 d. The mixture was allowed to cool and the solvent was removed under vacuum. The crude mixture was then recrystallized in 1:1:0.1 methanol:petroleum ether:acetone. Red crystals were then collected on a filter and washed with cold methanol (0.43 g, 0.7 mmol, 50%) (400 MHz, D_2O): 9.10 (d, *J*=8Hz, 4H), 8.50 (d, *J*=8Hz, 4H),6.70 (m, 4H), 6.67(m, 2H), 5.81 (s, 4H), 1.79 (s, 12H). ^{13}C NMR (400 MHz, D_2O): 160.93, 150.20, 145.29, 134.19, 126.95, 107.64, 101.43, 55.47.

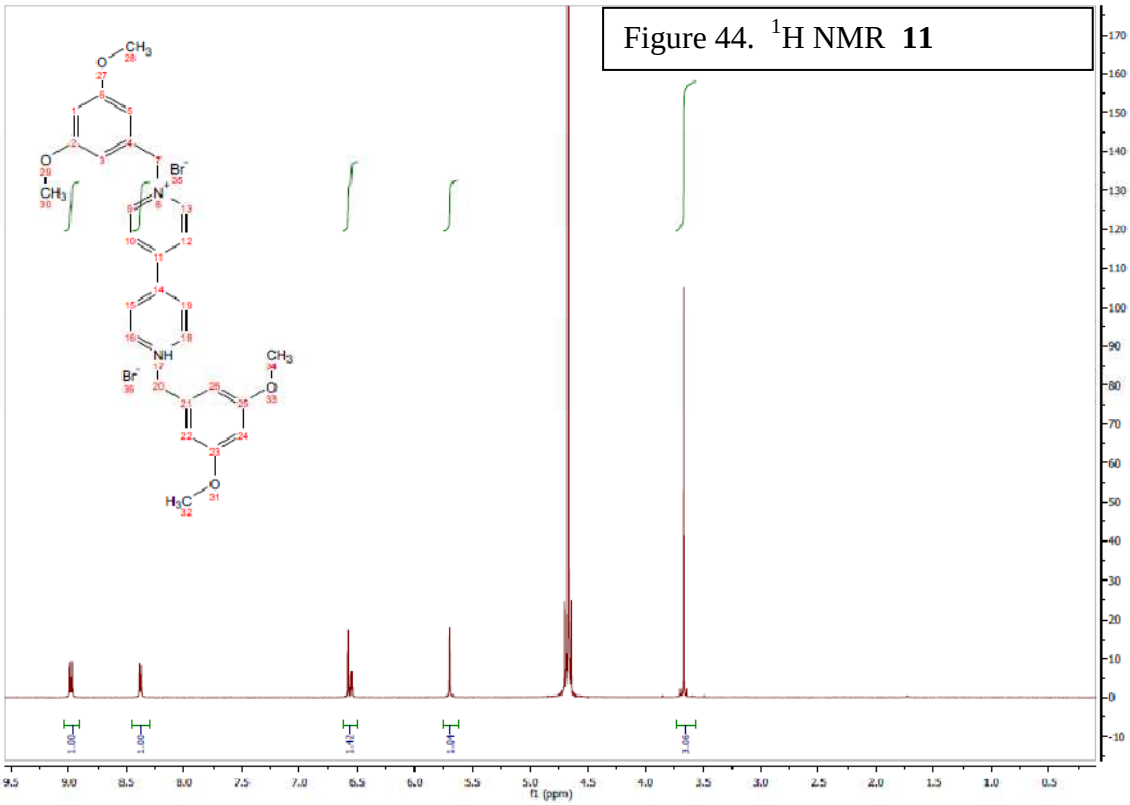

Figure 44. ^{1}H NMR **11**

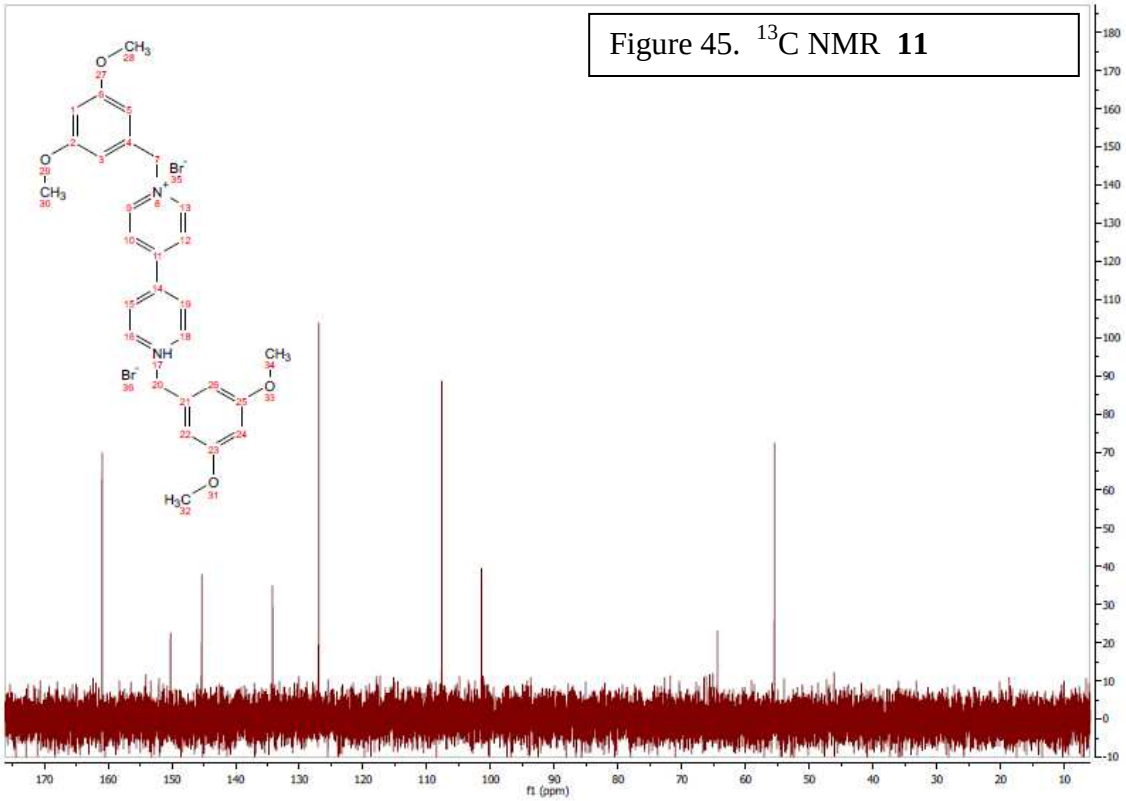

Figure 45. ^{13}C NMR **11**

Chapter 4: Kinetic investigations toward the design of molecular sensors

4.1 Introduction

Molecular sensors have vast potential for application in the medical field, including the potential to screen for cancer cells in the early stages.[19] A simple molecular sensor consists of a receptor and a signaling group, the latter of which turns on and off based upon interactions with the receptor.[19] One of the most promising types of signaling groups are fluorescent dyes, due to the potential for fast on and off signaling, and the ability of instrumentation to detect fluorescent signals with high sensitivity.[19] However, it is difficult to choose a corresponding receptor that will not only communicate with such a signaling group, but also be exclusively selective for the desired biomarker of cancer, which could be a protein, DNA, or antibody. This problem is further compounded by the possibility that a specific cancer may not have a known or unique biomarker, or, even if a biomarker is known, there may not be a known receptor that is specific for that particular biomarker.[19]

These issues can largely be solved by targeting the cancer cells themselves using an array based sensing methodology[20], which employs multiple non-specific molecular sensors that, when taken together, can provide a unique fluorescent profile for a specific cancer cell, not unlike a fingerprint. For example, if two molecular sensors are combined with a cancer cell one by one, then the fluorescent intensity of each sensor can be plotted as a coordinate in a two dimensional graph. Specific cancer cells in known states of progression, repeatedly measured, would be expected to consistently be

plotted in a general area of the two dimensional grid, creating a unique profile for each type of cell. Then, if an unknown cancer cell was plotted in the same way, it could be identified by its position on the two dimensional graph which is compared to a database of profiles of other cancer cells in various stages.

This proposed method is especially ideal for the early detection of cancer when the cells may not be easily identified by other methods, and could be a cheaper and faster way to screen for cancer, and could eventually lead to convenient flow though technology. This method can be further improved by the increase of dimensions used in creating profiles of cancer cells, by using a greater number of sensors or by using those that experience fluorescence at more than one wavelength. Computer matching software can be used to match multi-dimensional profiles of known biomarkers to unknown species with a high degree of accuracy. Interestingly, this method, which could be referred to as an "artificial nose", does not rely on in depth knowledge of the biochemistry of the particular cancer cell, making it highly attractive in areas of cancer research that are still progressing.

4.2 Specific Aims

Herein, a molecular sensor is proposed that describes the use of cucurbit[7]uril as a shuttle that allows for communication between the receptor and signaling group of the molecular sensor. (Figure 46) Before the receptor interacts with a cell surface, it is encapsulated by CB[7] with a high binding constant that is 100 to 1000 fold higher than any other potential binding site on the molecular sensor or on the cell itself, to ensure that CB[7] spends most of its time interacting with the receptor by a supramolecular interaction. Then, if a small percentage of CB[7] briefly shuttles down

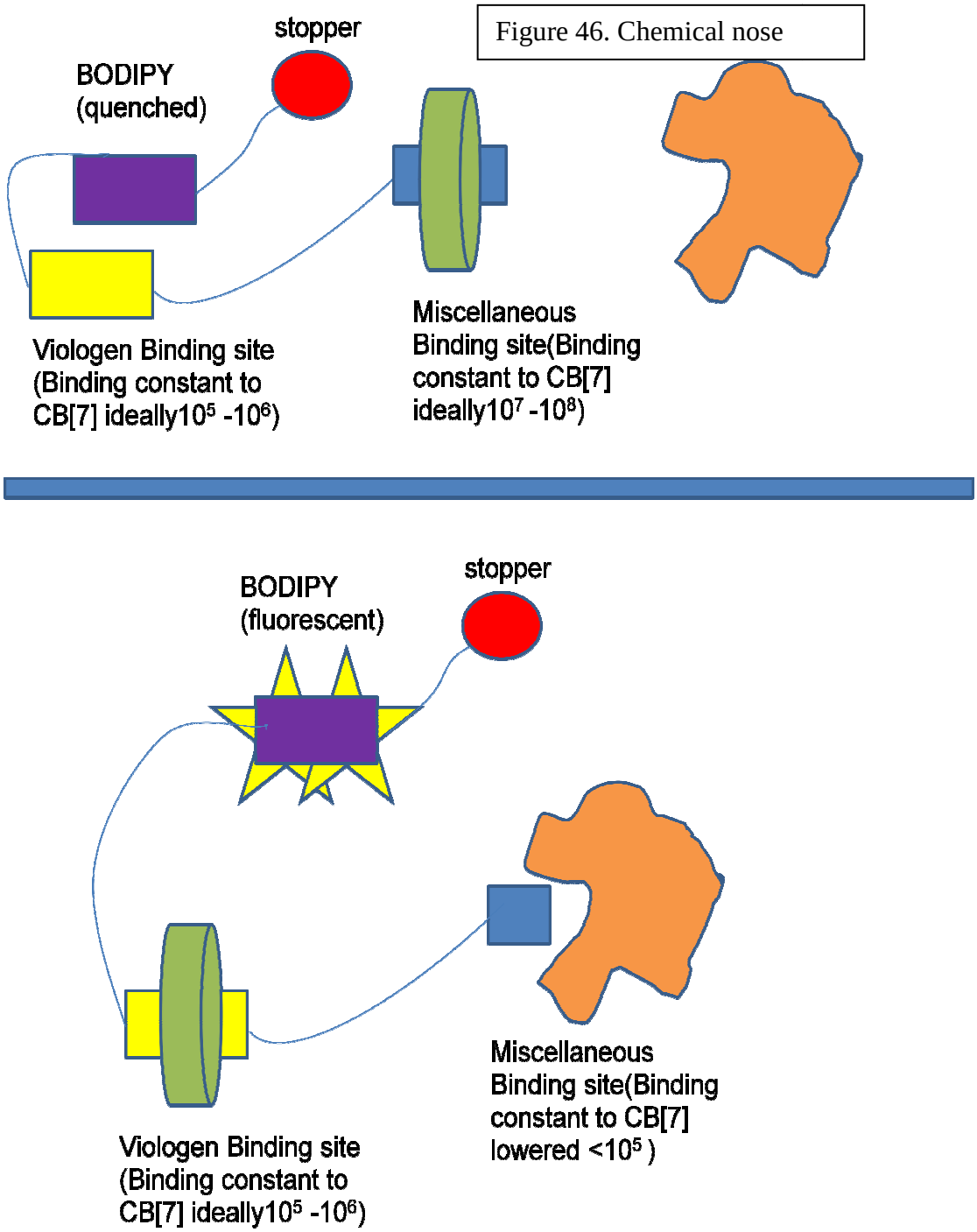

Figure 46. Chemical nose

the axle of the molecular sensor to a weaker binding site, the cell surface then has an opportunity to come into contact with the receptor. At this point, the binding constant between CB[7] and the receptor might be reduced by the incoming steric bulk and

electronic interactions from the cell surface. The weaker binding site could be strategically chosen to trigger the fluorescence "on" event. Presumably, different cells would interact with the molecular sensor slightly differently, and the fluorescence increase from the baseline could be measured with high sensitivity for each type of cancer cell. A variety of sensors with identical structures but different receptors could gather an array of information that is specific to certain cancer cells.

Cancer cell receptors containing different functionality types have already been explored in the literature[19] and consist primarily of alkyl chains, which may or may not contain hydroxy or ammonium groups or a combination thereof. Alkyl chains and cationic moieties are excellent candidates for encapsulation by CB[7], therefore; it would be feasible to equip the proposed molecular sensor with a variety of suitable receptors from the literature[21] that bind strongly to CB[7] in the range of 10^7-10^8 M^{-1}. However, the selection of the second, weaker binding site on the molecular sensor is a much more challenging proposition, and is the critical focus of this chapter. Not only must the internal docking site have a binding constant in the range of 10^5-10^6 M^{-1}, it must also somehow trigger a fluorescence signal.

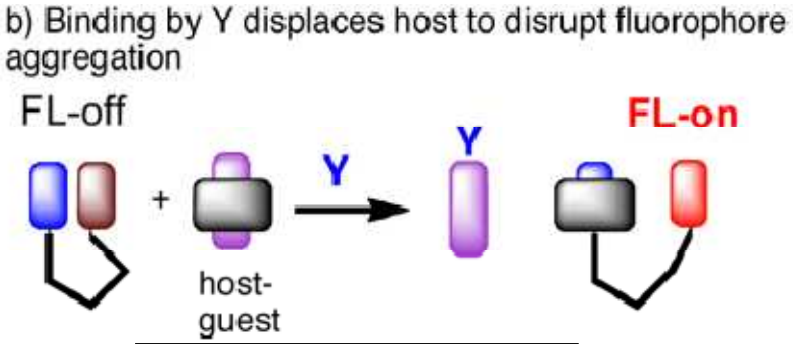

Figure 47. BODIPY on/off

A promising system for this trigger consists of a Boron dipyrromethene (BODIPY) fluorophore that can be temporarily quenched by a viologen by electron transfer[11] (Figure 47). The studies describes herein were complementary to an effort by Anuradha Singh of the Halterman group to develope a quencher-fluorophore dyad that, upon encapsulation of viologen by CB[7], interrupted the quenching of BODIPY.[27] This effect would provide the desired flourescence "on" for the proposed molecular sensor, which is triggered by CB[7]. Unfortunately, a suitable viologen with a binding constant in the range of 10^5-10^6 M^{-1}did not exist before this study. Therefore, my work began with a survey of dipyridine and viologen binding constants. I also studied the binding modes of CB[7] on a particularly promising axle in order to predict whether BODIPY would be properly shielded from fluorescent quenching. Also, in collaboration with Dr. Kalmar and Professor Ashby, I investigated the kinetic formation and dissociation rate constants of the 1:1 complex.

The proposal outlined above afforded a unique opportunity to focus on the supramolecular equilibrium binding locations and the equilibrium binding constants of CB[7] with a variety of viologen and pyridinium species which have not previously been studied. For the purposes of this study, the desired compound is a viologen, or a dipyridyl compound with the potential to be protonated, that binds with CB[7] with an equilibrium binding constant of 10^5-10^6 M^{-1}. However, it is anticipated that the results of this study could be potentially useful for variety of applications in the general area of molecular machines. The viologen and dipyridyl compounds chosen for this study contained several features in common (Figure 48).

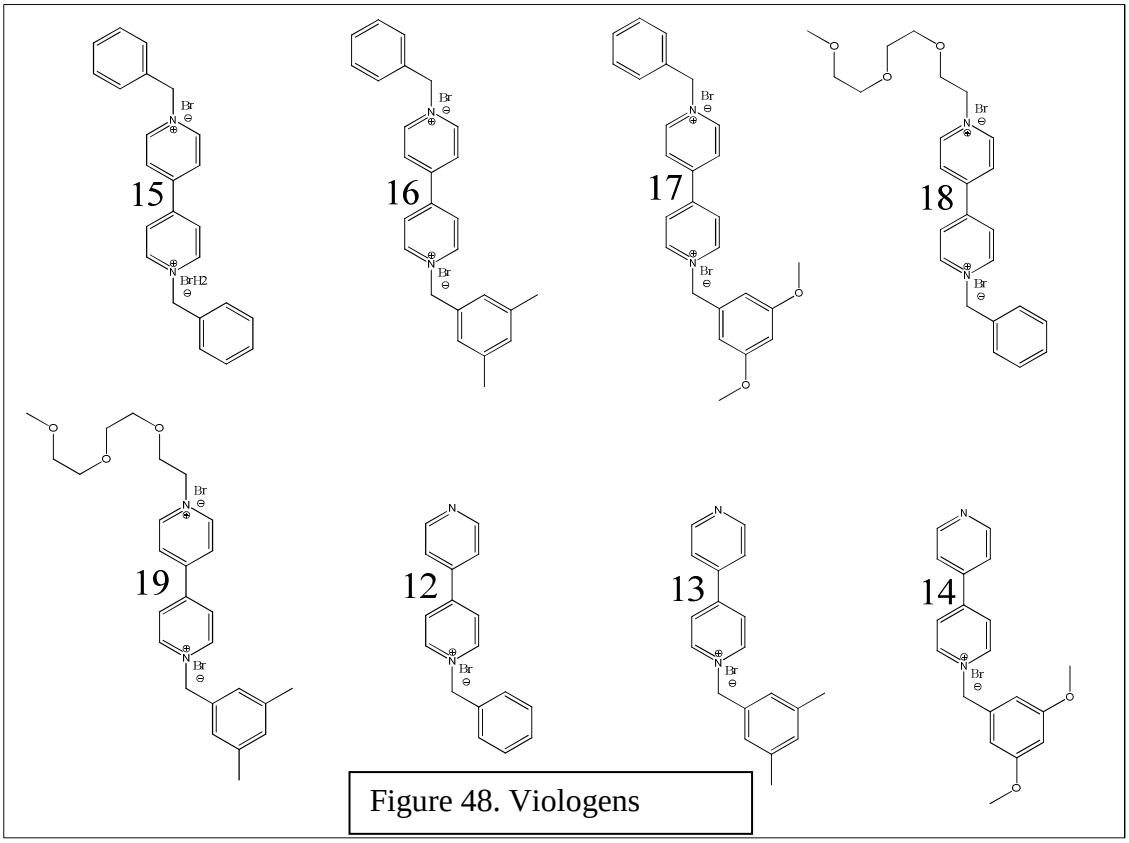

Figure 48. Viologens

First, each compound had at least one end that was sterically open on at least one side to allow the threading of CB[7] onto the axle. Second, with the exception of control compounds **15** and **13**, the end groups on the axle where chosen to destabilize the binding with CB[7] in order to achieve a lower binding constant. This destabilization was attempted by added steric substituents at the meta positions of the phenyl group, or by incorporating electronegative elements such as ether groups.

4.3 Synthesis

Compounds **15**, **12**,**13**, and **14** were synthesized by methods described in Chapter 3. Compounds **16** and **17** were synthesized from compounds **13** and **14**, respectively, in acetonitrile with a three-fold excess of benzyl bromide, and recrystallized in ethanol.[23] Compounds **18** and **19** were synthesized from a common

precursor, mono-substituted dipyridine **21.** In the synthesis of **18** and **19**, compound **20** was combined with a three-fold excess of a benzyl bromide derivative in

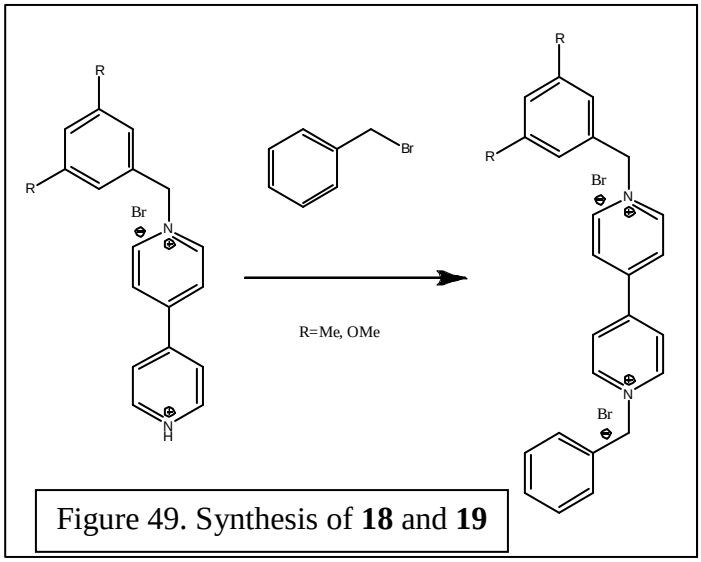

Figure 49. Synthesis of **18** and **19**

chloroform and refluxed under nitrogen for two days. (Figure 49). Chloroform was evaporated and the crude mixture was washed on a filter with acetonitrile and ether to remove starting materials. The filtrate was discarded and the remaining yellow solid was recrystallized in MeOH which gave high yields, **18** in 95% yield and **19** in 91% yield.

Precursor **21** was prepared from triethylene glycol (Figure 50) combined with a slight excess of tetrabromocarbon in methylene choloride at 0^{o}C, and a two-fold excess triphenylphospine solution was slowly added to activated the alcohol and allow S_N2 substitution by bromide to give compound **20**. Upon workup by extraction and purification by column, **20** was obtained in 85% yield. **20** was then combined with 4,4-bipyridine in large excess in acetonitrile under reflux. The di-substituted side product was not obtained, and so the resulting mixture was purified by taking advantage of the water solubility of compound **21**. Acetonitrile was evaporated and distilled water was added to the crude mixture. Excess 4,4-dipyridine precipitated from solution and was filtered out and discarded. The remaining filtrate was washed three times with toluene

and three times with ether. The water layer was then evaporated to give 54% yield of pure yellow solid **21**.

4.4 Equilibrium binding constant studies

Many different methods exist for calculating the equilibrium constants of various species with a variety of hosts has been established in the literature. The specific method used in this study was pioneered by Mock et. al. and Isaacs et. al.,[21] who successfully used ^{1}H-NMR competition experiments referenced to an absolute *K*a value. For our purposes, the reference compound selected for this study was $(Me)_3SiCD_2CD_2COOH$ **22** (Figure 51), which has a binding constant of 1.82×10^7 M^{-1} to CB[7]. **22** has an ^{1}H-NMR shift at 0.0 ppm in its unbound state, and has a shift at −0.7 when bound to CB[7]. Because this compound demonstrates slow exchange on the ^{1}H NMR timescale, both peaks can be integrated to determine an accurate ratio of bound and unbound **22**. In addition, because the binding constant of **22** is so high, it can be expected that a 1:4 ratio of CB[7] and **22** would result in only bound compound **22**. However, if a second guest is introduced, it will compete with compound **22** for inclusion in CB[7]. The ratio of bound and

Figure 50. Synthesis of **21**

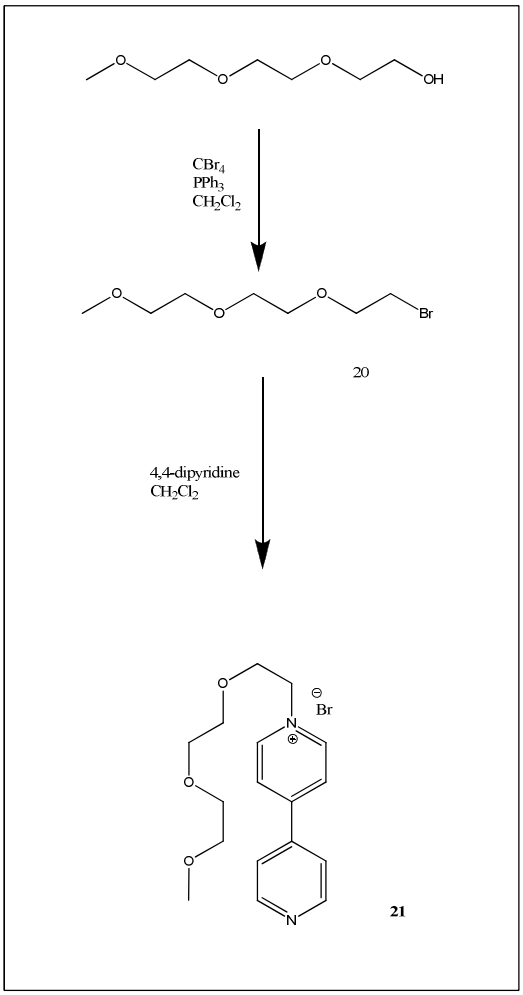

unbound **22** that appears on H^1 NMR is determined by the mathematical relationship between the equilibrium binding constant of **22** and the competing guest and the concentrations of all species in solution (Figure 51). Therefore, the relative equilibrium binding constant of the competing guest and **22** can be determined, and the absolute binding constant of **22** can then be used to calculate the absolute binding constant of the competing guest.

Figure 51. Compound **22**

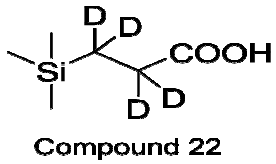

Compound 22

X=competing guest
Krel = ([CB[7]•N][X]free) / ([CB[7]•X][N]free)
[N]Total = [N]free + [CB[7]•N]
[CB[7]]Total = [CB[7]•N] + [CB[7]•X]
[X]Total = [X]free + [CB[7]•X]

This method of determining equilibrium binding constants was first tested with a known compound due to the precision required in the purification of synthetic compounds and the accurate measurements of both weight and volumes in the preparation of ^{1}H-NMR solutions. The equilibrium binding constant of 1,1'-dimethyl-4,4'-bipyridine-1,1'-diium iodide **23** (Figure 52) was prepared by combining an excess of methyl iodide with 4,4-bipyridine in acetonitrile at reflux for one day. Then, three solutions of 0.125 mM CB7, 0.5 mM

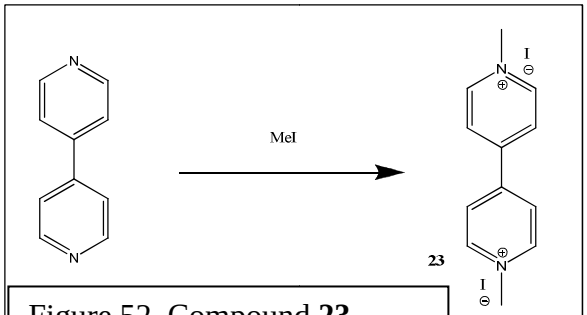

Figure 52. Compound **23**

22, and 4.0 mM **23** were prepared in 50 mM $Na(O_2CCD_3)$-buffered D_2O (pD = 4.5). **22** demonstrated slow exchange kinetics on the NMR time scale resulting in clear peaks for bound and unbound **22** at −0.7 and 0.0 ppm, respectively. From the average of ratios of the bound and unbound **22** of three solutions, the 1 : 1 binding constant of **23** : CB[7] was determined to be $K_1 = (1.8\pm0.2)\times10^7\ M^{-1}$. The expected literature value is $1.32\pm0.2\times10^7\ M^{-1}$. Error analysis was carried out according to literature.[21]

Once the method for determining equilibrium bind constants was verified, measurements were conducted for compounds **12-19**. The procedure was the same as for compound **22**, varying the concentration of guests until **23** showed clear and significant peaks for bound and unbound species at -0.7 and 0.0 ppm. The binding constants were then calculated in the same way for compounds **12-19** (Table 1). It is important to note that these studies were conducted in acidic solution, so that compound **12**, **13**, and **14** would be in their protonated form with two cationic nitrogen atoms, which is consistent with the form these compounds would have to take if incorporated into a molecular axle. Compounds **12-15** showed remarkably similar, high binding constants with CB[7] in the range of 10^7-$10^8\ M^{-1}$, presumably due to the presence of the benzyl group, which has shown to give rise to a stable, external binding described in Chapter 3. The highest binding constant was achieved by compound **15**, which contained two benzyl groups and thus two stable docking sites for CB[7]. The least stable binding guest among compounds **15-18** and **13** was compound **13**, due to having only on docking site. Among compounds **16-18**, the compound with the most

Table 1. K_1 values (Guest : CB[7] 1 : 1)

15	$(2.6\pm0.8)\times10^8$
16	$(2.2\pm0.7)\times10^8$
17	$(1.5\pm1.1)\times10^8$
18	$(1.9\pm0.2)\times10^8$
19	$(6.9\pm1.6)\times10^5$
12	$(6.6\pm1.4)\times10^7$
13	$(7.9\pm1.4)\times10^5$
14	$(8.8\pm2.3)\times10^5$

destabilization was compound **17**, which had the dual ability to sterically hinder CB[7], but was also able to repel the encapsulating host by electronic interaction. Compounds **19**, **13**, and **14** were the most destabilizing compounds of the group, **13** and **14** in particular because of only one binding site that was hindered sterically. However, compound **19** was determined to have the lowest equilibrium binding constant with CB[7] due to a binding site that was sterically hindered due to 3,5-dimethylbenzyl, and electronically repulsive due to triethylene glycol.

4.5 Further studies of molecular sensor model compound

Only three survey compounds (**19**, **13**, and **14)** were found to have equilibrium binding constants in the target range of 10^5-10^6 M^{-1}. Compound **19** happened to have smallest binding constant, and was ultimately chosen for further study for two reasons. First, the TEG substituent would be an ideal linker between binding sites in the molecular sensor, because its electronegative properties would ensure that it would not compete for association with CB[7]. Second, the 3,5-dimethyl benzyl group was determined to be an effective stopper in Chapter 3, and would provide a barrier between BODIPY and the internal binding site along the axle of the molecular sensor.

In order to increase the likelihood that CB[7]'s will disrupt the fluorescence quenching, it must be threaded onto the viologen in an internal position. Therefore; the binding mode became a target of study. The proton NMR of Compound **19** with one equivalent of CB[7] is shown above (Figure 53). Due to the broadening of the benzyl peaks at 7.0 ppm and the methyl peak at 2.2 ppm, it is clear that CB[7] is binding near the 3,5-dimethyl benzyl group of the viologen. However, it is unclear as to whether CB[7] has threaded onto the rotaxane, or is acting as a capping group on the methyls. If

the CB[7] is threading onto the viologen as desired, the internal protons of CB[7] (5.6 ppm) could be expected to interact through space via the nuclear overheuser effect with

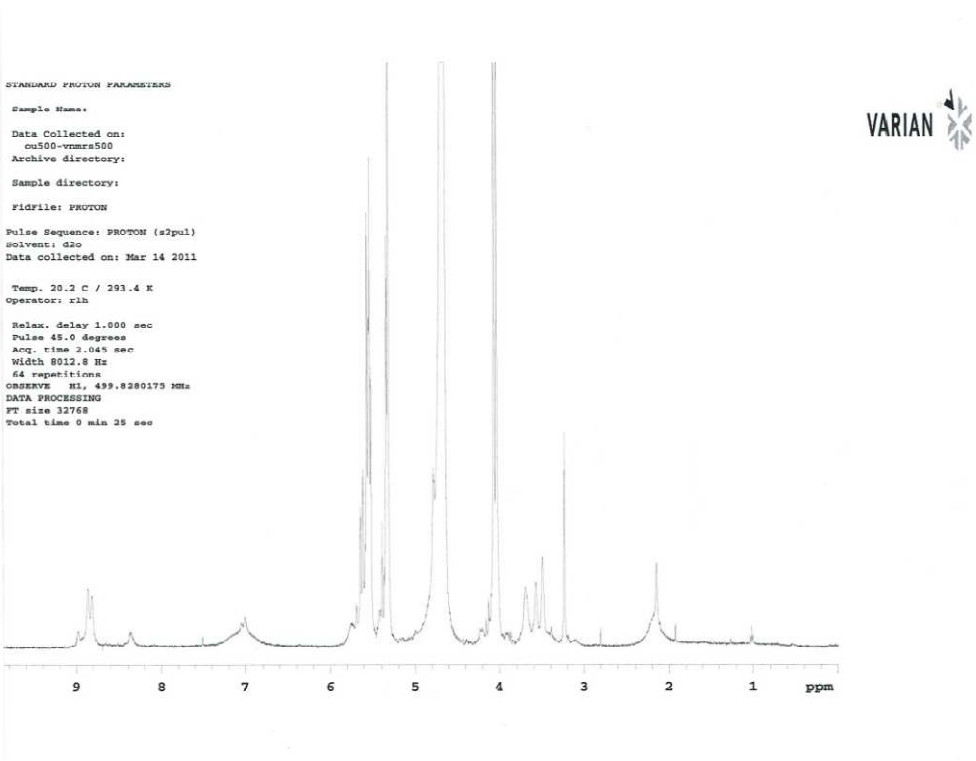

Figure 53. ^{1}H NMR **19**

the protons on the viologen axle. The ^{1}H NMR shifts at 9.0 and 8.9 represent the alpha protons of the viologen. When the ROESY[24] experiment was conducted to investigate thru space interaction, it was found that, after 36 hours, there was a positive correlation with the viologen peak at 8.9 (Figure 54). This indicates that CB[7] did thread and that the correlation is with the alpha protons on the dipyridine which must be the near the

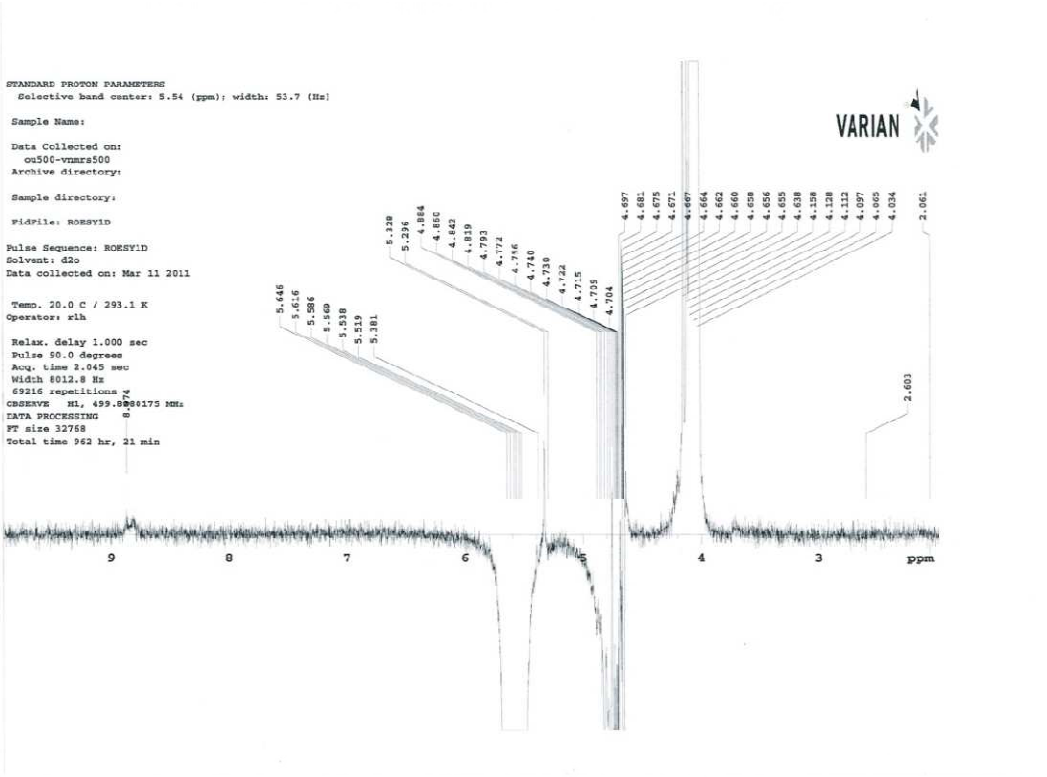

Figure 54. ROESY **19**

3,5-dimethylbenzyl group as established earlier. This is further supported by data obtained in Chapter 3, which suggested that an undesirable capping type of binding should cause the methyl signal to shift upfield 0.6 ppm. In this case, upon addition of one equivalent of CB[7], the methyl signal shifted downfield 0.1 ppm, supporting internal binding.

In order to create a more complete picture of this system, further investigation into the fast kinetics of compound **19** was conducted in collaboration with Dr. Michael Ashby's group.[25] A spectral change can be seen with the formation of a 1:1 host-guest

complex, with the absorbance maximum of the viologen **19** experiencing a slight red shift, about 10 nm.

This result was used to identify species in stopped-flow kinetic experiments. The formation and dissociation rate constants were found to be $k_1 = (6.01\pm0.03)\times10^6\ M^{-1}s^{-1}$ and $k_{-1} = (5.27\pm0.04)\times10^1\ s^{-1}$, respectively. In addition, the stability constant of the 1 : 1 adduct was determined to be $K = (1.23\pm0.04)\times10^5\ M^{-1}$ at 25 C by UV-Vis spectroscopy. This was in good agreement with the value obtained in this chapter by ^{1}H-NMR competition studies.

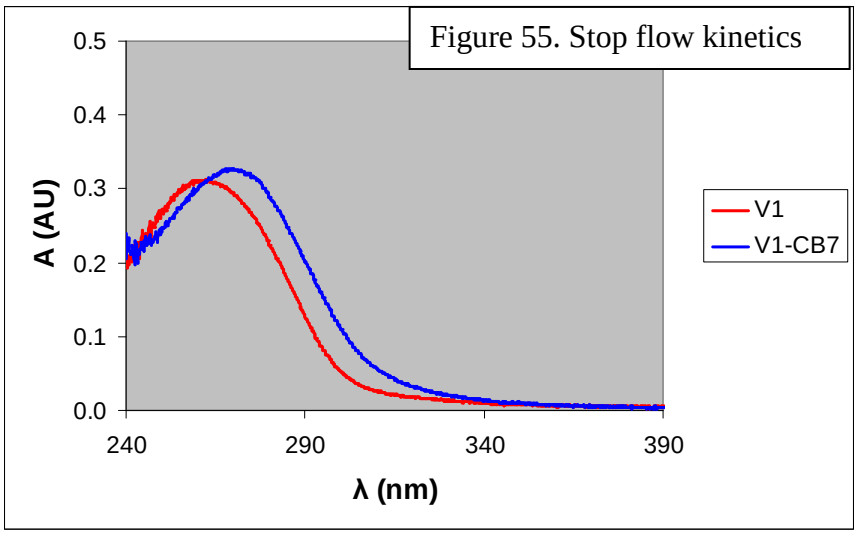

Figure 55. Stop flow kinetics

($K_1 = (6.9\pm1.6)\times10^5\ M^{-1}$), and could be accounted for by more dilute conditions in the fast kinetic studies. The kinetic studies also determined a one step kinetic model in which one equivalent of CB[7] threads on and off one equivalent of Compound **19**, and so the 1:1 adduct does not show evidence of any 2:1 species present in solution. The specific use of fast kinetic studies are the first study of its kind for any cucurbituril host.

The results of these studies were foundational to research by Dr. Anuradha Singh and Professor Ronald Halterman et. al. to develop a quencher-fluorophore dyad that, upon encapsulation of viologen by CB[7], interrupted the quenching of BODIPY

which increase fluorescence 30-fold.[22] (Figure 56) The kinetic information that

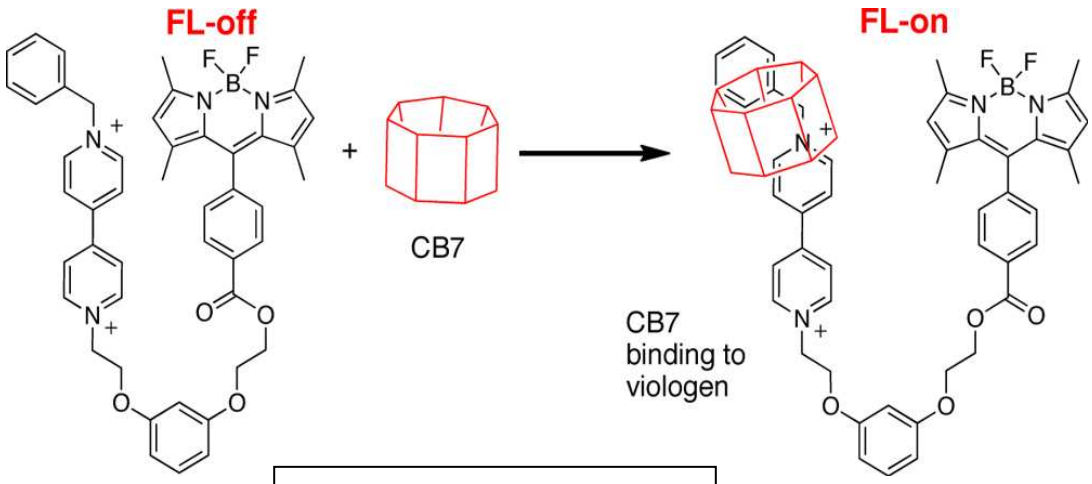

Figure 56. BODIPY dyad

informed the choice of binding moities did not exist before this study. By incorporating competitive binding sites and further modifications, this work could lead to the development of a set of molecular noses, which could be studied for their response to various important biomarkers for disease.

4.6 Experimental

Synthesis of 1,1'-dimethyl-4,4'-bipyridine-1,1'-diium bromide 23- 4,4'-dipyridine (0.5 g, 3.2 mmol) and methyl iodide (1.1 g, 8 mmol) were combined in acetonitrile and heated to reflux for 24 hours. The reaction mixture was cooled and 30 mL of ethyl acetate was added, causing the red product to precipitate. The compound was collected by filter and washed three times with ethyl acetate in 85% yield. ^{1}H NMR (300 MHz, D_2O): 8.96 (d, *J*=9Hz, 4H), 8.42 (d, *J*=6Hz, 4H), 4.40 (s, 6H).[21]

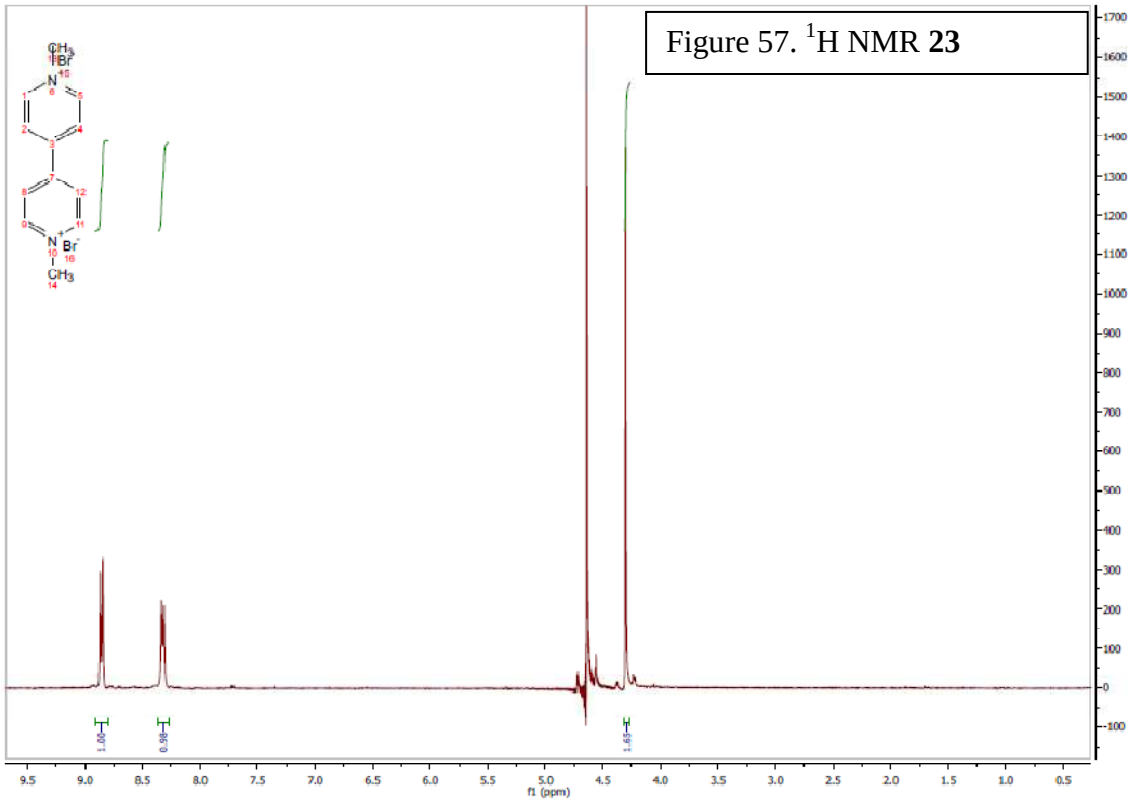

Figure 57. ^{1}H NMR **23**

Synthesis of 1,1'-dibenzyl-4,4'-bipyridine-1,1'-diium bromide 15 1-benzyl-4-(pyridin-4-yl)pyridinium bromide **13** (0.175 g, 0.54 mmol) and benzyl bromide (1.6 mmol) were added to dry acetonitrile (0.5 mL). The reaction mixture was heated to reflux for 48 h and then allowed to cool. The precipitate was collected on a filter and washed with acetonitrile and ether. The crude solid was then recrystallized in ethanol to give pure yellow-green product (0.072 g, 0.17 mmol, 31.7%). ^{1}H NMR (400 MHz, D_2O): 8.74 (d, *J*=7Hz, 4H), 8.11 (d, *J*=7Hz, 4H), 7.12 (s, 10H), 5.52 (s, 4H). ^{13}C NMR (400 MHz, D_2O): 150.12, 145.35, 132.03, 130.00, 129.50, 129.15, 126.94, 64.67. HRMS (ESI): *m/z* 338.1787$[M]^+$, ($M=C_{24}H_{21}N_2^+$ requires 338.1772).[26,27]

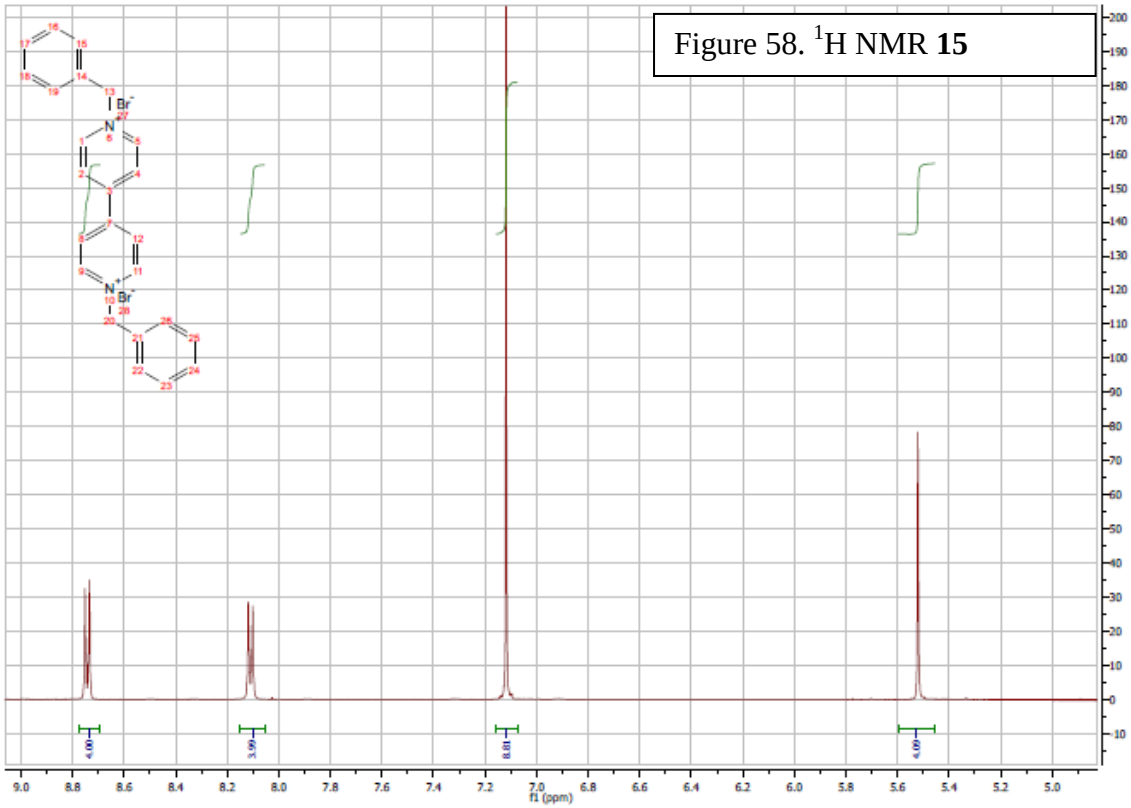

Figure 58. ^{1}H NMR **15**

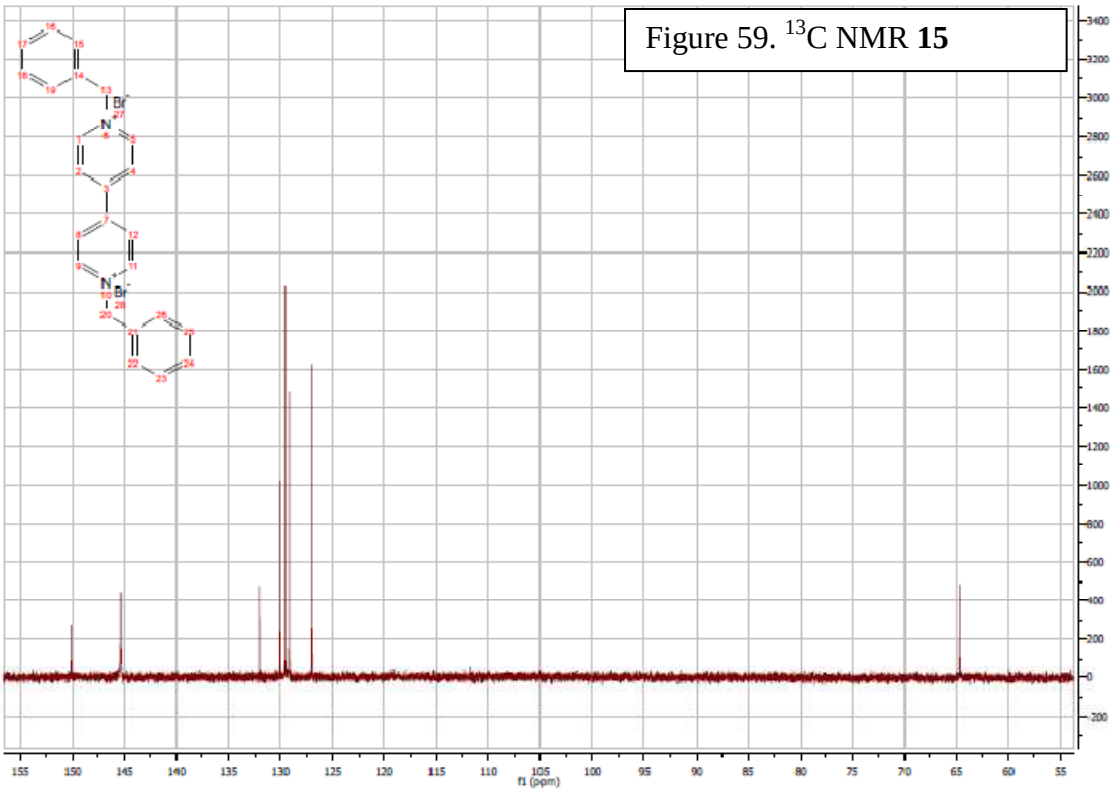

Figure 59. ^{13}C NMR **15**

Synthesis of 1-benzyl-1'-(3,5-dimethylbenzyl)-4,4'-bipyridine-1,1'-diium bromide 16- 1-benzyl-4-(pyridin-4-yl)pyridinium bromide **13** (0.411 g, 1.25 mmol) and 3,5-dimethylbenzyl bromide (3.8 mmol) were added to dry acetonitrile (25 mL). The reaction mixture was heated to reflux for 48 h and then allowed to cool. The precipitate was collected on a filter and washed with acetonitrile and ether. The crude solid was then recrystallized in ethanol to give pure yellow product (0.48 g, 0.91 mmol, 73%). ^{1}H NMR (400 MHz, D_2O): 8.74 (d, *J*=12Hz, 4H), 8.72(d, *J*=12Hz, 4H), 8.11 (d, *J*=6Hz, 4H), 8.10 (d, *J*=6Hz, 4H), 7.12 (s, 5H), 6.81 (s, 1H), 6.74 (s, 2H), 5.52 (s, 2H), 5.43 (s, 2H), 1.93 (s, 6H). ^{13}C NMR (400 MHz, D_2O): 150.12, 150.10, 145.33, 145.23, 139.86, 132.12, 132.02, 131.26, 129.99, 129.49, 129.11, 126.91, 126.87, 126.57, 64.66, 64.66, 20.02. HRMS (ESI): *m/z* 365.2015$[M-H]^+$, ($M=C_{26}H_{25}N_2^+$ requires 365.2012).

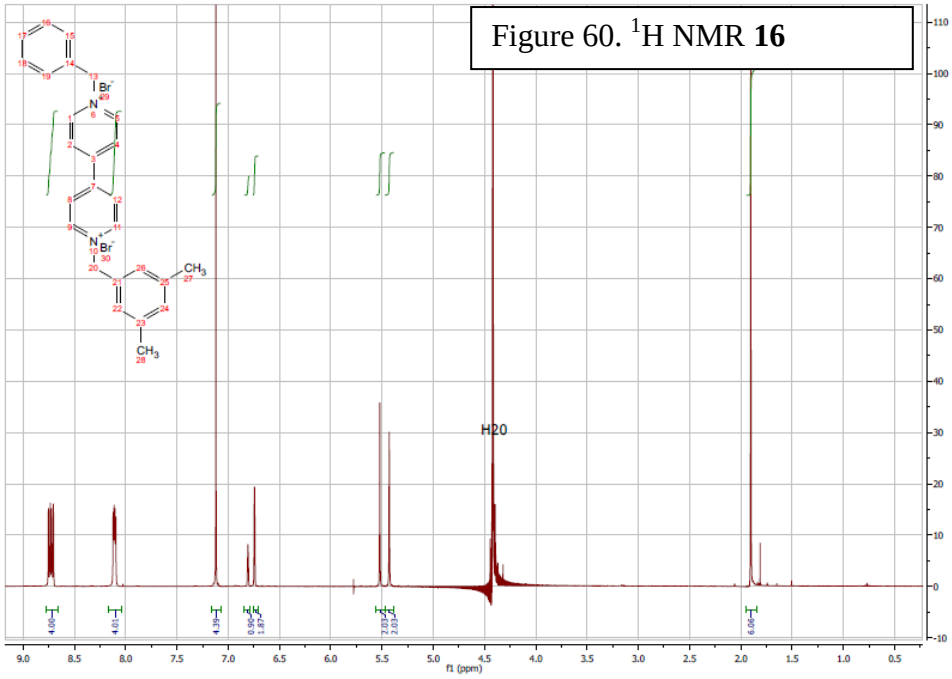

Figure 60. ^{1}H NMR **16**

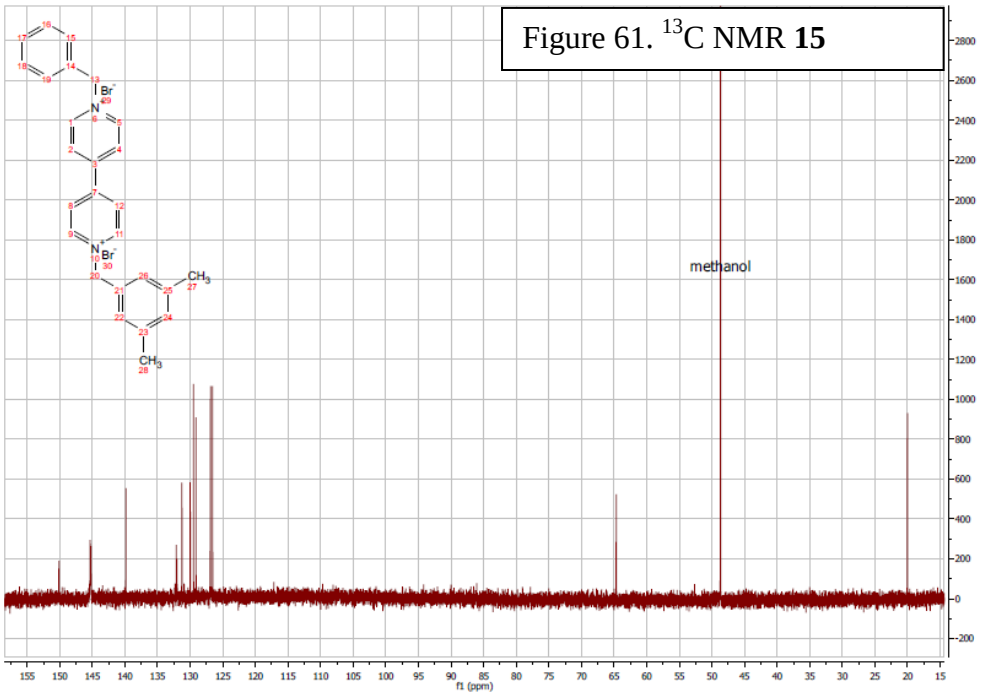

Figure 61. ^{13}C NMR **15**

Synthesis of 1-benzyl-1'-(3,5-dimethoxybenzyl)-4,4'-bipyridine-1,1'-diium bromide

17- 1-benzyl-4-(pyridin-4-yl)pyridinium bromide **12** (0.502 g, 1.3 mmol) and benzyl bromide (3.9 mmol) were added to dry acetonitrile (25 mL). The reaction mixture was heated to reflux for 48 h and then allowed to cool. The precipitate was collected on a filter and washed with acetonitrile and ether. The crude solid was then recrystallized in ethanol to give of a pure yellow product (0.6 g, 1.1 mmol, 84%). ^{1}H NMR (400 MHz, D_2O): 8.74 (d, *J*=7Hz, 4H), 8.72 (d, *J*=7Hz, 4H), 7.12 (s, 5H), 6.32 (d, *J*=2Hz, 2H), 6.29 (t, *J*=7Hz, 1H), 5.52 (s, 2H), 5.44 (s, 2H), 3.41 (s, 6H). ^{13}C NMR (400 MHz, D_2O): 160.93, 150.24, 150.09, 145.35, 145.28, 134.19, 132.02, 130.00, 129.50, 129.14, 126.93, 109.99, 107.63, 101.42, 64.68, 64.40, 55.45. HRMS (ESI): *m/z* 398.1989[M]$^{2+}$, ($M=C_{26}H_{26}N_2O_2^{2+}$ requires 398.1983).[23]

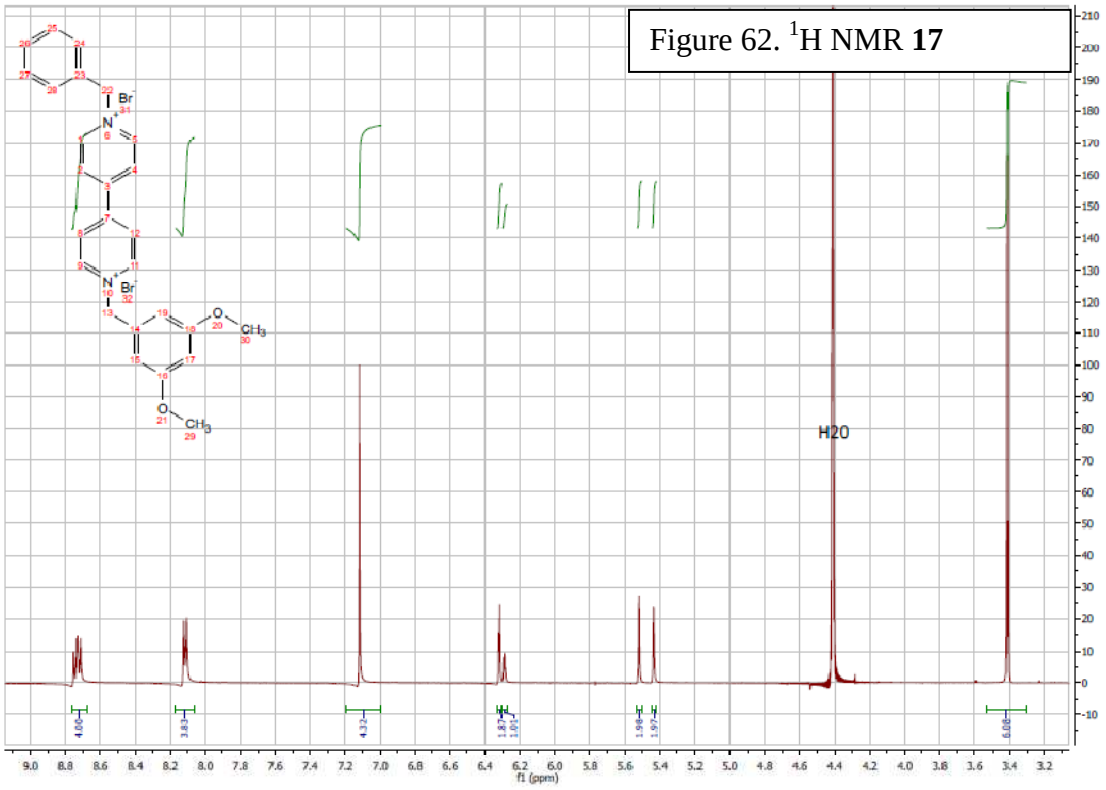

Figure 62. ^{1}H NMR **17**

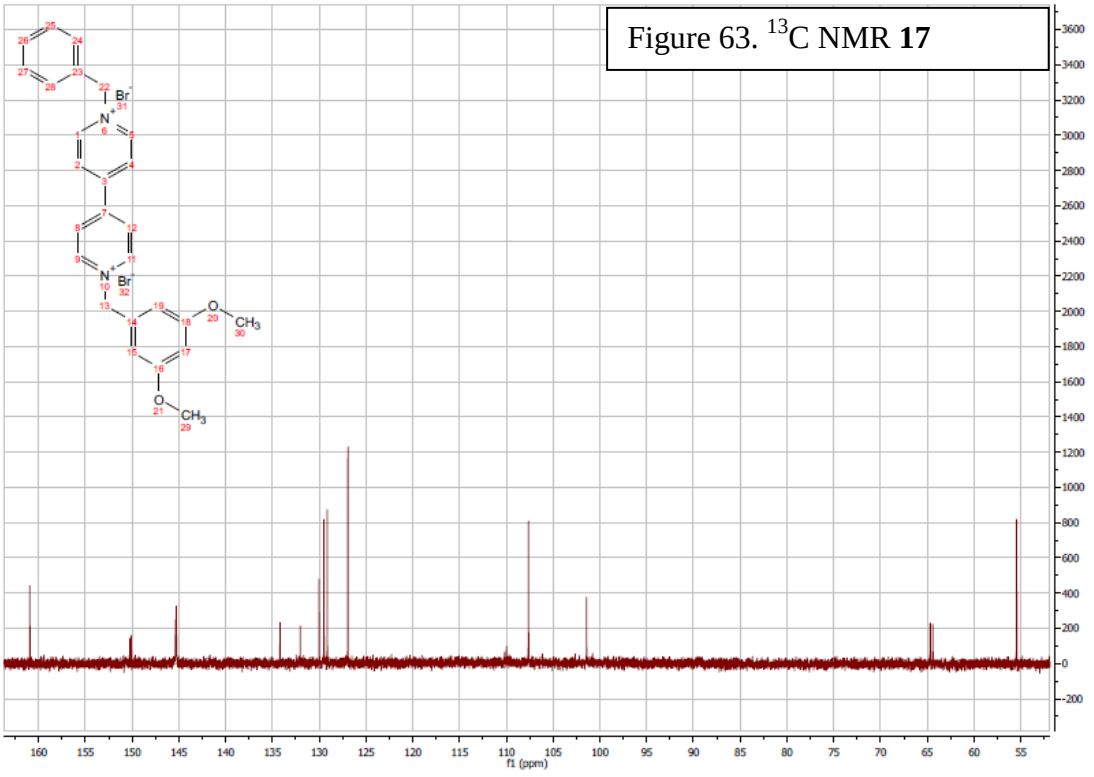

Figure 63. ^{13}C NMR **17**

Synthesis of 1-bromo-2-(2-(2-methoxyethoxy)ethoxy)ethane 20- 2-(2-(2-methoxyethoxy)ethoxy)ethanol (2.00 g, 12.2 mmol) and carbon tetrabromide (4.85 g, 14.7 mmol) was dissolved in methylene choloride under nitrogen. The temperature was lowered to 0C and a one molar solution of triphenylphospine (4.79 g, 36.6 mmol) in methylene chloride was added dropwise. The reaction mixture was stirred at 0C for four hours and then allowed to come to room temperature. Methylene chloride was evaporated from the crude mixture. The crude solid was then triturated by adding ether and filtering off the solid side product three times. Finally, a column of 1:1 ether:pet. ether was run on silica gel to give pure product (2.3 g, 10.4 mmol, 85%). ^{1}H NMR (300 MHz, $CDCl_3$): 3.81 (t, *J*=6Hz, 2H), 3.67 (m, 6H), 3.55 (m, 2H), 3.47 (t, *J*=6Hz, 2H), 3.36 (s, 3H). [6]

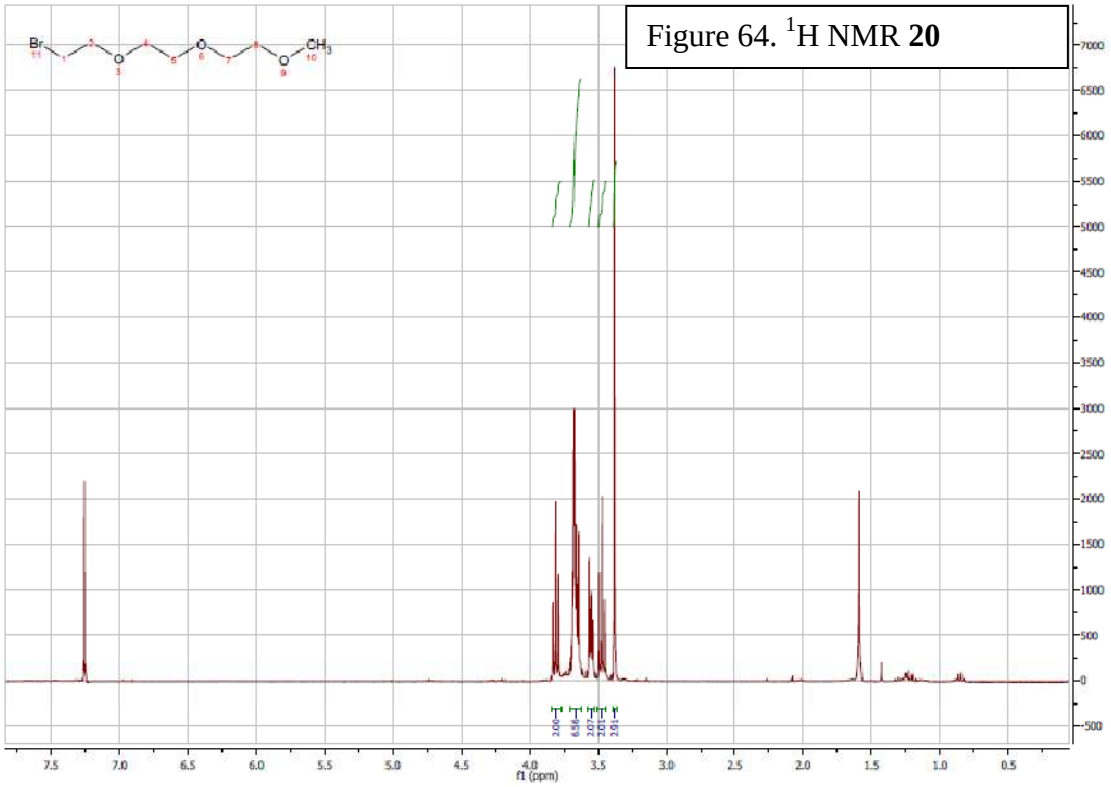

Figure 64. ^{1}H NMR **20**

Synthesis of 1-(2-(2-(2-methoxyethoxy)ethoxy)ethyl)-4-(pyridin-4-yl)pyridinium 21 - 4,4-dipyridine (6.309g, 39.6 mmol) and 1-bromo-2-(2-(2-methoxyethoxy)ethoxy)ethane **20** (3.01 g, 13.2 mmol) was added to dry acetonitrile (50 mL). The mixture was allowed to reflux under nitrogen for 18 h. Acetonitrile was evaporated and distilled water was added to the crude mixture. Excess 4,4-bipyridine precipitated from solution and was filtered out and discarded. The remaining filtrate was washed three times with toluene and three times with ether. The water layer was then evaporated to give pure yellow solid (2.7 g, 7.1 mmol, 54%). ^{1}H NMR (400 MHz, D_2O): 8.81 (d, *J*=6Hz, 2H), 8.60 (d, *J*=6Hz, 2H), 8.24 (d, *J*=6Hz, 2H), 7.74 (d, *J*=6Hz, 2H), 4.64 (m, 2H), 3.89 (t, *J*=6Hz, 2H), 3.50 (m, 2H), 3.44 (m, 2H), 3.36 (m, 2H), 3.33 (m, 2H), 3.10 (s, 3H).[27]

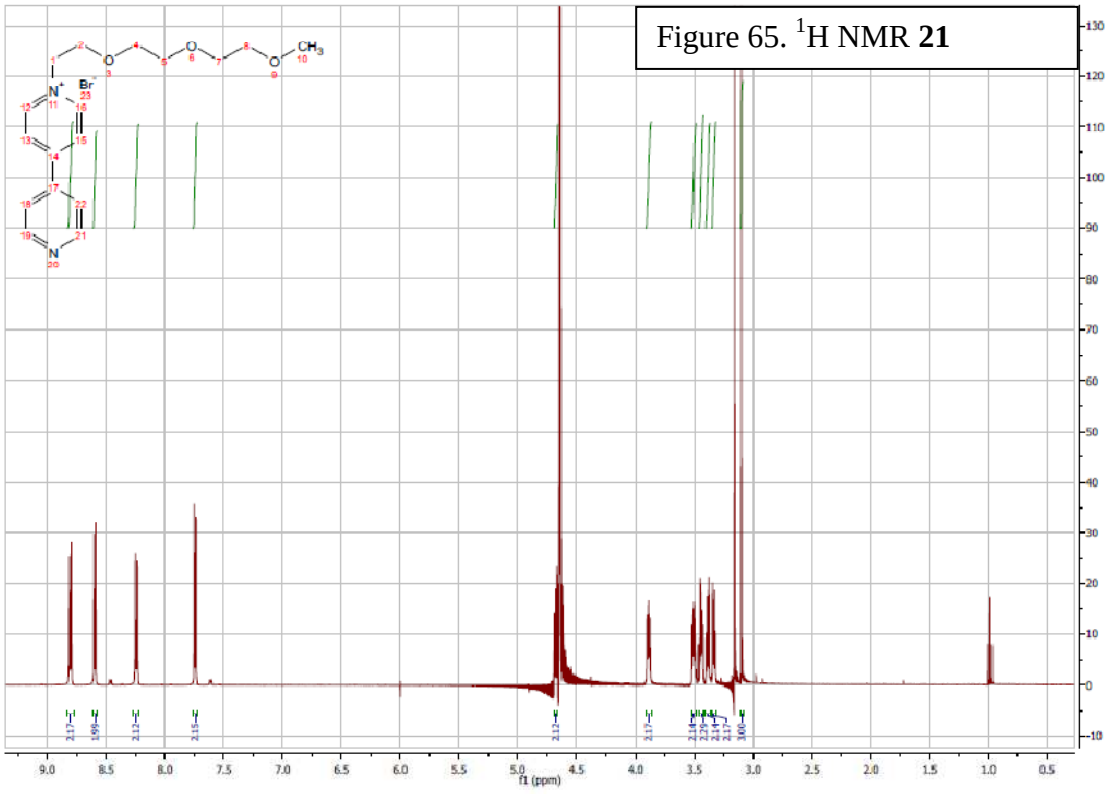

Figure 65. ^{1}H NMR **21**

Synthesis of 1-benzyl-1'-(2-(2-(2-methoxyethoxy)ethoxy)ethyl)-4,4'-bipyridine-1,1'-diium bromide 18 - 1-tri(ethylene-glycol)-4,4'-bipyridinium (0.914 g, 2.4 mmol) and 3,5-dimethylbenzylbromide (7.2 mmol) were combined with chloroform (50 mL) and refluxed under nitrogen for 2 d. Chloroform was evaporated and the crude mixture was washed on a filter with acetonitrile and ether. The filtrate was discarded and the remaining yellow solid was recrystallized in MeOH (1.3 g, 2.3 mmol, 95%). ^{1}H NMR (400 MHz, D_2O): 8.99 (d, *J*=7Hz, 2H), 8.95 (d, *J*=7Hz, 2H), 8.36 (m, 4H), 7.35 (s, 5H), 5.76 (s, 2H), 4.74 (t, *J*=4Hz, 2H), 3.52 (m, 2H), 3.44 (m, 4H), 3.37 (m, 2H), 3.12 (s, 6H). ^{13}C NMR (400 MHz, D_2O):. 150.18, 150.12, 145.88, 145.39, 132.03, 130.01, 129.51, 129.12, 126.90, 126.58, 70.79, 69.64, 69.27, 69.23, 68.38, 64.69, 61.20, 57.79. HRMS (ESI): *m/z* 393.2173 $[M-H]^+$, ($M=C_{24}H_{29}N_2O_3^+$ requires 393.2173).

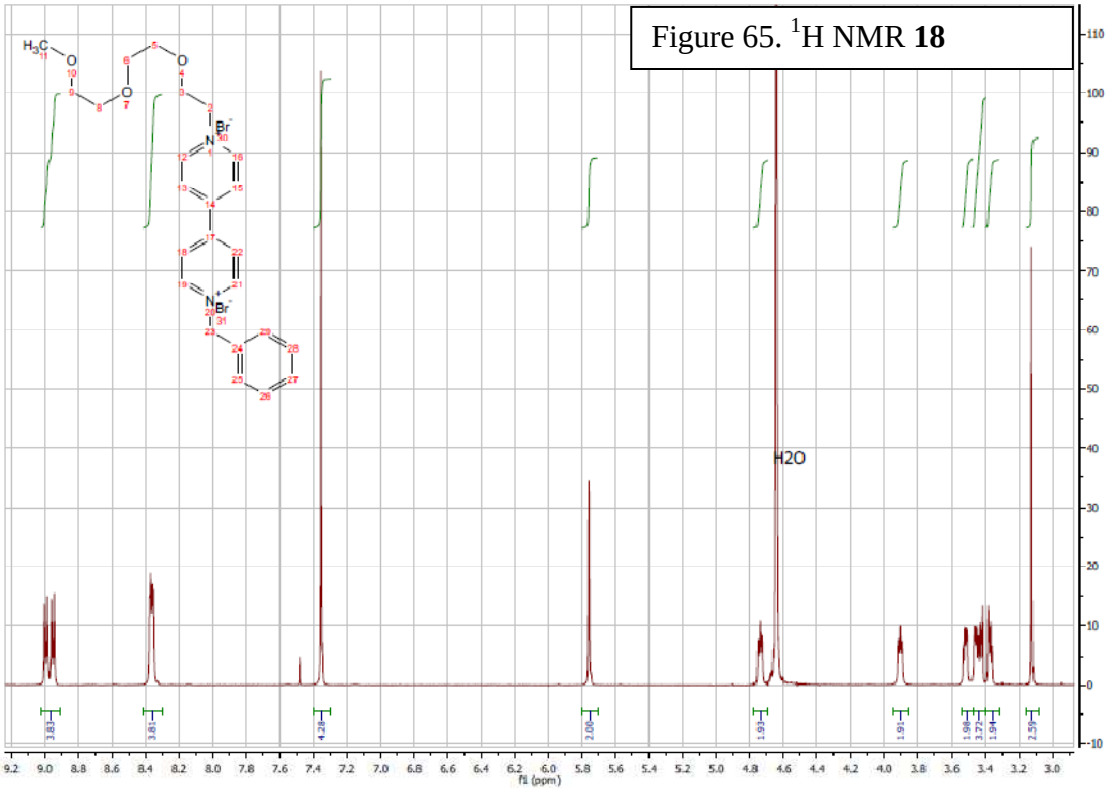

Figure 65. ^{1}H NMR **18**

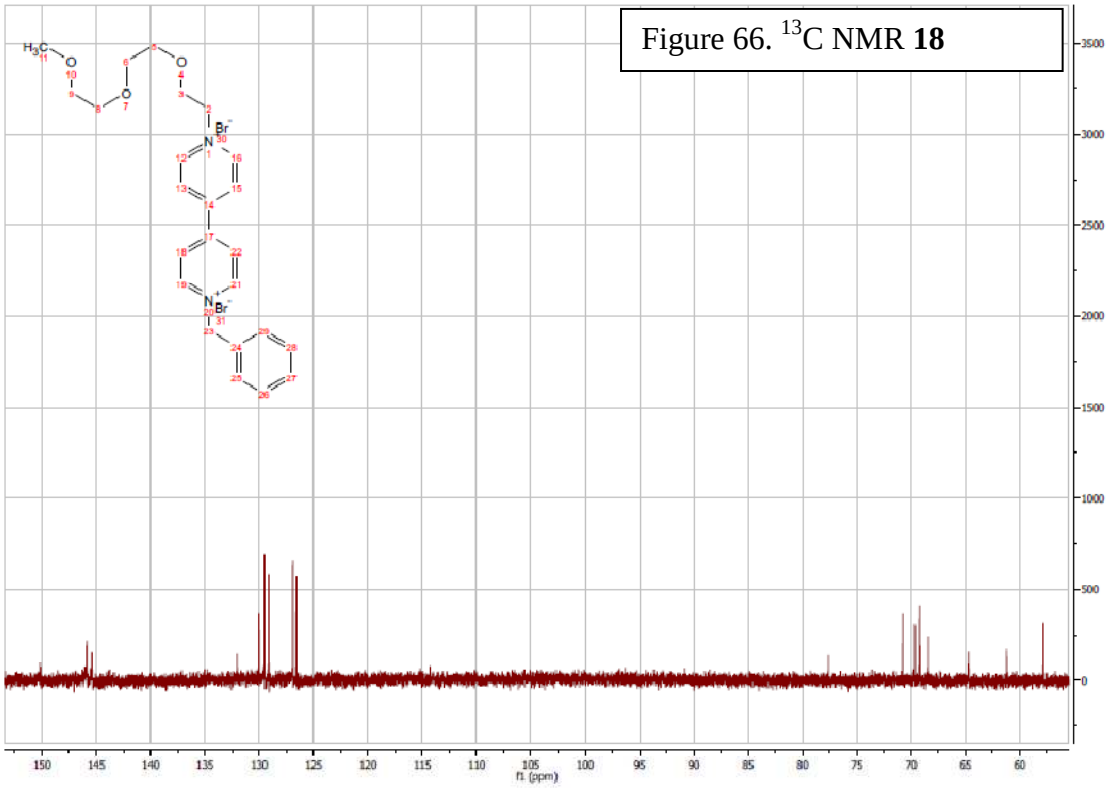

Figure 66. ^{13}C NMR **18**

Synthesis of 1-tri(ethylene-glycol)-1'-methyl-m-xylyl-4,4'-bipyridinium dication 19 - 1-tri(ethylene-glycol)-4,4'-bipyridinium (0.92 g, 2.4 mmol) and 3,5-dimethylbenzylbromide (1.43 g, 7.2 mmol) were combined with chloroform (50 mL) and refluxed under nitrogen for 2 d. Chloroform was evaporated and the crude mixture was washed on a filter with acetonitrile and ether. The filtrate was discarded and the remaining red solid was recrystallized in methanol which yielded product (1.3 g, 2.2 mmol, 91%). ^{1}H NMR (300 MHz, D_2O): 8.97 (m, 4H), 8.36 (m, 4H), 7.03 (s, 1H), 6.99 (s, 2H), 5.67 (s, 2H), 4.75 (t, *J*=4 Hz 2H), 3.91 (t, *J*=4 Hz, 2H), 3.52 (m, 2H), 3.42 (m, 2H), 3.36 (m, 2H), 3.12 (s, 3H), 2.14 (s, 6H) . ^{13}C NMR (400 MHz, D_2O): 179.32, 150.2, 145.94, 145.35, 139.98, 132.28, 131.36, 127.00, 126.70, 70.90, 69.77, 69.37, 69.33, 68.49, 64.78, 61.30, 57.96, 22.06, 20.19. HRMS (ESI): *m/z* 421.2498 $[M-H]^+$, ($M=C_{26}H_{33}N_2O_3^+$ requires 421.25).

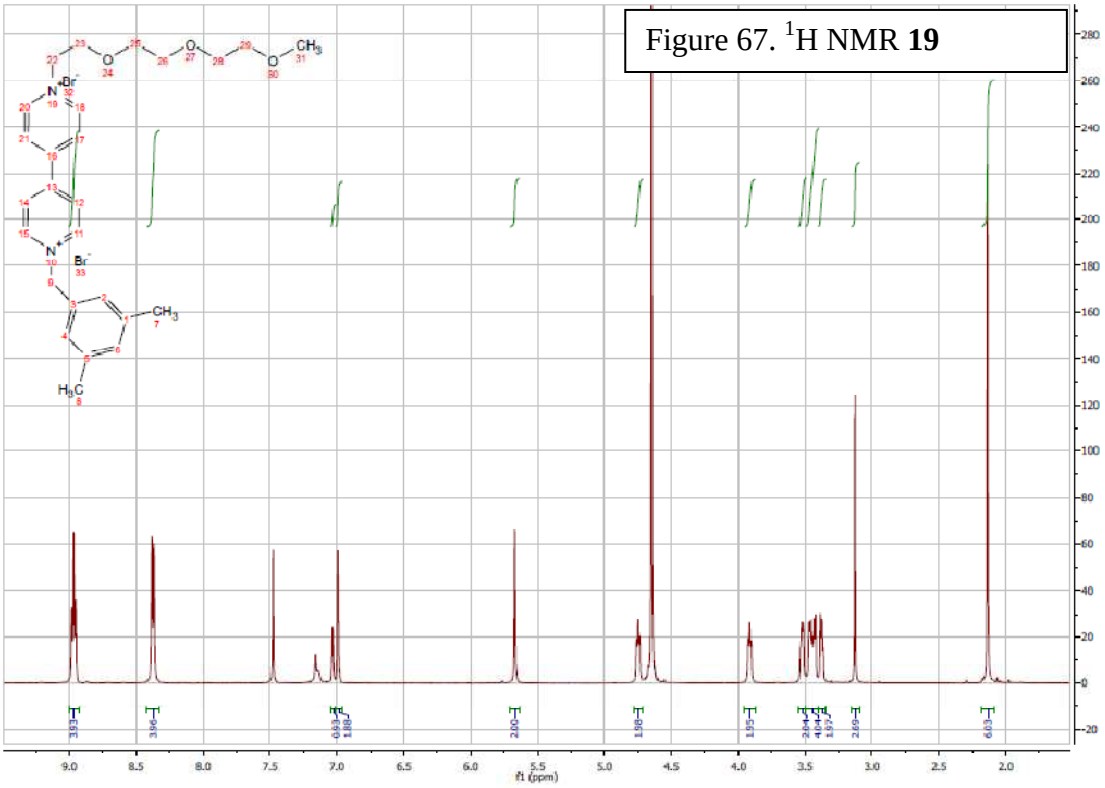

Figure 67. ^{1}H NMR **19**

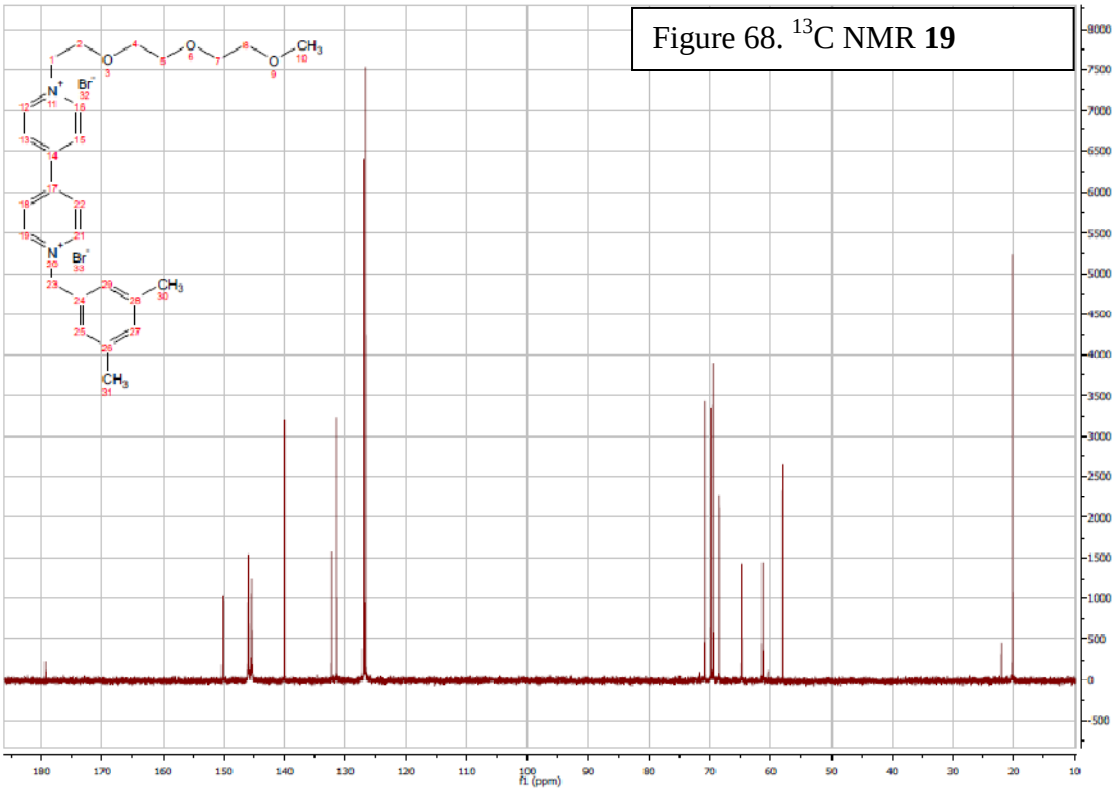

Figure 68. ^{13}C NMR **19**

^{1}H-NMR stability study of 23. The equilibrium binding constant of 1,1'-dimethyl-4,4'-bipyridine-1,1'-diium iodide **23** with cucurbit[7]uril CB[7] was determined by analyzing the competitive binding of **23** compared to that of the reference compound $(Me)_3SiCD_2CD_2COOH$ **22** using ^{1}H-NMR (400 MHz). The stability constant of the 1 : 1 adduct of CB[7] and **22**[21] is 23 = $(1.8\pm0.2)\times10^7$ M^{-1}. The procedure followed was developed by Mock and Isaacs[21]. Three solutions of 0.125 mM CB[7], 0.5 mM **22**, and 4.0 mM **23** were prepared in 50 mM $Na(O_2CCD_3)$-buffered D_2O (pD = 4.5). **22** demonstrated slow exchange kinetics on the NMR time scale resulting in clear peaks for bound and unbound **22** at -0.7 and 0.0 ppm, respectively. From the average of ratios of the bound and unbound **22** of three solutions (which was determined with a ±12 % std. dev.), we determined the binding constant of **23** : CB[7] 1 : 1 to be $K_1 = (1.8\pm0.2)\times10^7$ M^{-1}. The expected literature value is $1.32\pm0.2\times10^7$ M^{-1}. Error analysis was carried out according to literature.[21]

Figure 70. ^{1}H NMR competition studies compound **23**

Spectrum A

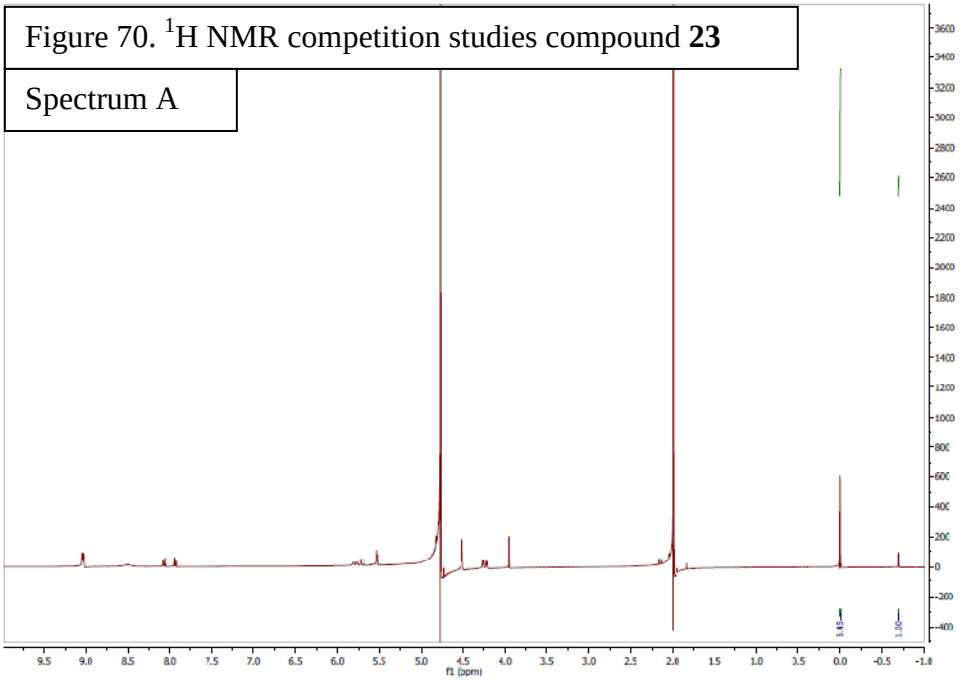

Spectrum B

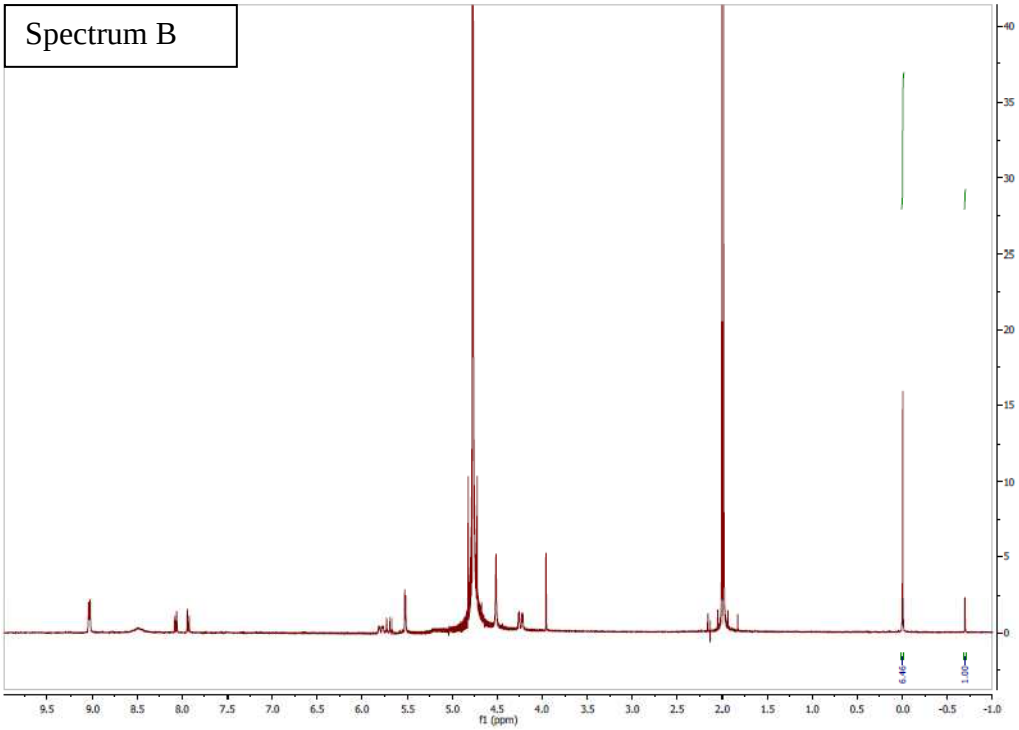

Spectrum C

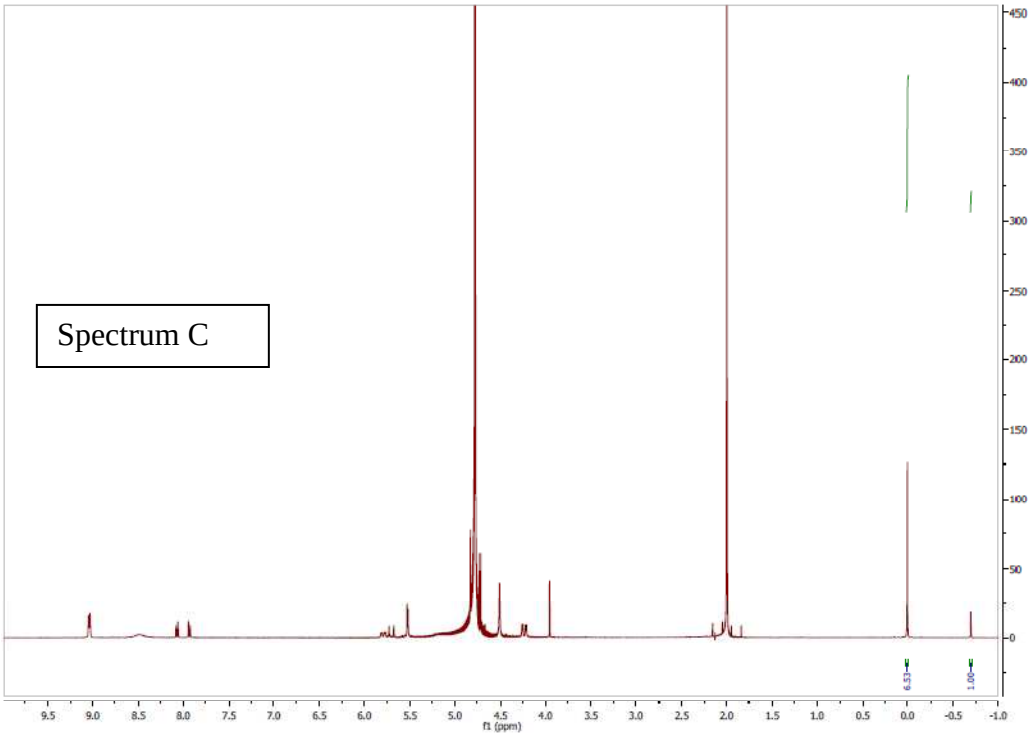

^{1}H-NMR stability study of 15. The equilibrium binding constant of 1,1'-dibenzyl-4,4'-bipyridine-1,1'-diium bromide **15** with cucurbit[7]uril CB[7] was determined by analyzing the competitive binding of **15** compared to that of the reference compound $(Me)_3SiCD_2CD_2COOH$ **22** using ^{1}H-NMR (400 MHz). The stabilitiy constant of the 1 : 1 adduct of CB[7] and **22**[21] is $K = (2.6\pm0.8)\times10^8$ M^{-1}. The procedure followed was developed by Mock and Isaacs[21]. Three solutions of 0.125 mM CB7, 2.0 mM **22**, and 0.5 mM **15** were prepared in 50 mM $Na(O_2CCD_3)$-buffered D_2O (pD = 4.5). **22** demonstrated slow exchange kinetics on the NMR time scale resulting in clear peaks for bound and unbound **22** at -0.7 and 0.0 ppm, respectively. From the average of ratios of the bound and unbound **22** of three solutions (which was determined with a ±14 % std. dev.), we determined the binding constant of **15** : CB[7] 1 : 1 to be $K_1 = (2.6\pm0.8)\times10^8$ M^{-1}. Error analysis was carried out according to literature.[21]

Figure 71. ^{1}H NMR competition studies compound **15**

Spectrum A

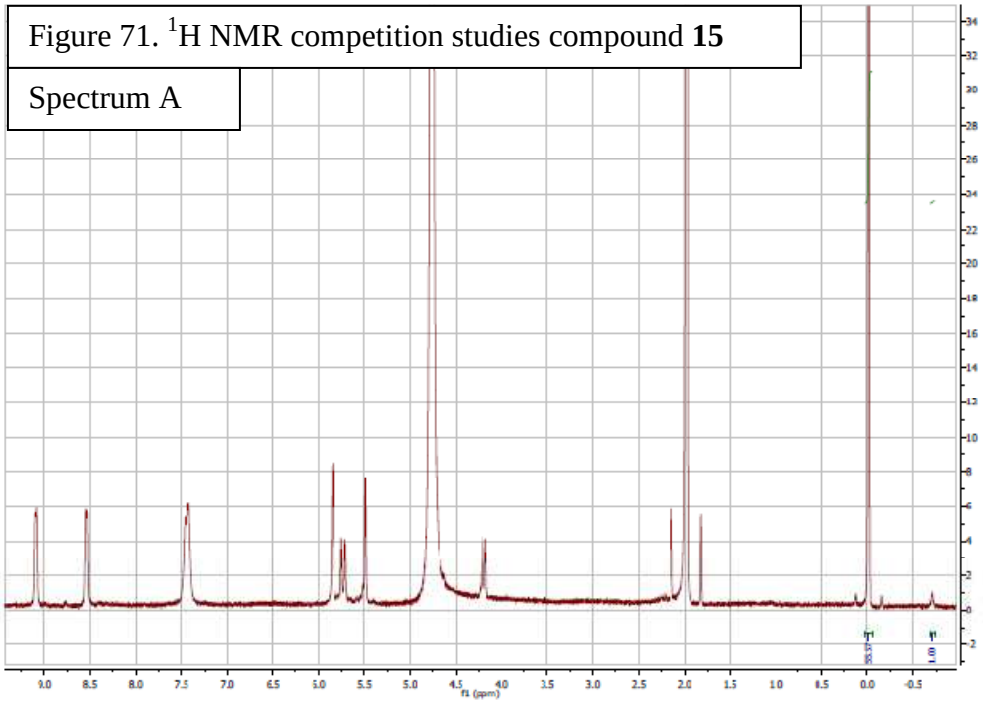

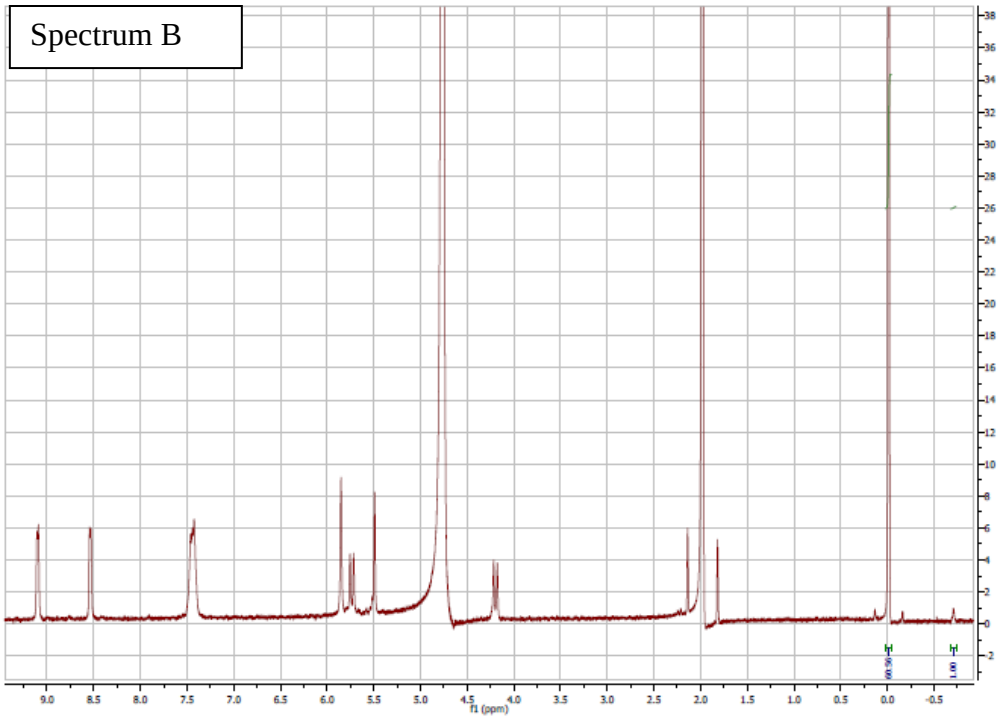

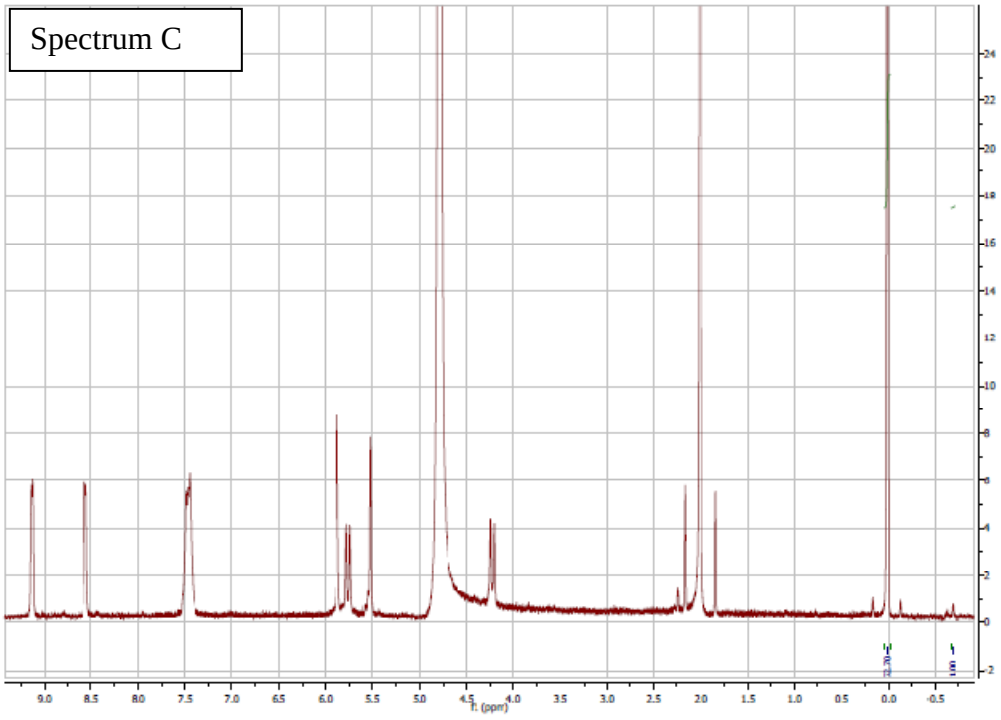

^{1}H-NMR stability study of 16. The equilibrium binding constant of 1-benzyl-1'-(3,5-dimethylbenzyl)-4,4'-bipyridine-1,1'-diium bromide **16** with cucurbit[7]uril CB[7] was

determined by analyzing the competitive binding of **16** compared to that of the reference compound $(Me)_3SiCD_2CD_2COOH$ **22** using ^{1}H-NMR (400 MHz). The stability constant of the 1 : 1 adduct of CB[7] and **22**[21] is K = $(1.8\pm0.2)\times10^7$ M^{-1}. The procedure followed was developed by Mock and Isaacs[21]. Three solutions of 0.125 mM CB7, 2.0 mM **22**, and 0.5 mM **16** were prepared in 50 mM $Na(O_2CCD_3)$-buffered D_2O (pD = 4.5). **22** demonstrated slow exchange kinetics on the NMR time scale resulting in clear peaks for bound and unbound **22** at -0.7 and 0.0 ppm, respectively. From the average of ratios of the bound and unbound **22** of three solutions (which was determined with a ±16 % std. dev.), we determined the binding constant of **16** : CB[7] 1 : 1 to be K_1 = $(2.2\pm0.7)\times 10^8$ M^{-1}. Error analysis was carried out according to literature.[21]

Figure 72. ^{1}H NMR competition studies compound **16**

Spectrum A

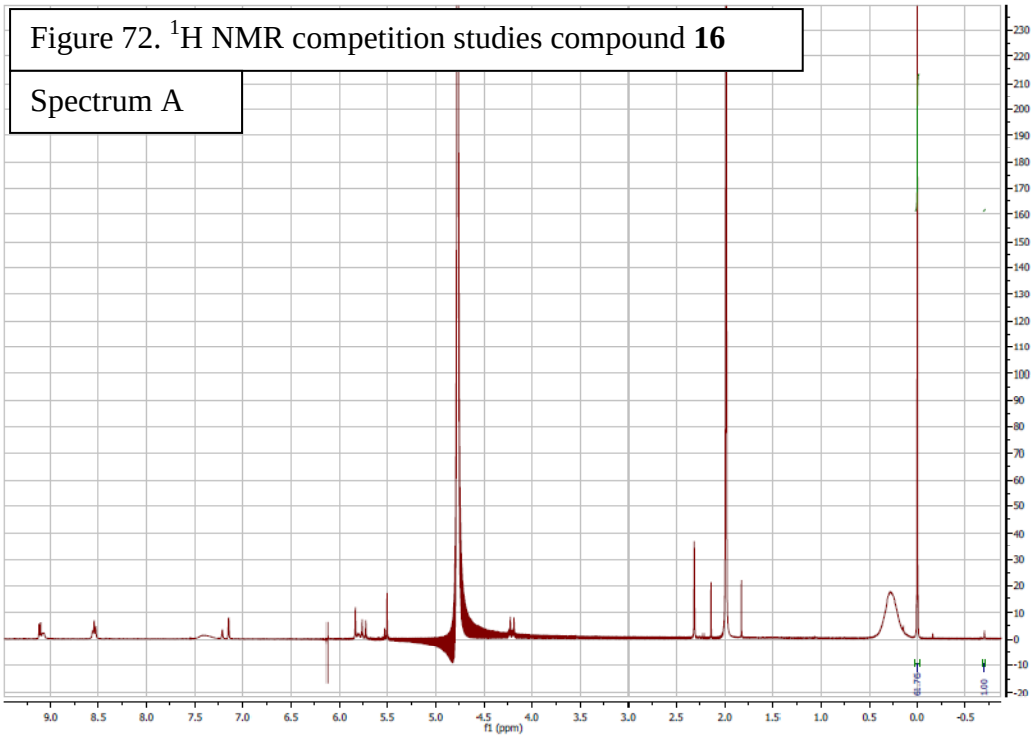

Spectrum B

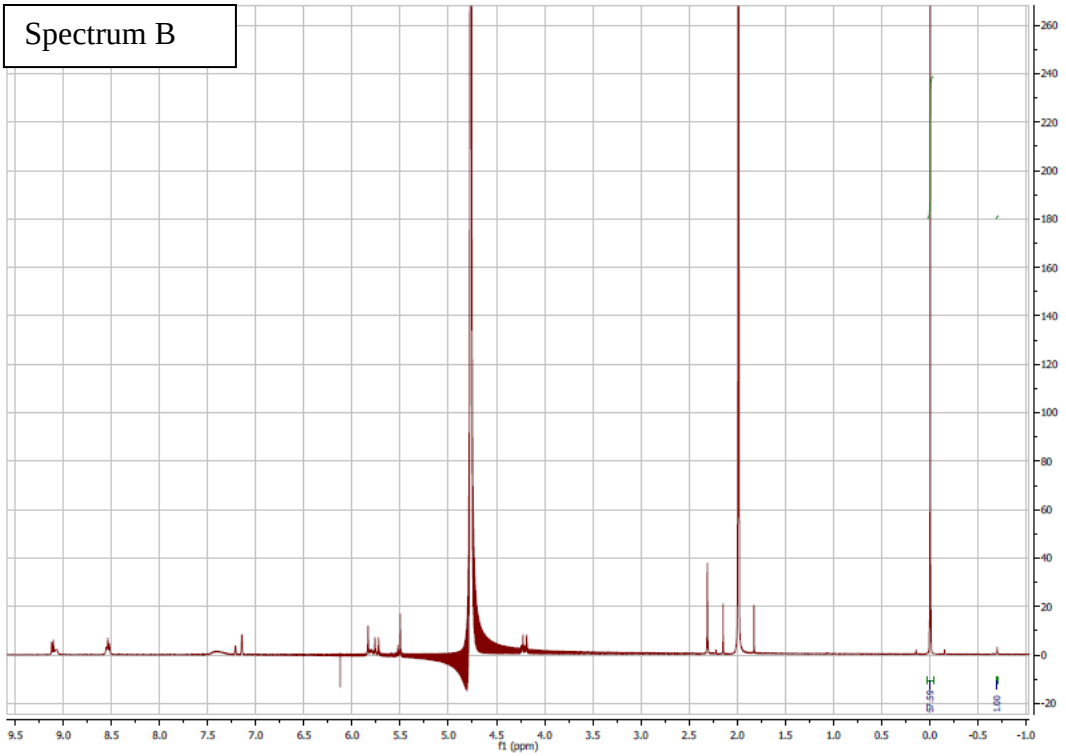

Spectrum C

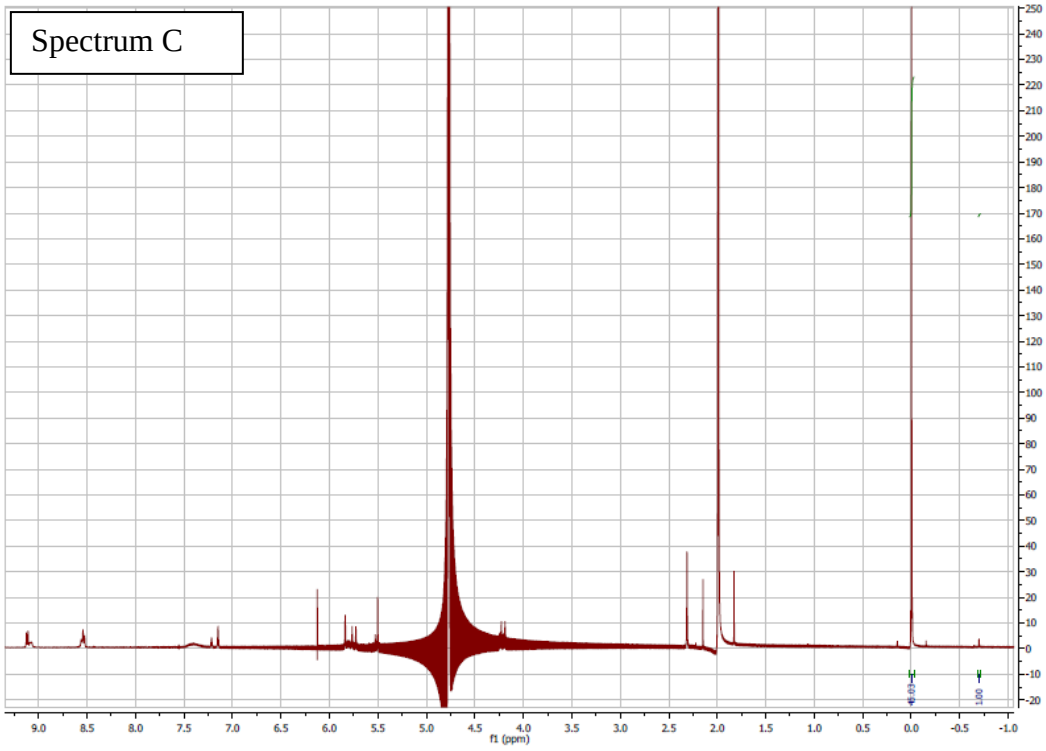

^{1}H-NMR stability study of 17. The equilibrium binding constant of 1-benzyl-1'-(3,5-dimethoxybenzyl)-4,4'-bipyridine-1,1'-diium bromide **17** with cucurbit[7]uril CB[7] was determined by analyzing the competitive binding of **17** compared to that of the reference compound $(Me)_3SiCD_2CD_2COOH$ **22** using ^{1}H-NMR (400 MHz). The stabilitiy constant of the 1 : 1 adduct of CB[7] and **22**[21] is $K = (1.5\pm1.1)\times10^8$ M^{-1}. The procedure followed was developed by Mock and Isaacs[21]. Three solutions of 0.125 mM CB[7], 2.0 mM **22**, and 0.5 mM **17** were prepared in 50 mM $Na(O_2CCD_3)$-buffered D_2O (pD = 4.5). **22** demonstrated slow exchange kinetics on the NMR time scale resulting in clear peaks for bound and unbound **22** at -0.7 and 0.0 ppm, respectively. From the average of ratios of the bound and unbound **22** of three solutions (which was determined with a ±36 % std. dev.), we determined the binding constant of **17** : CB[7] 1 : 1 to be $K_1 = (1.5\pm1.1)\times10^8$ M^{-1}. Error analysis was carried out according to literature.[21]

Figure 73. ^{1}H NMR competition studies compound **17**

Spectrum A

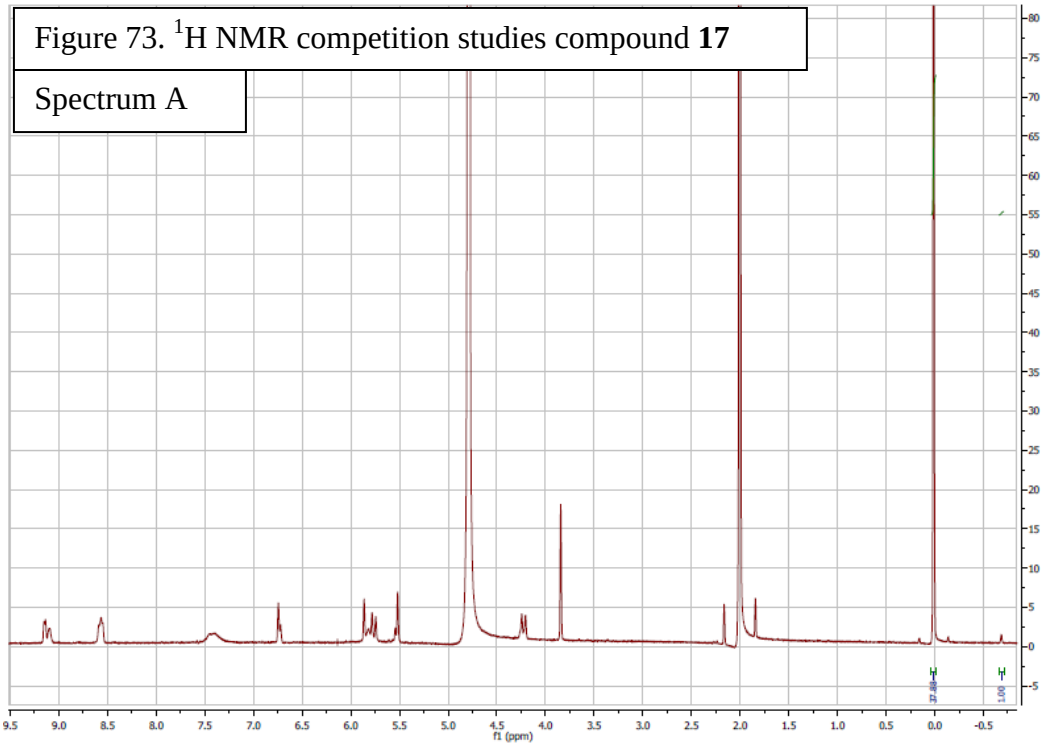

Spectrum B

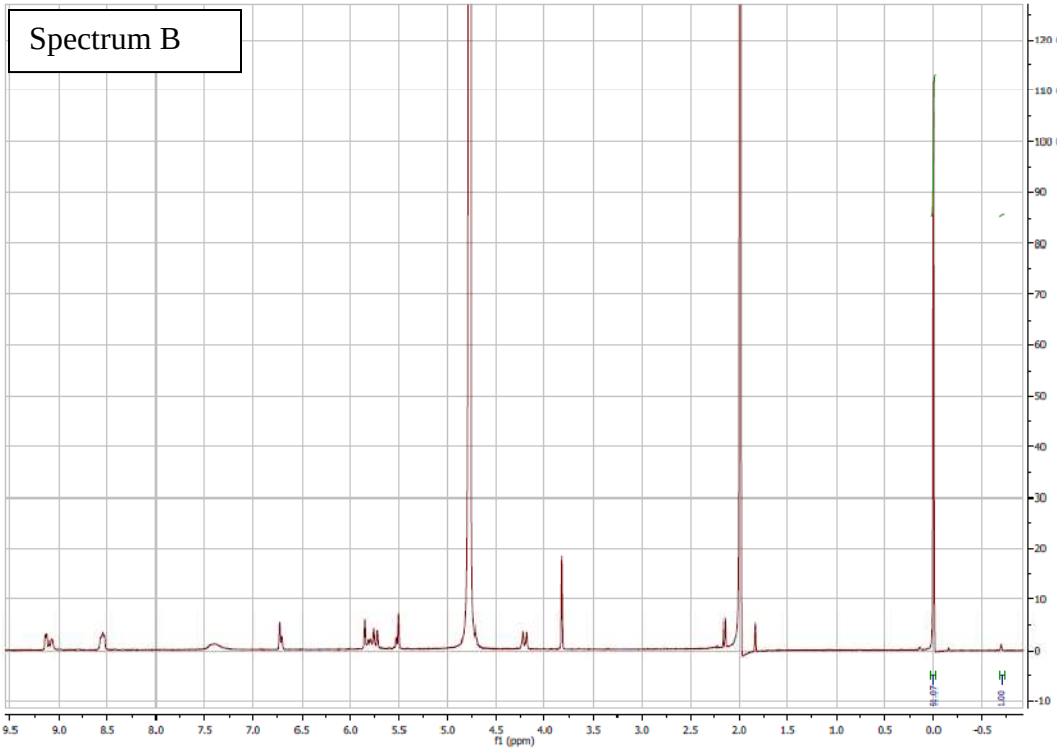

Spectrum C

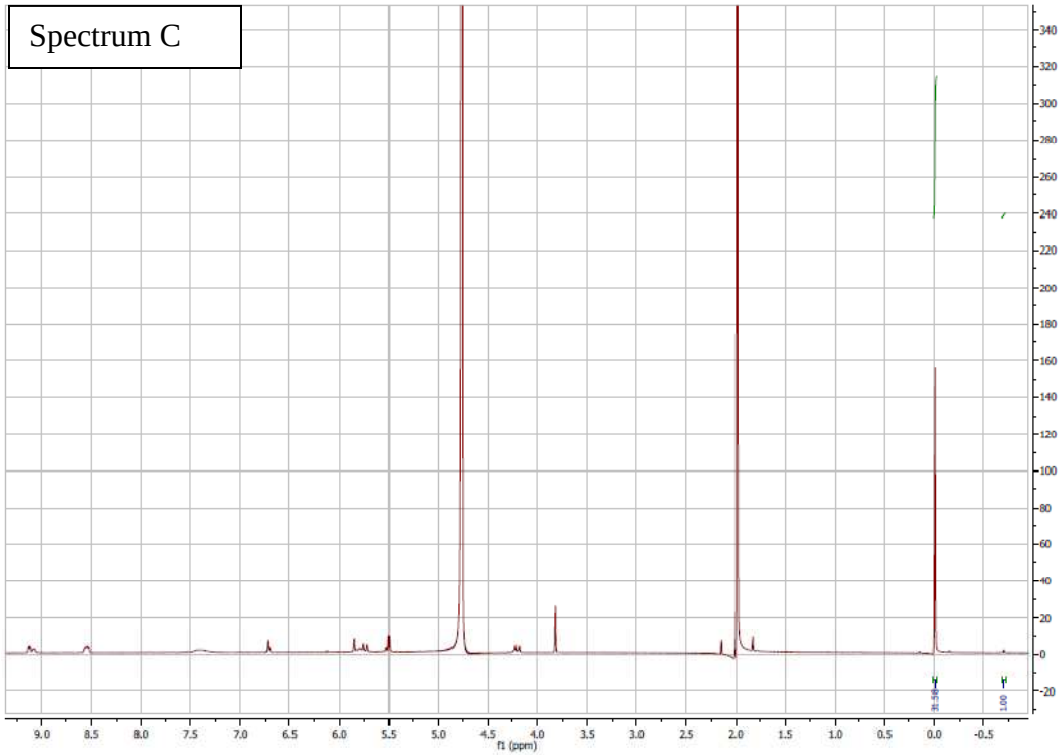

^{1}H-NMR stability study of 18. The equilibrium binding constant of 1-benzyl-1'-(2-(2-(2-methoxyethoxy)ethoxy)ethyl)-4,4'-bipyridine-1,1'-diium bromide **18** with cucurbit[7]uril CB[7] was determined by analyzing the competitive binding of **18** compared to that of the reference compound $(Me)_3SiCD_2CD_2COOH$ **22** using ^{1}H-NMR (400 MHz). The stabilitiy constant of the 1 : 1 adduct of CB[7] and **22**[21] is $K = (1.8\pm0.2)\times10^7\ M^{-1}$. The procedure followed was developed by Mock and Isaacs[21]. Three solutions of 0.125 mM CB[7], 2.0 mM **22**, and 0.5 mM **18** were prepared in 50 mM $Na(O_2CCD_3)$-buffered D_2O (pD = 4.5). **22** demonstrated slow exchange kinetics on the NMR time scale resulting in clear peaks for bound and unbound **22** at -0.7 and 0.0 ppm, respectively. From the average of ratios of the bound and unbound **22** of three solutions (which was determined with a ±3 % std. dev.), we determined the binding constant of **18** : CB[7] 1 : 1 to be $K_1 = (1.2\pm0.8)\times10^7\ M^{-1}$. Error analysis was carried out according to literature.[21]

Figure 74. ^{1}H NMR competition studies compound **18**

Spectrum A

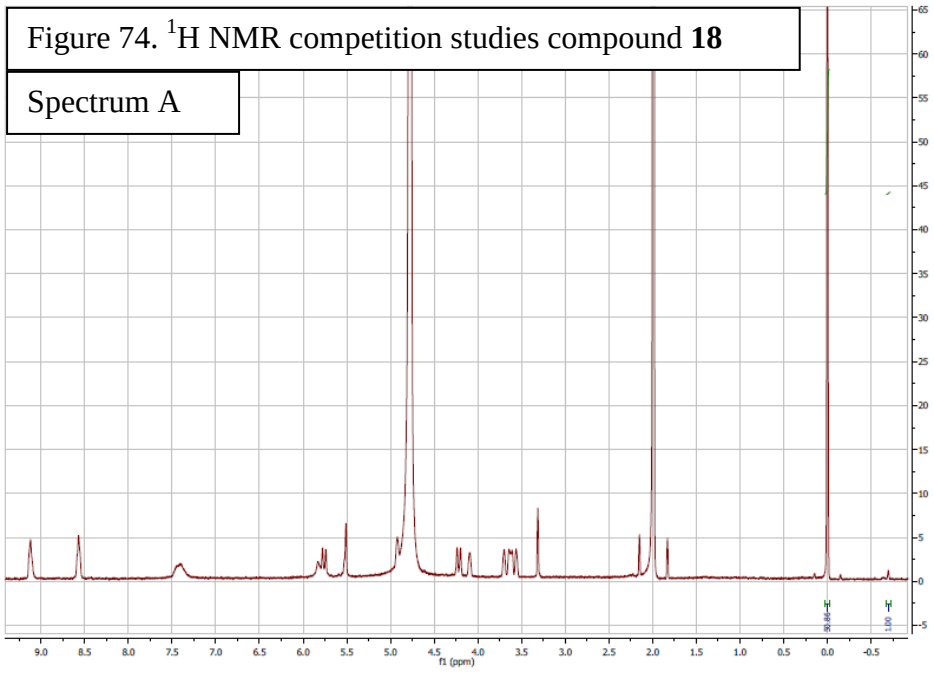

Spectrum B

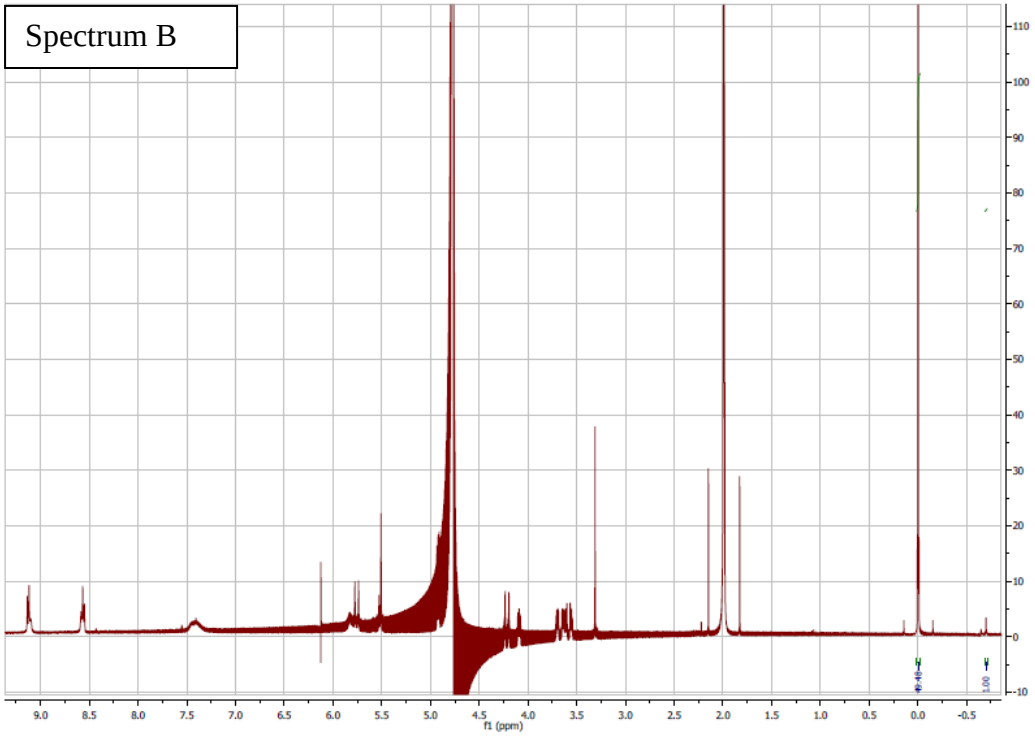

Spectrum C

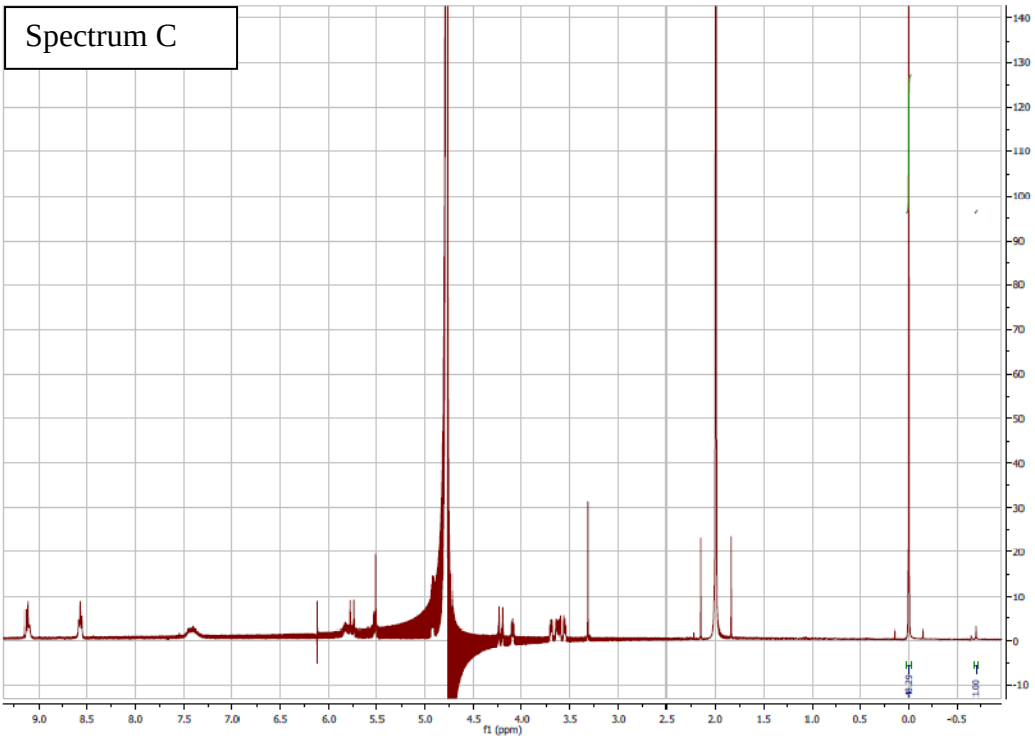

^{1}H-NMR stability study of 19. The equilibrium binding constant of 1-tri(ethylene-glycol)-1'-methyl-m-xylyl-4,4'-bipyridinium dication **19** with cucurbit[7]uril CB[7] was determined by analyzing the competitive binding of **19** compared to that of the reference compound $(Me)_3SiCD_2CD_2COOH$ **22** using ^{1}H-NMR (400 MHz). The stabilitiy constant of the 1 : 1 adduct of CB[7] and **22**[21] is $K = (1.82\pm0.22)\times10^7\ M^{-1}$. The procedure followed was developed by Mock and Isaacs[21]. Three solutions of 0.125 mM CB[7], 0.50 mM **22**, and 4.0 mM **22** were prepared in 50 mM $Na(O_2CCD_3)$-buffered D_2O (pD = 4.5). **22** demonstrated slow exchange kinetics on the NMR time scale resulting in clear peaks for bound and unbound **22** at -0.7 and 0.0 ppm, respectively. From the average of ratios of the bound and unbound **22** of three solutions (which was determined with a ±10 % std. dev.), we determined the binding constant of **19** : CB[7] 1 : 1 to be $K_1 = (6.9\pm1.6)\times10^5$. Error analysis was carried out according to literature.[21]

Figure 75. ^{1}H NMR competition studies compound **19**

Spectrum A

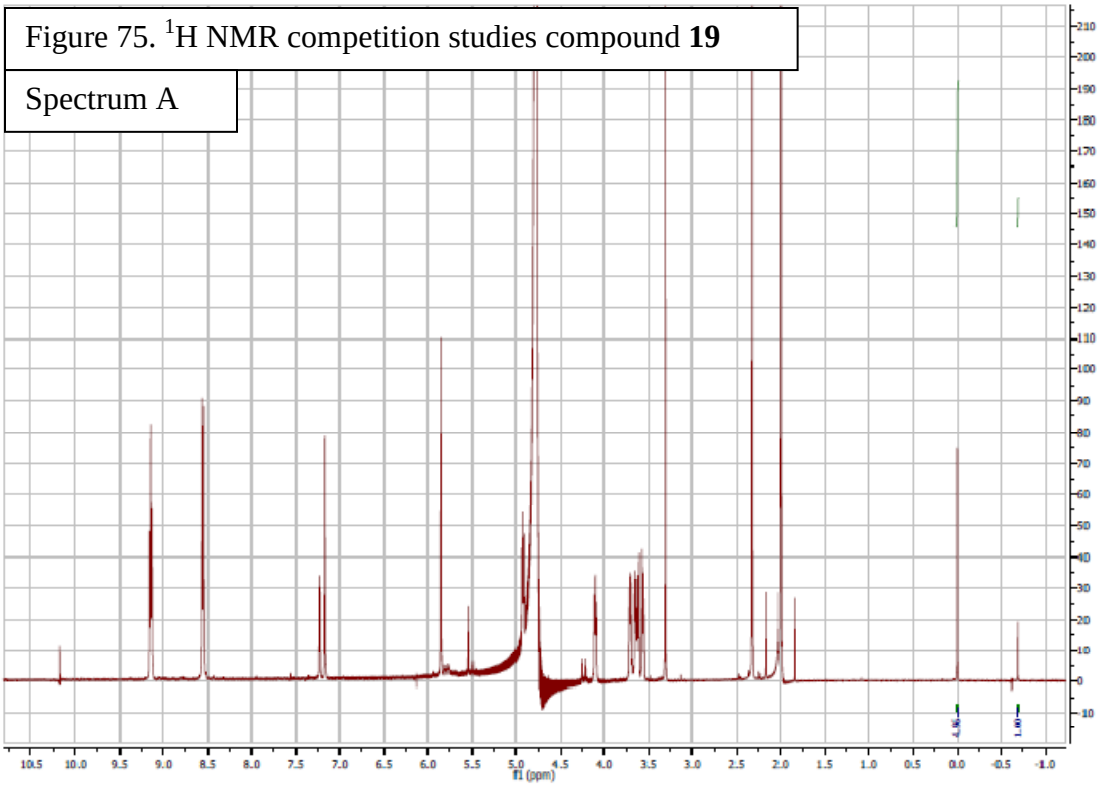

Spectrum B

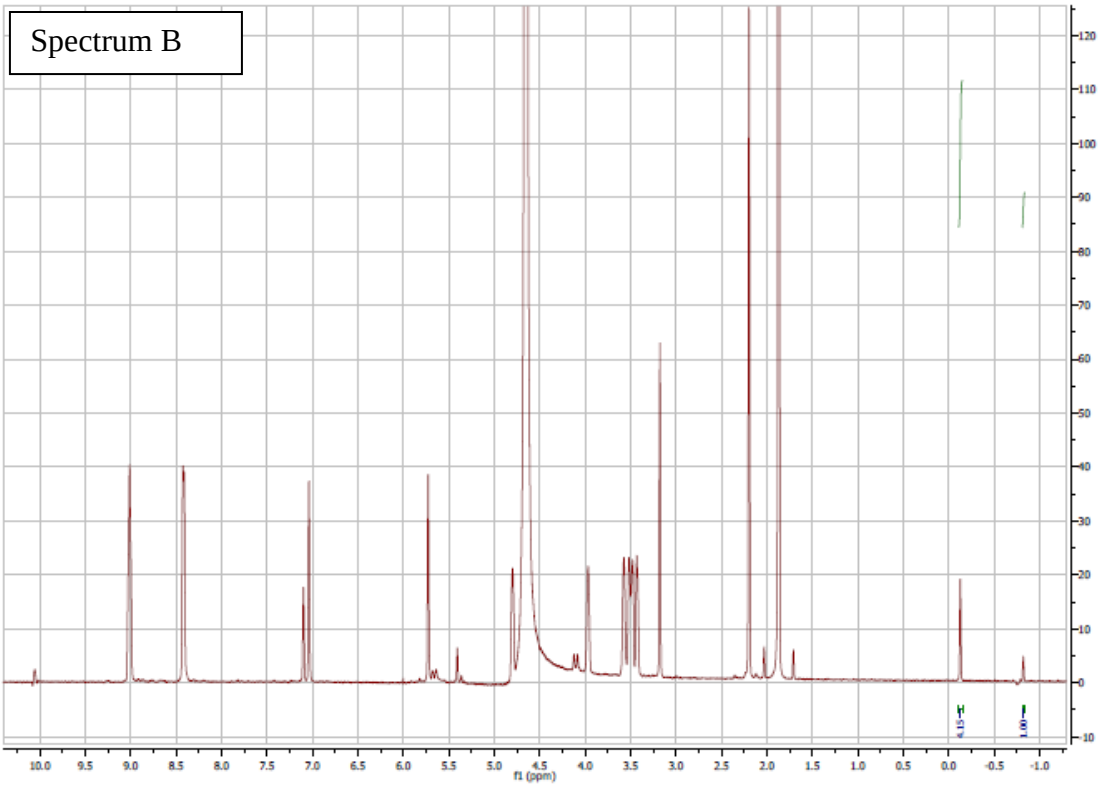

Spectrum C

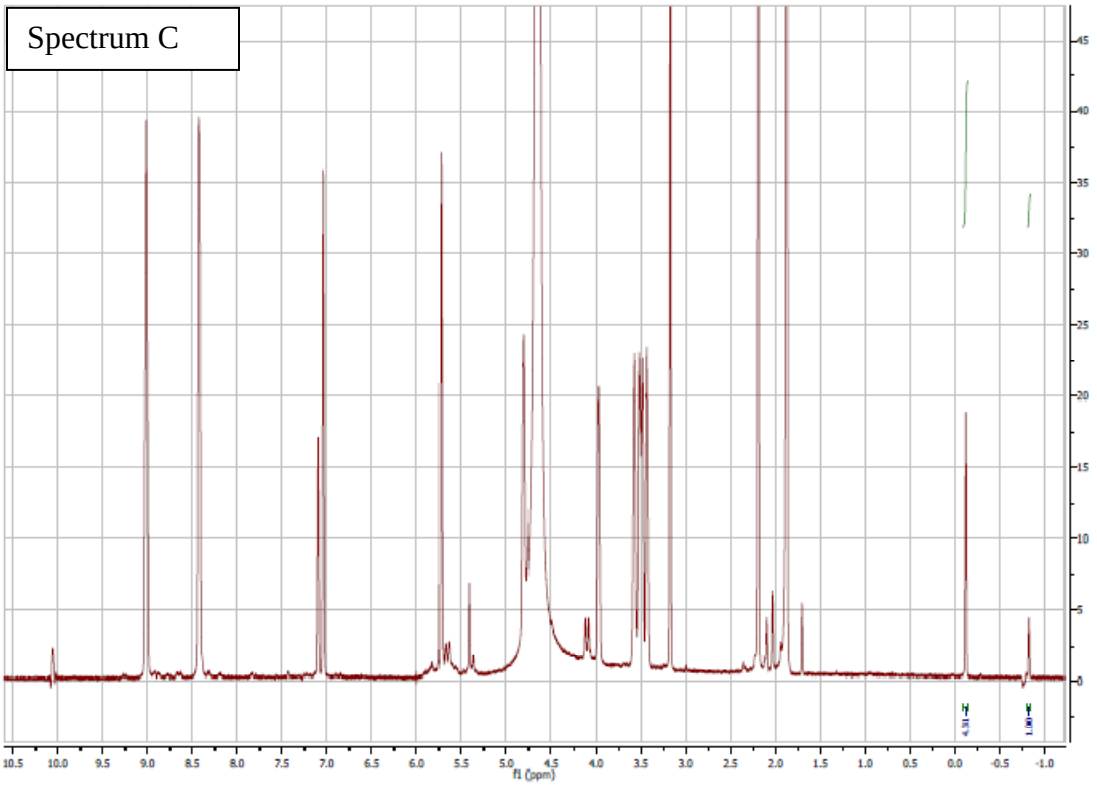

^{1}H-NMR stability study of 12. The equilibrium binding constant of 1-benzyl-4-(pyridin-4-yl)pyridinium bromide **12** with cucurbit[7]uril CB[7] was determined by analyzing the competitive binding of **12** compared to that of the reference compound $(Me)_3SiCD_2CD_2COOH$ **22** using ^{1}H-NMR (400 MHz). The stabilitiy constant of the 1 : 1 adduct of CB[7] and **22**[21] is $K = (6.6\pm1.4)\times10^7\ M^{-1}$. The procedure followed was developed by Mock and Isaacs[21]. Three solutions of 0.125 mM CB[7], 2.0 mM **22**, and 0.5 mM **12** were prepared in 50 mM $Na(O_2CCD_3)$-buffered D_2O (pD = 4.5). **22** demonstrated slow exchange kinetics on the NMR time scale resulting in clear peaks for bound and unbound **22** at -0.7 and 0.0 ppm, respectively. From the average of ratios of the bound and unbound **22** of three solutions (which was determined with a ±9 % std. dev.), we determined the binding constant of **12** : CB[7] 1 : 1 to be $K_1 = (6.6\pm1.4)\times10^7$. Error analysis was carried out according to literature.[21]

Figure 76. ^{1}H NMR competition studies compound **12**

Spectrum A

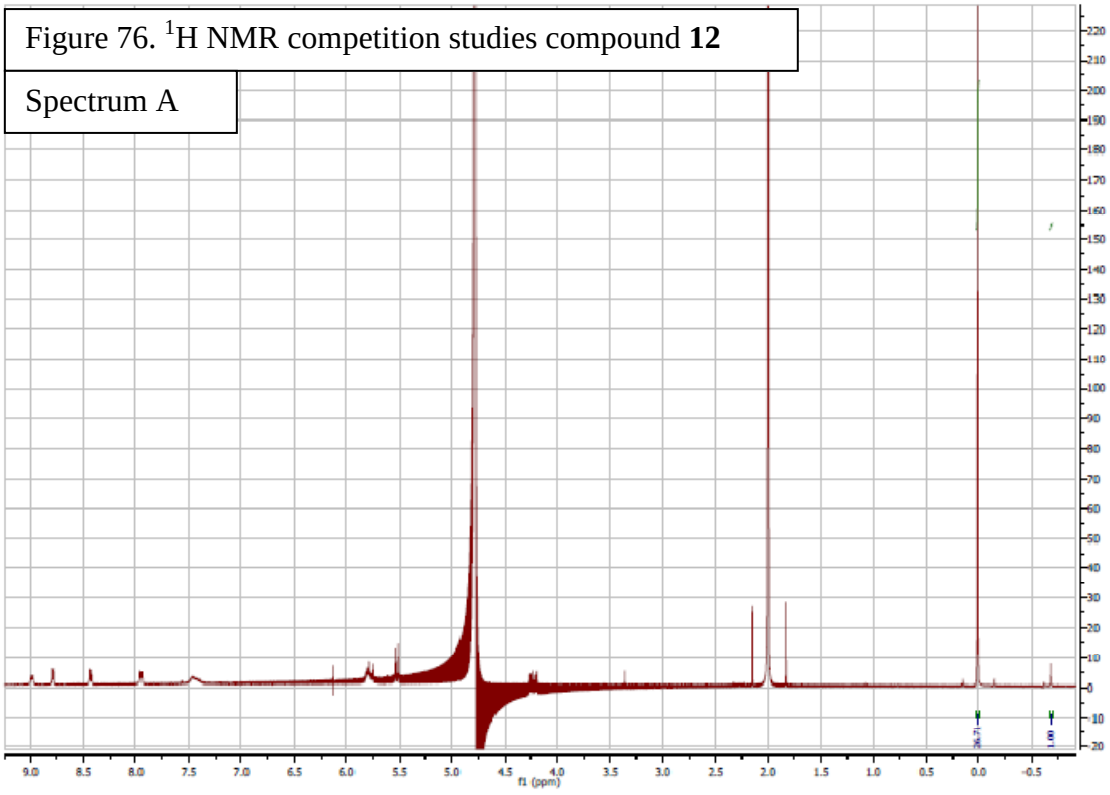

Spectrum B

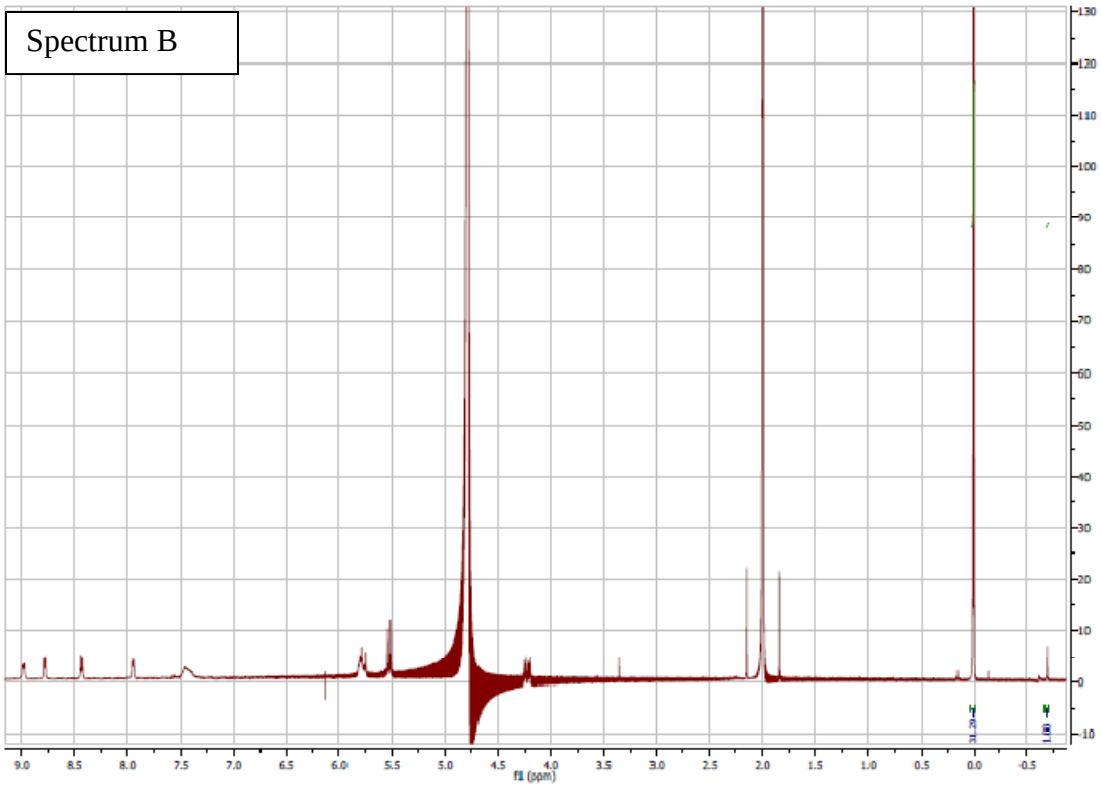

Spectrum C

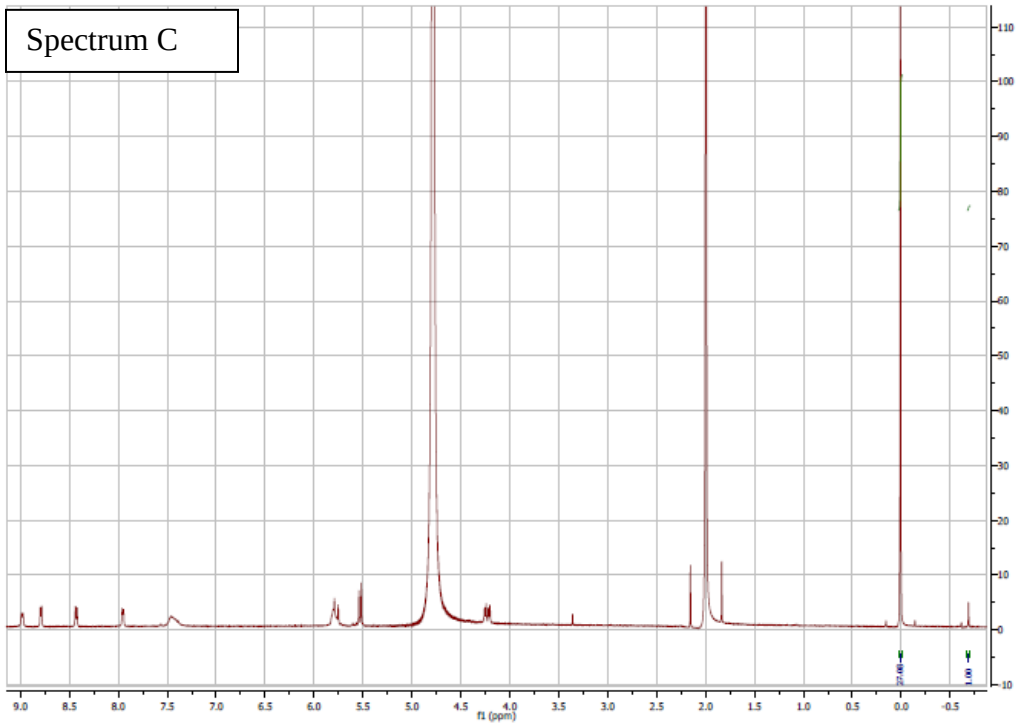

^{1}H-NMR stability study of 13. The equilibrium binding constant of 1-(3,5-dimethylbenzyl)-4-(pyridin-4-yl)pyridinium **13** with cucurbit[7]uril CB[7] was determined by analyzing the competitive binding of **13** compared to that of the reference compound $(Me)_3SiCD_2CD_2COOH$ **22** using ^{1}H-NMR (400 MHz). The stabilitiy constant of the 1 : 1 adduct of CB[7] and **22**[21] is $K = (7.9\pm1.4)\times10^{5}$ M^{-1}. The procedure followed was developed by Mock and Isaacs[21]. Three solutions of 0.125 mM CB7, 0.5 mM **22**, and 4.0 mM **13** were prepared in 50 mM $Na(O_2CCD_3)$-buffered D_2O (pD = 4.5). **22** demonstrated slow exchange kinetics on the NMR time scale resulting in clear peaks for bound and unbound **22** at -0.7 and 0.0 ppm, respectively. From the average of ratios of the bound and unbound **22** of three solutions (which was determined with a ±7 % std. dev.), we determined the binding constant of **13** : CB[7] 1 : 1 to be $K_1 = (7.9\pm1.4)\times10^{5}$ M^{-1}. Error analysis was carried out according to literature.[21]

Figure 77. ^{1}H NMR competition studies compound **13**

Spectrum A

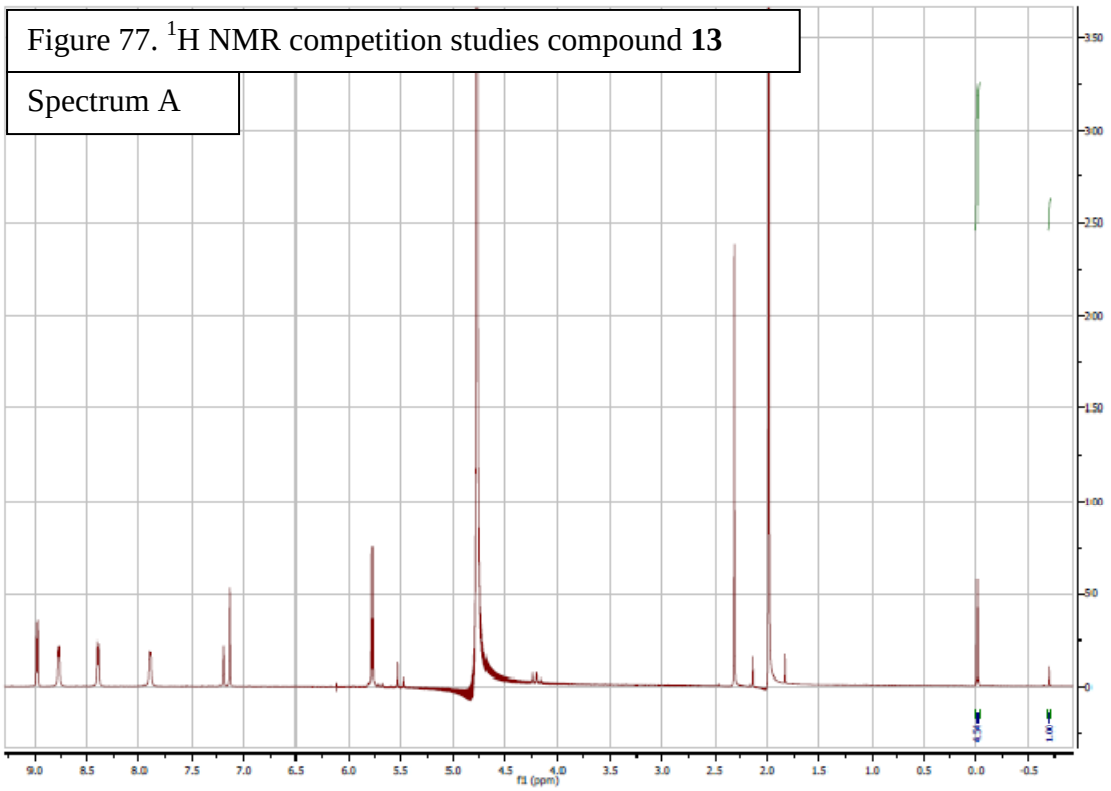

Spectrum B

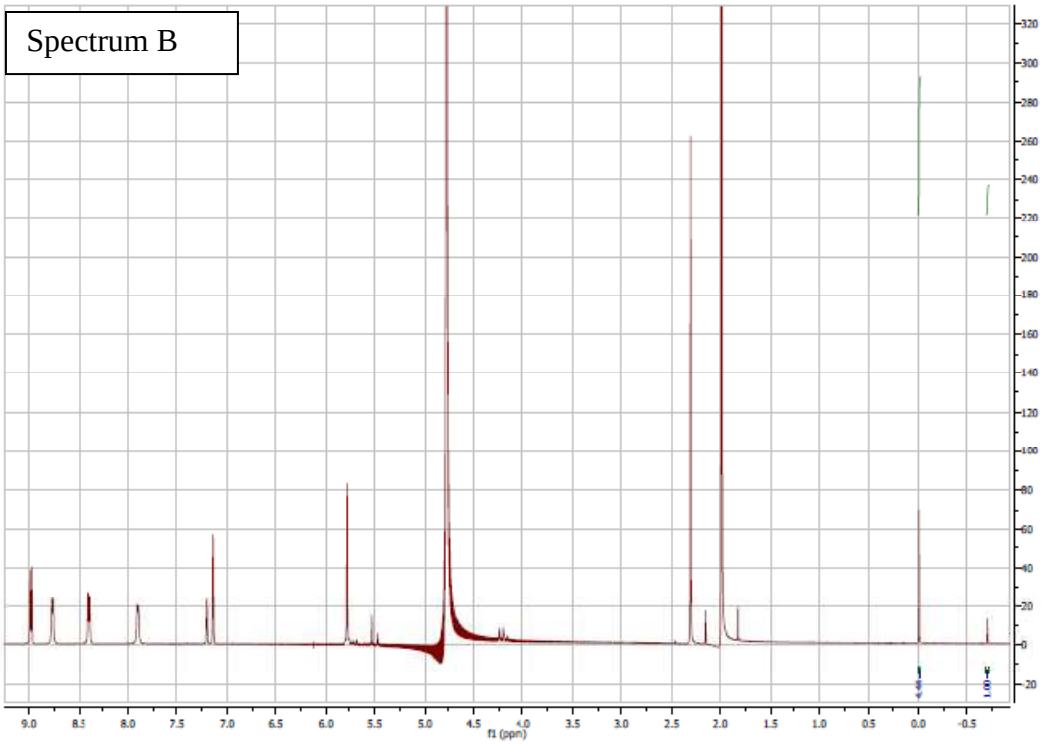

Spectrum C

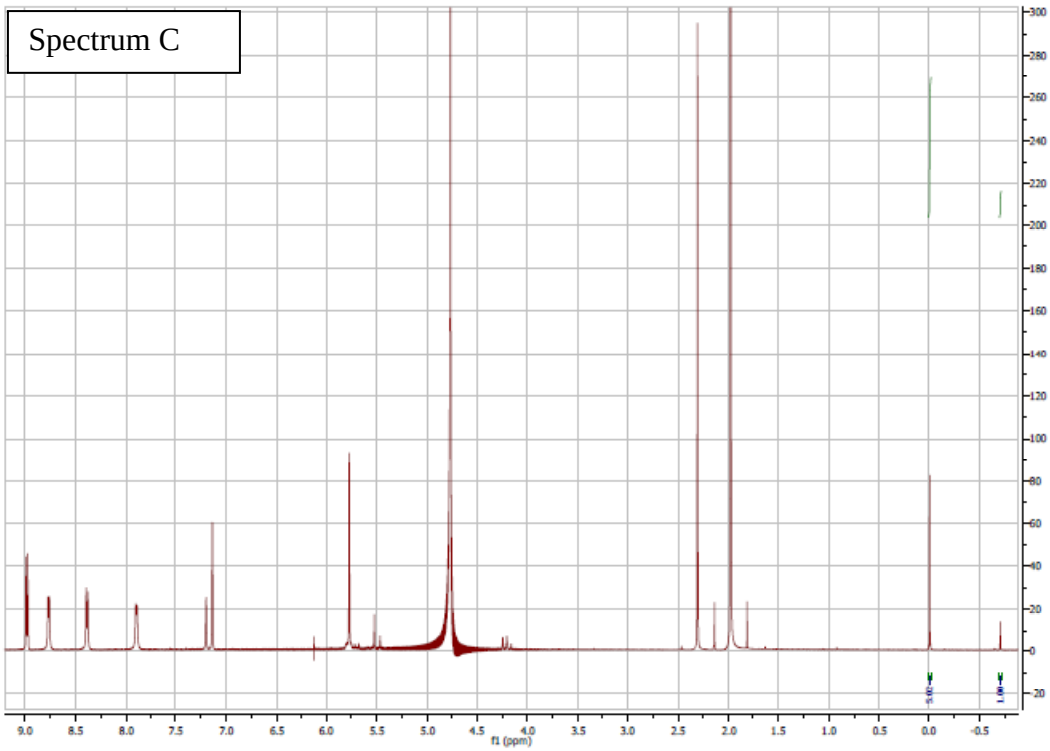

^{1}H-NMR stability study of 14. The equilibrium binding constant 1-(3,5-dimethoxybenzyl)-4-(pyridin-4-yl)pyridinium **14** with cucurbit[7]uril CB[7] was determined by analyzing the competitive binding of **14** compared to that of the reference compound $(Me)_3SiCD_2CD_2COOH$ **22** using ^{1}H-NMR (400 MHz). The stabilitiy constant of the 1 : 1 adduct of CB[7] and **22**[21] is $K = (1.8\pm0.2)\times10^7$ M^{-1}. The procedure followed was developed by Mock and Isaacs[21]. Three solutions of 0.125 mM CB[7], 0.5 mM **22**, and 4.0 mM **14** were prepared in 50 mM $Na(O_2CCD_3)$-buffered D_2O (pD = 4.5). **22** demonstrated slow exchange kinetics on the NMR time scale resulting in clear peaks for bound and unbound **22** at -0.7 and 0.0 ppm, respectively. From the average of ratios of the bound and unbound **22** of three solutions (which was determined with a ±12 % std. dev.), we determined the binding constant of **14** : CB[7] 1 : 1 to be $K_1 = (1.8\pm0.2)\times10^7$ M^{-1}. Error analysis was carried out according to literature.[21]

Figure 78. ^{1}H NMR competition studies compound **14**

Spectrum A

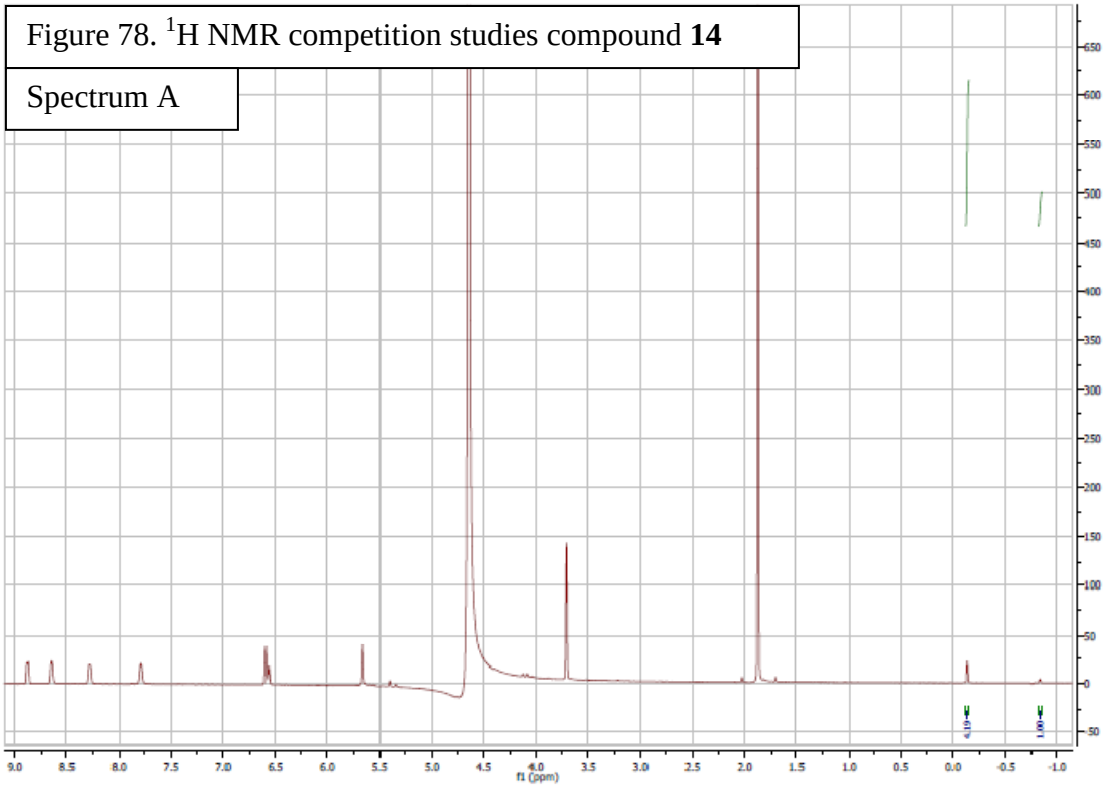

Spectrum B

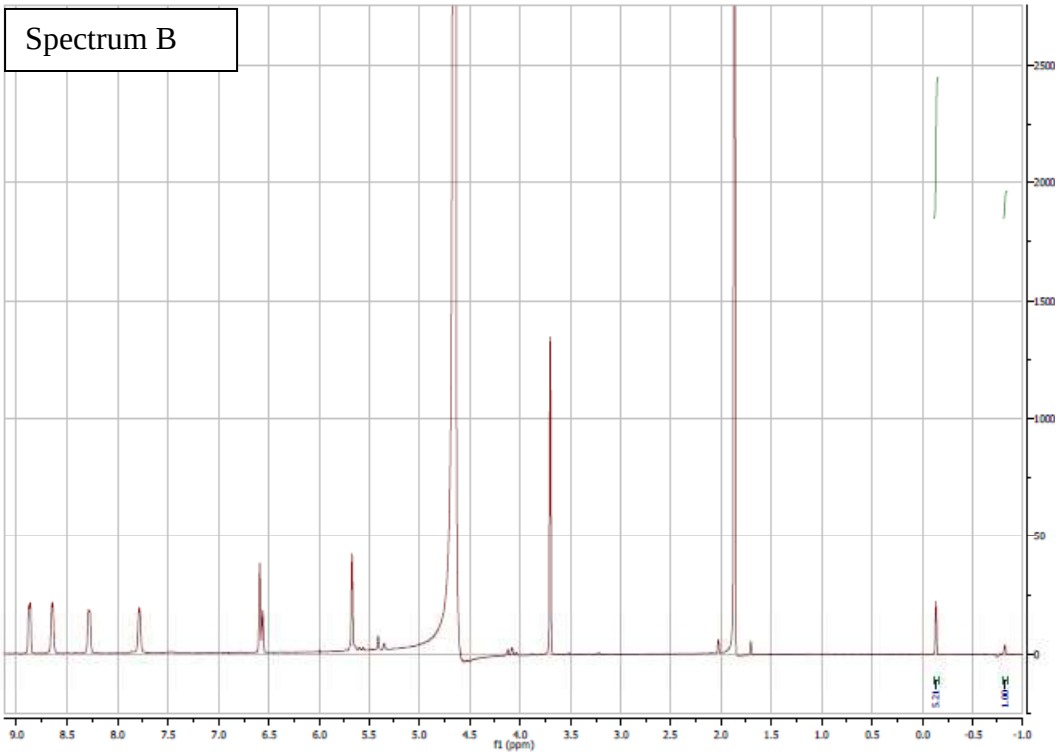

Spectrum C

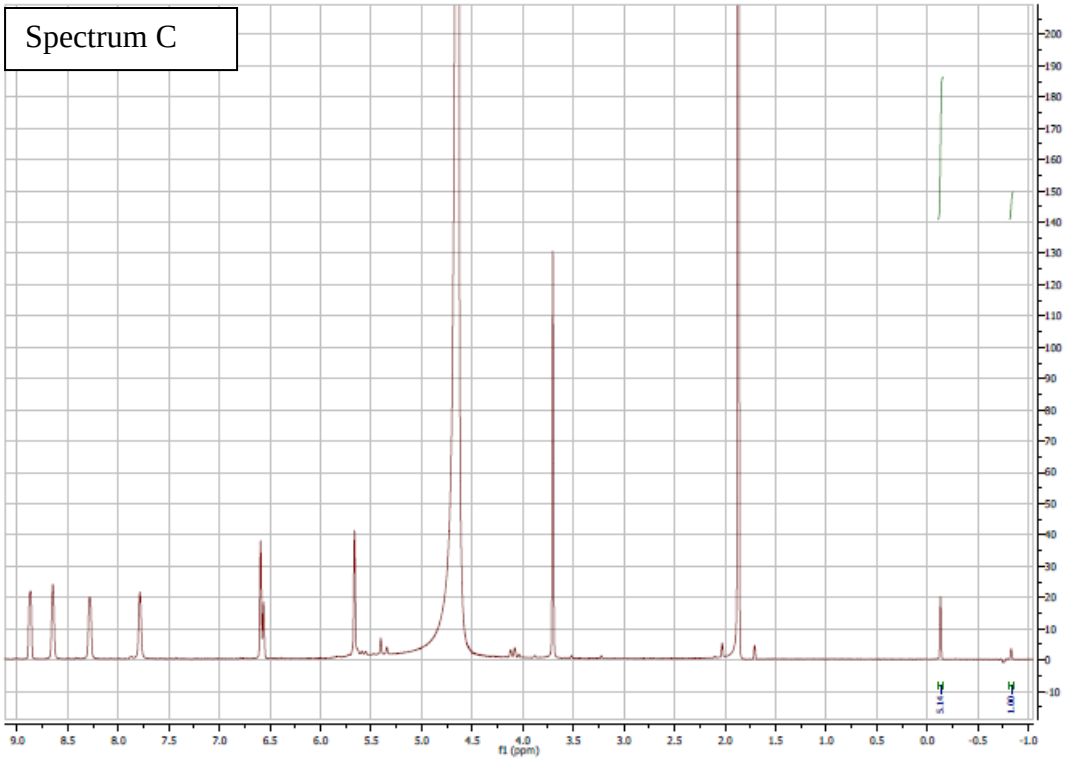

Chemicals and solutions. Ion exchanged and MILLIPORE ultrafiltered (Milli-Q synthesis A10) water was used to prepare all solutions. Acetate buffers (pH = 4.5) were made from NaOAc and $HClO_4$. An Orion Sure-Flow Ross combined-pH electrode attached to an Orion Expandable ionAnalyzer E920 was employed for the pH measurements. The electrode was calibrated following IUPAC recommendations. For UV-vis absorbance measurements an HP8452A diode array photometer and a cell with 1.00 cm pathlength were used.

Stopped-flow technique. Stopped-flow experiments were performed using a Hi-Tech SF-61 DX2 instrument equipped with both a photomultiplier tube (PMT) for single-wavelength detection and a diode-array for multiple wavelength detection. A reference PMT is employed in this instrument. Absorbance traces were collected using a Xe arc lamp and an optical cell with a 1.00 cm pathlength. The dead-time of the stopped-flow instrument was measured by the reaction of 2,6-dichlorophenol-indophenol (DCIP) with ascorbic acid (AA) under pseudo-first order conditions with AA in excess. By plotting the experimentally obtained k_{obs} values against [AA], deviation from linearity was observed above $k_{obs} = 600\ s^{-1}$ for the High-Tech instrument, which means that higher k_{obs} values can be determined only with the slight elevation of relative error. The dead time of the High-Tech instrument is 1.35±0.03 ms. The timescale of the recorded stopped-flow kinetic curves was corrected with the dead time of the instrument which enhanced the precision of further data treatment (e.g. mathematical data fitting) The temperature during all the stopped-flow measurements

was maintained at 25.0±0.1 ºC using Lauda RC-20 circulators equipped with chilled water heat exchangers.

DEDUCTION OF THE INTEGRATED RATE LAW (SIMPLE MODEL)

The simplest one-step kinetic model, which describes the equlibrium formation, is the following:

1) $V + CB7 \rightarrow V{\cdot}CB7$ with: k_1

-1) $V{\cdot}CB7 \rightarrow V + CB7$ with: k_{-1}

The differential rate law and the expression of the equilibrium constant is:

$$\frac{d[V]}{dt} = -k_1[V][CB7] + k_{-1}[V \cdot CB7] \quad \text{and} \quad K_1 = \frac{k_1}{k_{-1}} = \frac{[V \cdot CB7]_{Eq}}{[V]_{Eq}[CB7]_{Eq}} \qquad (1)$$

and (2)

where square brackets indicate time dependent actual concentrations, and $[V]_{Eq}$, $[CB7]_{Eq}$, $[V{\cdot}CB7]_{Eq}$ are the corresponding equilibrium concentrations under the applied conditions. The integrated rate law can be deduced by introducing *x* as the time dependent concentration which shows the distance of the system from equilibrium at a given instance:

$[V]=[V]_{Eq}+x$
$[CB7]=[CB7]_{Eq}+x$
$[V \cdot CB7]=[V \cdot CB7]_{Eq}-x$

By substituting *x* into eq. 1 and integrating, one obtains:

$$\frac{x\left(\xi+k_1[V\cdot CB7]_{Eq}\right)}{[V\cdot CB7]_{Eq}\left(\xi+k_1 x\right)}=\exp\left(-\xi t\right) \qquad \text{where:} \quad \xi=k_1\left([V]_{Eq}+[CB7]_{Eq}\right)+k_{-1}[V\cdot CB7]_{Eq}$$

(S1)

Because the reaction is fast even on the stopped-flow time scale, only the last 30 – 60 % of the process can be followed, where *x* is already small compared to the equilibrium concentrations ($[V]_{Eq}$, $[CB7]_{Eq}$ and $[V\cdot CB7]_{Eq}$) under the applied conditions. Therefore $\xi >> k_1 x$ is fulfilled and the rate equation becomes a special case:

$$[V]=[V]_{Eq}+\frac{\xi[V\cdot CB7]_{Eq}}{\xi+k_1[V\cdot CB7]_{Eq}}\exp\left(-\xi t\right)$$

(3)

which is a single exponential expression.

Chapter 5: Conclusion

The study of technology at the molecular level is the perhaps the final frontier in materials science, and is fertile ground for the application of supramolecular chemistry. In particular, this study has highlighted the reasons that the application of cucurbit[7]uril should be dominating this emerging field. First, CB[7] can bind a wide range of small molecules with high equilibrium binding constants. Not only has this study increased the library of kinetic data of known compounds that can be encapsulated by CB[7], but it has strategically chosen those compound to contain the fascinating properties of viologens with usable equilibrium binding constants in the range of 10^5-10^8 M^{-1}, allowing for future strategic incorporation of these compounds in molecular sensors and shuttles. These studies have in addition set the precedent for studying the on and off kinetics of CB[7] with high accuracy via stop flow techniques. Further, these studies were foundational to efforts by Dr. Anuradha Singh to develop a quencher flourophore dyad consisting of viologen and BODIPY.

In addition, this study has confirmed and advanced the knowledge that encapsulation by CB[7] often enhances the properties of its guest or provides some type of protective effect. It has been clearly demonstrated that fluorescent dyes Rhodamine B and Pyronin Y are protected from photedegradation during the harsh cycling of current provided by CV. This is significant because molecular machines can be stimulated by redox and this will be a factor in the upcoming years.

Excitingly, these studies confirmed many of the viologen/CB[7] binding mode theories put forward by Dr. Kaifer that predict whether a viologen will bind in an internal or external position. Ultimately, external binding will always be observed if the

viologen substituent is hydrophobic enough, but sterically hindered and electronegative groups will upset the delicate balancing act in favor of internal binding. These position predictions are vital not only to the successful creation of a rotaxane, but could potentially be useful to elicit desirable properties from rotaxanes and pseudo-rotaxanes. The studies in this paper suggest a third mode of binding that is unique to internal and external binding, a condition referred to 'capping' throughout this study in reference to the 3,5-dimethyl viologen compounds.

Another major success of this research was to establish two effective stoppering groups of 3,5-dimethylbenzyl and 3,5-methoxybenzyl. Unfortunately these compounds were not proven to be able to achieve the rotaxane-closing reaction, but certainly they were proven to be too bulky for CB[7] to shuttle over, and so could be used as a stoppering group on one side of a rotaxane, particularly in longer axle that incorporates triethylene glycol functionality. The evidence for this that was provided in chapter 3 was further enforced in chapter 4 during the analysis of the binding mode of the cancer model. Additionally, these moieties determined the binding mode of CB[7] by their steric bulk and/or electronics, thus it is probable that they would be partially in control of the effectiveness of whatever molecular device they are incorporated into in the future.

Unfortunately, there were limitations to the knowledge gained in this study due to some of the drawbacks of cucurbit[7]uril. In particular, the successful attachment of a fluorescent dye to the surface of ITO in the presence of CB[7] was not attainable due to the lack of attachment of CB[7] to the system through a rotaxane or direct chemical linkage. This highlights the need for increased study to functionalize CB[7] so that it

can be permanently attached to wherever it needs to be. In addition, CB[7] is limited by its lack of solubility in non aqueous solvents which causes the formation of needed rotaxanes to be unnecessarily cumbersome. However, I am hesitant to suggest future studies in the area of getting CB[7] more soluable in organic solvents, becuase the majority of its allure lies in its high equilibrium binding constants largely obtained through hydrophobic interactions. Therefore, I think science would be better served in pursuing more water-friendly chemistry in the image of protein chemical transformations.

In conclusion, the studies herein have gathered sound data supporting the use of cucurbit[7]uril in a variety of molecular scale devices. Not only has previously held knowledge about the interactions of this macrocycle been confirmed, but the results here have increased the sphere of knowledge and may also inform future studies in this promising field.

References

1. a) Day, A.; Arnold, A. P.; Blanch, R.J.; Snushall, B. "Highly Symmetric columnar channels in metal-free cucurbit[n]uril hydrate crystals (n=6,8)." *Journal of Organic Chemistry*. **2001.** *66*, 8094. b) Kim, J.; Jung, I.; Kim, S. E.; Kang, J.; Sakamoto, S.; Yamaguchi, K.; Kim, K. "New Cucurbituril Homologues: Syntheses, isolation, Characterization, and X-ray Crystal Structures of Cucurbit[n]uril (n=5, 7, and 8)."*Journal of the American Chemical Society*. **2000**.*122*, 540. c) Lagona, J.; Mukhopadhyay, P.; Chakrabarti, S,; Isaacs, L. "The Cucurbit[n]uril Family." *Angewandte Chemie, Int. Ed*. **2005**. *44*, 4844.

2. a) Spencer, N.; Stoddart, J. F.; Anelli, P. L. "A molecular shuttle." *J. Am. Chem. Soc.* **1991**. *113*, 5131 – 5133. Spencer, N.; b) Stoddart, J. F.; Anelli, P. L. "A molecular shuttle." *J. Am. Chem. Soc.* **1991**. *113*, 5131 – 5133 c) Aricó, F.; Badjic, J.; Cantrill, S.; Flood, A.; Leung, K.; Liu, Y.; Stoddart, J. F. "Templated Synthesis of Interlocked Molecules". *Topics in Current Chemistry.* **2005**. *249*, 203–259. d) Terada, K.; Kobayashi, K.; Haga, M. "Synthesis, electrochemical, and molecular inclusion properties of 'canopied' trinuclear ruthenium complexes with six anchoring groups on an ITO electrode." *Dalton Trans. **2008***. 4846–4854.

3. a)Vladimir Sindelar, V.; Moon, K.; Kaifer, A. "Binding Selectivity of Cucurbit[7]uril: Bis(pyridinium)-1,4-xylylene versus 4,4-Bipyridinium Guest Sites."*Organic Letters.* **2004.** *16*, 2665-2668. b) Eelkema, R.; Maeda, K.; Odell, B.; Anderson, H. L. "Radical Cation Stabilization in a Cucurbituril Oligoaniline Rotaxane." *J. Am. Chem. Soc*. **2007**. *129*, 12384-12385.

4. a) Kalyanasundaram, K. *; Gratzel, M. "Applications of functionalized transition metal complexes in photonic and optoelectronic devices." *Coordination Chemistry Reviews.***1998**. *77*, 347–414. b) Gratzel, M. *Inorganic Chemistry.***2005**. *44*,6841.

5. a) Hardin, B. E.; Snaith, H. J.; McGehee, M. D. "The renaissance of dye-sensitized solar cells." *Nature photonics*. **2012**. *6*, 162-169. b) Karstens, T.; Kobs, K. "Rhodamine B and Rhodamine 101 as reference substances for fluorescence quantum yield measurements." *J. Phys. Chem.* **1980**. *84*, 1871-1872. c) Kellogg, R. E.; Bennett, R. G. "Radiationless intermolecular energy transfer. III. Determination of phosphorescence efficiencies." *J. Chem. Phys.* **1964**. *41*, 3042-3045. d) Kubin, R. F.; Fletcher, A. N. "Fluorescence quantum yields of some rhodamine dyes.*" J. Luminescence*. **1982**. *27*, 455-462. e) López A. F.; Ojeda, P. R.; Arbeloa, I. L. "Fluorescence self-quenching of the molecular forms of rhodamine B in aqueous and ethanolic solutions." *J. Luminesc.* **1989**. *44*, 105-112. f) Snare, M. J.; Treloar, F. E.; Ghiggino, K. P.; Thistlethwaite, P. J. "The photophysics of rhodamine B." *J. Photochem.***1982**. *18*, 335-346.

6. a) Nazeeruddin, P. P.; Pechy, P.; Renouard, T.; Zakeeruddin, S. M.; Humphry-Baker, R.; Comte, P.; Liska, {.; Cevey, L.; Costa, E.; Shklover, V.; Spiccia, L.; Deacon, G. B.;

Bignozzi, C. A.; Gratzel, M. "Engineering of Efficient Panchromatic Sensitizers for Nanocrystalline TiO_2- Based Solar Cells." *Journal of the American Chemical Society*.**2001**. *123*, 1613-1624. b) Ooyama, Y.; Harima, Y. "Molecular Designs and Syntheses of Organic Dyes for Dye-Sensitized Solar Cells." *European Journal of Organic Chemistry*.**2009**. *18*, 2903-2914. c) Gao, F. G.; Bard, A. J.; Kispert, L. D. " Photocurrent generated on a carotenoid-sensitized TiO2 nanocrystalline mesoporous electrode" *Journal of Photochemistry and Photobiology A: Chemistry*.**2000**. *130*, 49–56. d) Shan, Y.; Tang, J.; Lai, H.; Tan, H.; Yang, F.; Qiang Fang, Q.; Audebert, P.; Pron, A. "A novel pyridinium hemicyanine dye with carboxylate anchoring group and its application in dye-sensitized solar cells." *Tetrahedron Letters*. **2012**. *53*, 1341–1344. e) Terada, K.; Kobayashi, K.; Haga, M. "Synthesis, electrochemical, and molecular inclusion properties of 'canopied' trinuclear ruthenium complexes with six anchoring groups on an ITO electrode." *Dalton Trans.***2008**, 4846–4854.

7. a) Halterman, R. L.; Moore, J. L.; Mannel, L. M. "Disrupting aggregation of tethered rhodamine B dyads through inclusion in cucurbit[7]uril." *Journal of Organic Chemistry*. **2008**. *73*, 3266. b) Selwyn, J. E.; Steinfeld, J. I."Energy Transfer among combination of Acridine." *Journal of Physical Chemistry*. **1972**.*76*, 762. c) Rohatgi, K.K.; Singhal G. S. "Nature of bonding in Dye Aggregates." *Journal of Physical Chemistry***1966**. *70*, 1695-1701.

8. Ellis, S. B.; Glatzhofer, D. T.; Halterman, R. L. "Photoelectrochemistry of dye-cucurbit[7]uril (CB7) complexes."*Abstracts of Papers, 234th ACS National Meeting*, Boston, MA, United States. August 19-23. **2007**, PHYS 363.

9. Jyotirmayee, J. M.; Nau, W. M. "Ultrastable Rhodamine with Cucurbituril." *Angew. Chem Int*. **2005**. *44*, 3750-3754. Nau W. M.; Mohanty, J. "Taming fluorescent dyes with Cucurbituril." *Int J Photoenergy*. **2005**. *7*, 717.

10. a) DÌez-Gonzalez, S.; Correa, A.; Cavallo, L.; Nolan, S. P. "(NHC)copper(I)-catalyzed [3+2] cycloaddition of axides and mono- or disubstituted alkynes." *Chem. Eur. J.* **2006**. *12*, 7558-7564. b) Kolb, H.; Finn, M.; Sharpless, K. "Click Chemistry: Diverse Chemical Function from a Few Good Reactions". *Angewandte Chemie International Edition* **2001**. *40*, 2004–2021. c) I would like to thank and acknowledge Jason Moore for the synthesis and gift of this catalyst.

11. Alamiry, M.; Harriman, A.; Mallon, L.; Ulrich, G.; Ziessel, R. "Energy- and Charge-Transfer Processes in a Perylene-BODIPY-Pyridine Tripartite Array." *European Journal of Organic Chemistry*. **2008**. *16*, 2774-2782.

12. a) Halterman, R. L.; Moore, J. L.; Yip, W. T. "Cucurbit[7]uril Disrupts Aggregate Formation Between Rhodamine B Dyes Covalently Attached to Glass Substrates." *J Fluoresc.***2011**. *21*, 1467–1478. b) Martyn, T. A.; Moore, J. L.; Halterman, R. L.; Yip,

W. T. "Cucurbit[7]uril induces superior probe performance for single-molecule detection." *J. Am. Chem. Soc.* **2007**. *129*, 10338–10339.

13. Altieri, A.; Bottari, G.; Dehez, F.; Leigh, D. A.; Wong, J. K. Y.; Zerbetto, F. "Remarkable Positional Discrimination in Bistable Light- and Heat Switchable Hydrogen-Bonded Molecular Shuttles." *Angew. Chem. Int. Ed*. **2003**. *42*, 2296-2300.

14. Ashton, P. R.; Ballardini, R.; Balzani, V.; Baxter, I.; Credit, A.; Fyfe, M.; Gandolfi, M. T.; Gomez-Lopez, M.; Martinez-Diaz, M.; Piersanti, A.; Spencer, N.; Stoddart, J. F.; Venturi, M.; White, A.; Williams, D. "Acid-Base controllable molecular shuttles." *J. Am. Chem. Soc.* **1998.** *120*, 11932-11942.

15. Armaroli, N.; Balzani, V.; Collin, J.; Gavina, P.; Sauvage, J. –P.; Ventura, B. "Rotaxanes Incorporating Two Different Coordinating Units in Their Thread: Synthesis and Electrochemically and Photochemically Induced Molecular Motions." *J. Am. Chem. Soc*. **1999**. *121*, 4397-4408.

16. a)Vladimir Sindelar, V.; Moon, K.; Kaifer, A. "Binding Selectivity of Cucurbit[7]uril: Bis(pyridinium)-1,4-xylylene versus 4,4-Bipyridinium Guest Sites."*Organic Letters.* **2004.** *16,* 2665-2668. b) Eelkema, R.; Maeda, K.; Odell, B.; Anderson, H. L. "Radical Cation Stabilization in a Cucurbituril Oligoaniline Rotaxane." *J. Am. Chem. Soc*. **2007**. *129,* 12384-12385.

17. a) Ong, W.; Go´mez-Kaifer, M; Kaifer, A. E. "Cucurbit[7]uril: A Very Effective Hostfor Viologens and Their Cation Radicals." *Org. Lett*, **2002.** *10,*

18.a) Moon, K.; Kaifer, A. E. "Modes of Binding Interaction between Viologen Guests and the Cucurbit[7]uril Host." *Org. Lett.* **2004**, *6,* 185. (b) Sindelar, V.; Moon, K.; Kaifer, A. E. "Binding Selectivity of Cucurbit[7]uril:Bis(pyridinium)-1,4-xylylene versus 4,4-Bipyridinium Guest Sites."*Org. Lett.* **2004**, *6,* 2665.

19. a) Umali, A.P.; Anslyn, E.V. "A general approach to differential sensing using synthetic molecular receptors." *Curr. Opin. Chem. Biol.***2010**. *14,* 685–692. b) Scott, M.D.; Dutta, R.; Haldar, M.K.; Guo, B.; Friesner, D.L.; Mallik, S. "Differentiation of prostate cancer cells using flexible fluorescent polymers." *Anal. Chem.* **2012**. *84,* 17–20. c) Bajaj, A.; Miranda, O.R.; Phillips, R.; Kim, I.B.; Jerry, D.J.; Bunz, U.H.F.; Rotello, V.M. "Array-based sensing of normal, cancerous, and metastatic cells using conjugated fluorescent polymers." *J. Am. Chem. Soc.* **2010**. *132*, 1018–1022. d) El-Boubbou,; Zhu, K. D.C.; Vasileiou, C.; Borhan, B.; Prosperi, D.; Li, W.; Huang, X.F. "Magnetic glyco-nanoparticles: a tool to detect, differentiate, and unlock the glyco-codes of cancer via magnetic resonance imaging." *J. Am. Chem. Soc*.**2010**. *132,* 4490–4499. e) Bajaj, A.; Rana, S.; Miranda, O.R..; Yawe, J C.; Jerry, D.J.; Bunz, U.H.F.; Rotello, V.M. "Cell surface-based differentiation of cell types and cancer states using a gold nanoparticle-GFP based sensing array." *Chem. Sci.* **2010**. *1*, 134–138. f)

Bajaj, A.; Miranda, O.R.; Kim, I.B.; Phillips, R.L.; Jerry, D.J.; Bunz, U.H.F.; Rotello, V.M. "Detection and differentiation of normal, cancerous, and metastatic cells using nanoparticle-polymer sensor arrays." *Proc. Natl. Acad. Sci. USA.***2009**.*106,* 10912–10916.

20. Qian Liu, Q.; Yi-Cheun Yeh, Y.; a,1, Subinoy Rana, S.; a, Ying Jiang, Y.; a, Lin Guo, L.; b, Rotello, V. M. "Differentiation of cancer cell type and phenotype using quantum dot-goldnanoparticle sensor arrays." *Cancer Letters.***2013**. *334*, 196-201.

21.Liu,S.; Ruspic,C.; Mukhopadhyay, P.; Chakrabarti, S.; Zavalij,P.; Isaacs, L. "The Cucurbit[n]uril Family: Prime Components for Self-Sorting Systems." *J. Am. Chem. Soc.* **2005.** *127,* 15959-67.

22. Singh, A.; Yip, W.; Halterman, R. "Fluorescence-on response via CB7 binding to viologen-dye pseudorotaxanes." *Organic Letters.* **2012,** *14*, 4046-4049.

23) This synthesis was also conducted by Jillian Moore under the direct supervision of Shawna Ellis.

24. I would like to thank and acknowledge Susan Nimmo for her assistance with the ROESY experiment.

25. Kalmár, J; Ashby, M.; Ellis, S.; Halterman, R. L."Kinetics of formation of the host-guest complex of a viologen with cucurbit[7]uril."*Organic letters*. **2012**. *14*, 3248-51.

26) Samanta, D.; Sawoo, S.; Patra, S.; Ray, M.; Salmain, M.; Sarkar, A. "Synthesis of hydrophilic Fischer carbene complexes as organometallic marker and PEGylating agent for proteins." *J. Org. Metal. Chem.* **2005**, *690*, 5581-5590

27) Sindelar, V.; Moon, K.; Kaifer, A. "Binding Selectivity of Cucurbit[7]uril: Bis(pyridinium)-1,4-xylylene versus 4,4-Bipyridinium Guest Sites."*Organic Letters.* **2004.** *16*, 2665-2668.

29. a) Liu, S; Ruspic, C; Mukhopadhyay, P; Chakrabarti, S; Zavalij, P; Isaacs, L. *J. Am. Chem. Soc.* **2005**, *127*, (45) 15959-15967. b) Mock, W. L.; Shih, N. Y. *J. Org. Chem.* **1986**, *51*, 4440-4446.